PENNING TRAP MASS SPECTROSCOPY AT 0.1 PPB

VASANT NATARAJAN

Penning Trap Mass Spectroscopy at 0.1 ppb

by

Vasant Natarajan

B.Tech. Electrical Engineering, IIT Madras (1986)
M.S. Electrical Engineering, RPI (1988)

Submitted to the Department of Physics in
partial fulfillment of the requirements
for the degree of

Doctor of Philosophy

at the

Massachusetts Institute Of Technology

May, 1993

Signature of the Author Vasant Natarajan

Department of Physics
May 12, 1993

Certified by David E. Pritchard

David E. Pritchard
Professor of Physics
Thesis Supervisor

Accepted by _____

George F. Koster
Chairman, Department Committee
on Graduate Studies

Penning Trap Mass Spectroscopy at 0.1 ppb

by

Vasant Natarajan

Submitted to the Department of Physics
on May 12, 1993, in partial fulfillment of the
requirements for the degree of Doctor of Philosophy

Abstract

The MIT Penning trap mass spectrometer is currently the world's most accurate mass measurement tool, with a demonstrated precision below 0.1ppb. We have measured several ionic mass ratios with this precision and used them to obtain the atomic masses of ^{1}H, ^{2}H, ^{14}N, ^{16}O, ^{20}Ne, and ^{40}Ar with up to 1000 times greater accuracy than values from the 1983 atomic mass evaluation. From our data, we can extract such important quantities as the mass of the neutron and the deuteron binding energy.

We perform mass comparisons by alternately measuring the cyclotron frequency of single ions in the same magnetic field. The most important recent development in our experiment has been to extend this precision to two ions with a mass to charge ratio far from unity, known as non-doublets. We use a variant of the Ramsey separated oscillatory fields method to measure the frequency of both ions at the same trap voltage, eliminating errors from shifts in the equilibrium position of the ion with different applied voltages. This also enables us to check measurement errors with known non-doublet ratios such as $M[N_2^+]/M[N^+]$.

We achieve a precision of 0.1 ppb with less than one minute of integration time using a new signal processing technique that allows us to extract the frequency and phase of the ion's axial motion with minimal error. The final error in the mass ratio is dominated by temporal fluctuations in the magnetic field. We obtain about 20 independent measurements on the two ions in one run, enabling us to average these fluctuations. Systematic errors, due mainly to spatial inhomogeneities in the trapping fields, are shown to be below 0.05 ppb using different overdetermined sets of ratios.

Finally, we propose two new schemes for improving the precision towards our ultimate goal of 0.01 ppb or less. By simultaneously trapping a non-doublet pair of ions in the trap and measuring their ratio, we may solve the problem of magnetic field fluctuations while keeping the modes relatively unperturbed from ion-ion interaction. A classical amplitude squeezing technique may help reduce the effect of thermal fluctuations in the mode radii by up to a factor of 5.

Thesis Supervisor: Dr. David E. Pritchard
Title: Professor of Physics

To

Amma, Appa, Neelu and Radhika

"Now, in the East the notion of measure has not played nearly so fundamental a role. Rather, in the prevailing philosophy in the Orient, the immeasurable... is regarded as the primary reality. Thus, in Sanskrit... there is a word 'matra' meaning 'measure', in the musical sense, which is evidently close to the Greek 'metron'. But then there is another word 'maya' obtained from the same root, which means 'illusion'. This is an extraordinarily significant point. Whereas to Western society, as it derives from the Greeks, measure, with all that this word implies, is the very essence of reality, or at least the key to this essence, in the East measure has now come to be regarded commonly as being in some way false and deceitful. In this view the entire structure and order of forms, proportions, and 'ratios' that present themselves to ordinary perception and reason are regarded as a sort of veil, covering the true reality, which cannot be perceived by the senses and of which nothing can be said or thought."

– David Bohm in "*Wholeness and the Implicate Order*"

CONTENTS

1 INTRODUCTION

The unprecedented precision in mass measurements afforded by measuring the cyclotron frequency of a single trapped ion promises to introduce a new era in mass spectrometry and the measurement of fundamental constants. The MIT experiment, eight years after inception, is now at the forefront of this technology.

In the three years that I have worked on this experiment, we have gone from being considered upstarts in precision metrology to being acknowledged as among the best. In this thesis, I will present many of the improvements in our techniques that have helped us achieve this success. Our precision is now around 0.1 ppb* from one measurement run, usually lasting 4 hours, with a best result of 0.08 ppb. We still have to run in the wee hours of the morning when the subway has shut off and external magnetic field noise is at its lowest, since this constitutes our largest source of measurement uncertainty.

We have thoroughly studied systematic errors at this level of precision with two basic approaches. First, we have measured several overdetermined sets of ratios each of whose members should have independent systematic errors - their internal consistency is reassuring. We have also developed a new resonance scheme for comparing mass to charge ratios far from unity, called non-doublets. Non-doublet ratios such as $M[N_2^+]/M[N^+]$ and $M[Ar^+]/M[Ar^{++}]$ then act as calibrated values against which we can perform a second kind of check on our measurement errors. This is also a more stringent check since our errors usually scale as some high power of the mass ratio.

---

* Scattered through this thesis will be the words ppb and ppt. These refer to part per (US) billion, i.e. a relative accuracy of 10^{-9}, and part per (US) trillion, i.e. 10^{-12}.

We therefore feel confident about the results on the atomic masses of six light isotopes - ^{1}H, ^{2}H, ^{14}N, ^{16}O, ^{20}Ne, and ^{40}Ar - that I report in this thesis. The quoted errors, ranging from 0.09 ppb to 0.5 ppb, are the lowest reported to date for any atomic mass, to the best of our knowledge. They represent up to a thousand-fold improvement over the last globally adjusted atomic mass evaluation [WAA85] and should be the most precise contributor to the adjustment being finalized now [WAP93, AUD93]. Van Dyck and his group at the University of Washington are close to reaching our level of precision (they concentrate on light atoms such as H and He) and their results should be a good independent check on our values (see Chapter 5 for a comparison of their recent results).

The basic goals of this program have not changed since the inception of the experiment, though we are much closer. In this chapter, I will briefly cover the background material needed to understand the rest of the thesis, and put our experiment in historical perspective. Most of the material reviewed here is described quite well in the four excellent theses that have preceded mine on this experiment [FLA87, WEI88, COR90 and BOY92], and I refer the reader there for details.

1 MOTIVATION

A sensitive enough mass spectrometer can be used as an energy probe since Einstein's famous relationship associates a change in mass with any change in energy. The long term goal of this research program is to use our spectrometer as such a tool. Nuclear binding energies, which are typically a few MeV, cause differences of a part in 10^3 for atomic masses and have long been measured by mass spectrometers. With our accuracy, we can not only measure these energies to much higher precision, but can now start measuring chemical binding energies (of order a few eV) and use the instrument as a novel spectroscopic tool for atomic and molecular levels. Listed below are some of the more interesting applications of our experiment.

The neutrino mass

The rest mass of the electron neutrino is a fundamental question in science and has many implications for the standard model and cosmology. But the elusive nature of the neutrino makes it hard to measure its mass directly. One way to infer its mass is to measure the energy spectrum of a typical beta decay process such as

$$^3\mathrm{H} \rightarrow {}^3\mathrm{He}^+ + \mathrm{e}^- + \overline{\nu}_\mathrm{e}. \qquad (1\text{-}1)$$

Beta ray spectroscopists [RBS91, BBB92] measure the number of electrons emitted in the decay as a function of their kinetic energy. This number falls to zero at an energy defined as the endpoint, when all the energy available to the process is taken up by the emitted electron. A difference between the endpoint and the rest mass difference $M[^3\mathrm{H}–^3\mathrm{He}^+ - \mathrm{e}^-]$ is then the mass of the neutrino.

We can help the spectroscopists by measuring this rest mass difference from the mass ratio $M[^3\mathrm{H}^+]/M[^3\mathrm{He}^+]$. In order to be really useful to the spectroscopists, we have to measure the mass difference to better than 1eV, or the ratio to better than 0.3 ppb, which is well within our capability in terms of precision. Later, I will discuss some of our (as yet unsuccessful) attempts to perform this measurement. Van Dyck *et al.* [VFS93b] have recently reported a measurement of this difference with a precision of 1.7 eV or 0.57 ppb.

Fundamental constants - $N_A h$, α

A measurement of the molar Planck constant ($N_A h$) and the closely related fine structure constant (α) can be made by massing a photon (γ ray) [JOH84]. We can precisely measure the mass difference associated with the emission of a γ ray in atomic units. Wavelength spectroscopy on the γ ray (at a place such as NIST) yields the energy difference in macroscopic units. Equating the two ways of obtaining the energy difference, we find

$$\Delta E = \frac{hc}{\lambda} = \frac{\Delta M}{N_A}c^2 \quad \Rightarrow \quad N_A h = \lambda \Delta M c \qquad (1\text{-}2)$$

The molar Planck constant by itself is not very useful, since neither N_A nor h is known to the precision of their product. But it can be combined with a measurement of the Rydberg and the electron mass in atomic units to obtain α^2.

$$R_\infty = \frac{m_e e^4}{2h\hbar^2} = \frac{M_e}{N_A}\frac{\alpha^2 c^2}{2h} \quad \Rightarrow \quad \alpha^2 = \frac{2R_\infty (N_A h)}{M_e c^2} \qquad (1\text{-}3)$$

In order to really improve the knowledge of α^2, we need $N_A h$ to about 2 parts in 10^8. This means that we have to measure the mass difference to better than 0.01 ppb and the wavelength spectroscopists have to improve their precision by an order of magnitude - something that will require major advances at both ends. However, even at the part in

10^7 accuracy for $N_A h$ attainable now, this becomes an independent determination of α, with completely different physics from other schemes of measurement.

Atomic mass table and ^{28}Si

As we will see from the results reported in this thesis, we have the precision to greatly reduce the errors in the standard atomic mass table obtained from a least squares adjustment to all the relevant mass measurements [WAA85]. These masses are routinely used in nuclear physics calculations and for calculating such quantities as the isotope shift in atomic energy levels. Penning traps are being used not just for stable isotopes as in our lab, but also at reactor facilities to measure the masses of short-lived isotopes to high precision [BHK92].

Measuring the atomic mass of ^{28}Si and its most abundant isotopes might ultimately help in replacing the artifact mass standard with one based on Si. This is an attractive proposition since the technology for producing high purity single crystals in Si is very mature. Although the current limitation is the lack of precise knowledge of relative abundances of the Si isotopes, before this technology becomes viable the atomic masses will have to be improved beyond the present 25 ppb precision.

Weighing chemical binding energies

A precision of 0.01 ppb is equivalent to an energy resolution of 0.28 eV for a mass 28 ion. This is enough to measure chemical bonds to about 10% accuracy. Indeed, for many of the results reported here (at the 0.1 ppb level), we already have to account for chemical and electronic binding energies. There are surprisingly many simple ionic species that are inaccessible to conventional spectroscopic techniques either because they are too reactive or cannot be produced in large quantities.

With the invention of the Electron Beam Ion Trap (EBIT) [LMH88], it is now possible to easily produce highly charged ions of heavy nuclei. These have never been studied spectroscopically and mass measurements in Penning traps can prove to be very useful. For instance, a hydrogen-like uranium atom (i.e. completely stripped to its nucleus but for one core electron) has such a large nuclear wave function that the Lamb shift in the ground state is measurable just by measuring the mass of this ion! And we need only one ion to do this.

2 HISTORICAL INTRODUCTION

Charged particle traps now have a long history in precision measurements. F.M. Penning's original use of crossed electric and magnetic fields was to increase the time that electrons remained within a glow discharge [PEN36]. Dehmelt ultimately refined this idea to trap a single electron with a strong homogeneous magnetic field and an electrostatic quadrupole potential, and called it a Penning trap. Since then, Penning traps have been used for many fundamental measurements and, more recently, for mass measurements with single, trapped ions.

Penning trap measurements

The University of Washington group with such luminaries as Dehmelt, Wineland, Ekstrom, Van Dyck, Gabrielse and Brown, pioneered the use of Penning traps for fundamental constant work. They developed most of the theory for trapped particle motion (reviewed in [BRG86]), clever refrigeration techniques for cooling the modes [WID75], and detected the first single electrons. The measurement of the g-2 of the electron [VSD87], for which Dehmelt shared the Nobel Prize in 1989, remains one of the most precise measurements in the history of science.

In addition, they also measured the g-factor of the positron with similar accuracy and found it to be the same as for the electron. This becomes a strong test of CPT invariance for leptons. After single protons and other ions could be detected, the traps were used for mass comparisons. The proton to electron mass ratio is now most precisely obtained from a Penning trap comparison by Van Dyck's group [VMF86]. The Harvard-CERN group has successfully captured antiprotons in a Penning trap, which has yielded a precise value for the antiproton-proton mass ratio [GFO90].

The MIT experiment

The current project in precision metrology at MIT was conceived in 1983 and has had an 8 year long history. After settling on a commercial magnet and an RF SQUID for detection, the first version of the experiment was completed by 1986. When the first student (Flanagan) graduated, a large cloud of ions had been detected. By the time Robert Weisskopf wrote his thesis in 1988, a single N_2^+ ion had been detected. This was the first time a single molecular ion had ever been detected in a trap. These experiments

used our second generation of trap technology, Trap II, which had the split guard ring electrodes needed to drive and detect the radial modes.

Eric Cornell wrote his thesis in 1990 after helping to develop the mode coupling techniques used to make the first single ion mass ratio measurement $M[CO^+]/M[N_2^+]$, in 1989. He also worked on developing two ion measurement techniques to overcome the problems of field fluctuations. After these successes, we spent some time trying to see mass 3 ions for the ^{3}He-T measurement. But we soon gave up as the vacuum became unacceptably bad. We pulled up the experiment in May 1990 and started work on Trap III, which represented a global redesign with several improvements. As it turned out, we did correct a lot of the mistakes in the old design, but made quite a few of our own including accidentally quenching the magnet.

After energizing the magnet ourselves, we saw single ions again in May 1991. We started looking for the radial modes (with a certain amount of uncertainty since we were not sure of the exact current with which we had energized the magnet) when we ran into an unknown source of noise. It took us 3 months to track it down to a variable frequency motor controller for an air conditioning unit in our lab upstairs. We were back looking for the radial modes by the beginning of 1992. We found it in March and Kevin Boyce graduated with our second measurement of $M[CO^+]/M[N_2^+]$; the precision of 0.1 ppb this time was 4 times better than our previous measurement.

We then tried again to make a mass 3 measurement. This time we were able to see a single HD^+ ion, but were not able to reproducibly get rid of all the impurity ions without losing the good ion. We decided instead to start a comprehensive study of systematic errors and perform the useful measurements reported here in September 1992. Though our best precision is still only 0.08 ppb, we feel much more confident about our errors. Indeed, we found one small systematic error that had slipped into the $M[CO^+]/M[N_2^+]$ result reported at the AMCO-9 conference [VBD92, BOY92] when we completed this study; the corrected number differs by 0.2 ppb (see Chapter 5).

Other groups

There are currently several other groups using Penning traps for precision mass measurements. Van Dyck's group at Washington is the closest both in terms of precision and the mass range of interest [VFS92]. They use a trap about the same size as ours but

their detection scheme is to measure the axial frequency shift as the cyclotron orbit increases due to absorption of energy at the cyclotron frequency. Werth's group at the Universität Mainz in Germany launches ions from a Penning trap and uses time of flight to determine the cyclotron radius [GWW90]. When the cyclotron mode is resonantly excited, the time of flight decreases significantly because the cyclotron energy is converted into axial kinetic energy as the ion leaves the high field region. This is a destructive detector and also does not allow direct cooling of the modes. A similar technique is being used at CERN by Bollen *et al.* to determine the masses of unstable isotopes to about a part in 10^7 [BHK92]. For species with a lifetime of 50 s, a destructive measurement is not the problem.

Gabrielse's group at Harvard University is using Penning traps to measure the mass of antiprotons captured at CERN [GFO90]. They are also considering the possibility of making anti-hydrogen with the trapped antiprotons. Dunn's group at Boulder has been working on a trap project for a few years but has not yet published any results. They use a low noise cryogenic FET amplifier to detect the axial motion.

With all these groups starting to report precision results, it is widely believed in the mass spectrometry community that the next generation of atomic masses is probably going to come completely from Penning trap measurements with single ions. This technique is more than an order of magnitude better than any previous method of mass measurement. This can be seen from Fig. 1-1 where I trace the historical improvement in resolution and precision of mass spectrometers at measuring doublet ratios. The only rival technique now is Fourier transform ion cyclotron resonance in a cubic ion trap, usually done with a large cloud ions. This has much lower resolution (~2×10^7) than ours, but the signal peaks can be split by a factor of 100 to determine the doublet spacing, if all the coulobmic perturbations can be controlled [GMN93]. Penning trap ICR still is more than an order of magnitude better.

(a) 1951 The resolution (m/Δm) of this mass spectrometer was 5000. The doublet splitting was detemined by taking the average distance between corresponding half-heights on peaks [NIR51].

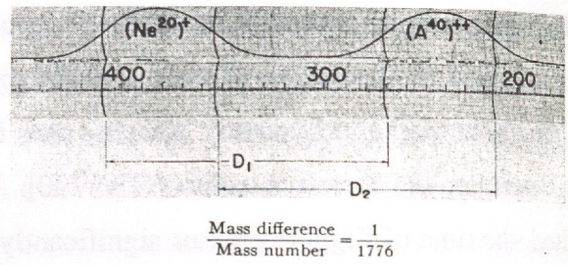

(b) 1967 This spectrometer had a resolution of 10^5. But for doublets, a peak matching technique was used to measure the splitting to better than 1% of the width of each peak. Therefore doublet ratios could be measured to a precision of 5×10^{-8} [JHB67].

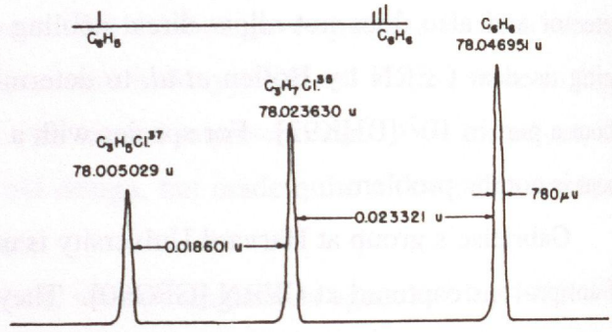

(c) 1993 This Fourier Transform Ion Cyclotron Resonance (FT-ICR) spectrometer has an "ultra-high" resolution of 2×10^7. The peaks are actually further spaced than shown because of a heterodyne excitation scheme. The doublet ratio can be measured to 1×10^{-9} by splitting the peaks carefully [GMN93].

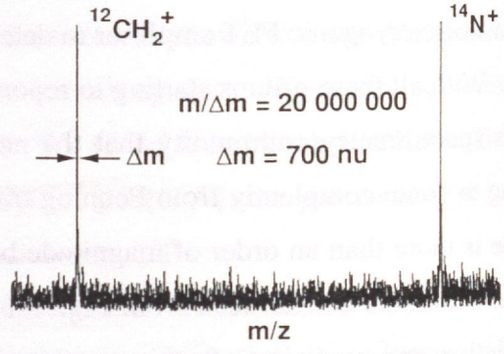

(d) 1993 (This Work) The MIT Penning trap mass spectrometer has a "resolution" of 3×10^9. The histograms are the fluctuations in the cyclotron frequencies for each ion, with Gaussian fits as a visual aid. The frequencies have been plotted on the same axis, but note that the break to bring them on scale is about 22 km! By averaging the measurements, the doublet ratio can be determined to 8×10^{-11}.

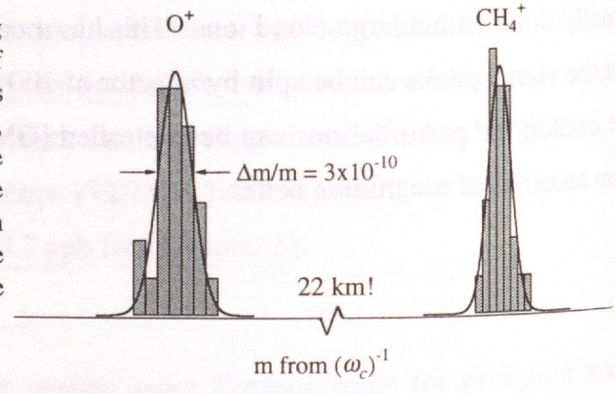

Fig. 1-1. Development of mass spectrometry. This figure shows the chronological improvement in the precision of mass measurements from 1950-1993. In all cases the two peaks shown form a doublet, although the doublet separations are not exactly the same.

3 BASIC PENNING TRAP PHYSICS

The Penning trap uses static electric and magnetic fields to trap charged particles in all three dimensions. In an ideal trap, a strong, uniform magnetic field along the $\hat{z}$ axis confines the particle radially while a weak, quadrupole electric field provides a linear restoring force in the axial direction. In practice, the fields are not perfect and there are several corrections to this simple picture. The theory for this has been well developed by the University of Washington group and summarized in a review article by Brown and Gabrielse [BRG86]. The mathematical theory relevant to our experiment has been developed in great detail by Robert Weisskopf in his thesis [WEI88].

The idea of using Penning traps for mass comparison is very simple. The cyclotron frequency of an ion in a magnetic field is given as $\omega_c = \frac{eB}{mc}$. If we measure this frequency for two singly charged ions in the same magnetic field, then the ratio of their cyclotron frequencies is the inverse ratio of their masses. Of course, in a trap the cyclotron frequency gets modified due to the presence of the electric field and we have to correct for this effect.

Single ion motion

In Fig. 1-2, I show the cross sectional view of our trap. The equipotential surfaces for a quadrupole electric field are hyperbolae of rotation. Our trap is formed with copper electrodes that are precision machined to have this shape. The potential inside the trap is then

$$\Phi(z,\rho) = \frac{z^2 - \frac{1}{2}\rho^2}{2d^2} V_T, \tag{1-4}$$

where V_T is the applied voltage between the ring and endcaps, z is the axial position, ρ is the radial position, and

$$d^2 \equiv \frac{{z_0}^2}{2} + \frac{{\rho_0}^2}{4} \tag{1-5}$$

is the characteristic size of the trap.

The equation of motion for a single ion of mass m and charge e is:

$$m\ddot{\mathbf{r}} = e\mathbf{E}(\mathbf{r}) + \frac{e}{c}\dot{\mathbf{r}} \times \mathbf{B}(\mathbf{r}). \tag{1-6}$$

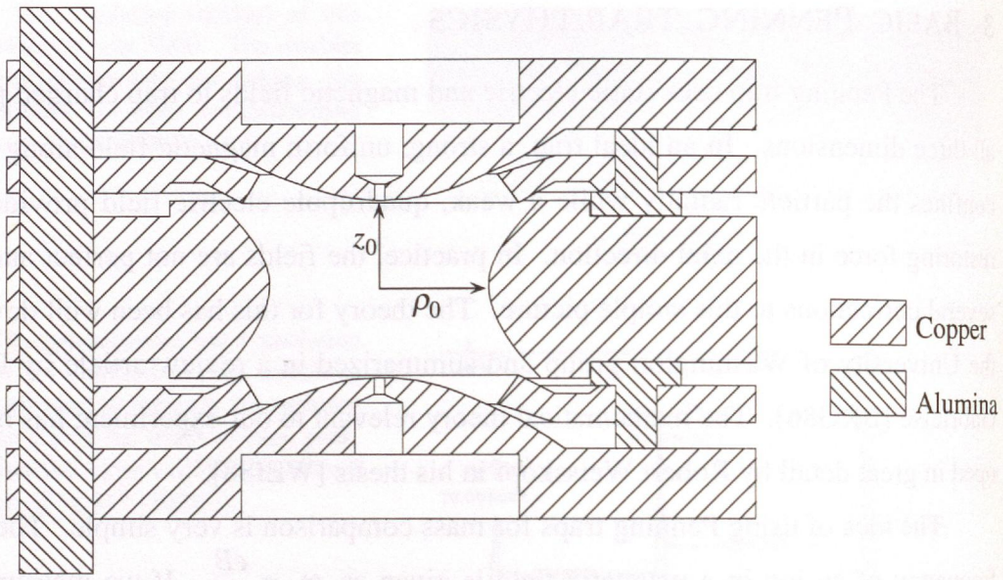

Fig. 1-2 Cross sectional view of an assembled trap. The endcap electrodes follow the equation $z^2 - \rho^2/2 = z_0^2$ while the ring electrode follows $z^2 - \rho^2/2 = \rho_0^2/2$. In our trap, $z_0 = 0.600$ cm and $\rho_0 = 0.696$ cm, giving a characteristic size $d^2 = 0.301$ cm^2.

In an ideal trap, the motion decomposes into three normal modes. In the axial direction, the linear electric field gives rise to harmonic motion at a frequency defined by

$$\omega_z^2 = \frac{eV_T}{md^2}. \tag{1-7}$$

The two modes in the radial plane are the trap cyclotron mode - at a frequency ω_c' corresponding to the normal cyclotron oscillation around the magnetic field lines, but slightly modified due to the electric field - and the magnetron mode - a slow drift at ω_m due to the $\mathbf{E}\times\mathbf{B}$ fields away from trap center. The eigenfrequencies can be derived from the radial equation of motion in the trap

$$\ddot{\boldsymbol{\rho}} - \omega_c \dot{\boldsymbol{\rho}} \times \hat{z} - \tfrac{1}{2}\omega_z^2 \boldsymbol{\rho} = 0. \tag{1-8}$$

We guess solutions of the form $\mathrm{Re}\left(\boldsymbol{\rho}_0 e^{i\omega t}\right)$ and plug it into the above equation to obtain the characteristic equation:

$$\omega^2 - \omega_c \omega + \tfrac{1}{2}\omega_z^2 = 0. \tag{1-9}$$

This yields the two solutions:

$$\omega_c' = \tfrac{1}{2}\left(\omega_c + \sqrt{\omega_c^2 - 2\omega_z^2}\right),$$
$$\omega_m = \tfrac{1}{2}\left(\omega_c - \sqrt{\omega_c^2 - 2\omega_z^2}\right). \quad (1\text{-}10)$$

The three trap modes behave as harmonic oscillators but differ greatly in the partition of energy between kinetic and potential. The axial motion has equal average kinetic and potential energy as for a mass bound harmonically on a spring. The cyclotron motion is mainly the circular motion in a magnetic field at high speed, so the energy is predominantly kinetic. On the other hand, the magnetron motion is a slow drift and the energy is almost entirely potential. In fact, the potential energy (and the total energy) in the magnetron mode decreases as we increase its radius, even as its kinetic energy increases. Therefore an ion at the center of the trap is in unstable equilibrium on top of this potential hill and does not leave the trap only because it has no way of losing energy and momentum.

As seen from Eq. 1-10, in an ideal trap we can extract ω_c by just measuring two modes: ω_c' and either ω_z or ω_m. What helps us do this in the presence of real life non-idealities, such as a small misalignment of magnetic and electric field axes (tilt) or machining imperfections in the electrodes leading to an eccentricity in the hyperboloids, is the following invariance theorem [BRG86]:

$$\omega_c^2 = \bar{\omega}_c'^2 + \bar{\omega}_z^2 + \bar{\omega}_m^2, \quad (1\text{-}11)$$

where I have temporarily added bars to indicate that these are the non-ideal frequencies we measure. For a typical ion of mass 28, the trap cyclotron frequency is about 4.5 MHz in our magnetic field of 8.528 T. We adjust the trap voltage to make the axial frequency 160 kHz, which gives a magnetron frequency of 2.8 kHz. We always work with this hierarchy of frequencies, i.e. the approximation $\omega_c' >> \omega_z >> \omega_m$ remains valid. Then, from the above relation, we only need to measure ω_c' to the desired precision; ω_z and ω_m need to be measured to correspondingly lower precision.

In practice, we usually measure only ω_c' and ω_z for each ion; for the magnetron frequency we use the following expression:

$$\omega_m = \frac{\omega_z^2}{2\omega_c'}(1+\delta), \quad (1\text{-}12)$$

where the quantity δ is an empirically determined factor that should be 0 in an ideal trap. Its non-zero value can be caused, for instance, by a tilt or an eccentricity in the hyperboloids. We therefore measure the magnetron frequency once to determine this factor and then use it for the rest of the run. In our trap, this factor has remained constant at about $\delta = 0.00026$ for different masses. If we assume that it is entirely due to a tilt in the electric field axis, this corresponds to a 0.6° misalignment, which is quite reasonable given our trap alignment technique. Assuming that $\delta = 0$ causes a shift in the cyclotron frequency of about 0.09 ppb (at mass 28), but the effect on a doublet ratio is less than 1 ppt because both ions are shifted almost equally (the effect can be as high as 0.05 ppb for a non-doublet). Therefore, at the current precision level, we do not need to know δ very accurately.

Detection

We directly detect only the axial motion of the ion. We use an RF SQUID to sense the image current induced in the endcaps by the oscillating ion. This acts as a high impedance current source which we match to the low input impedance of the SQUID using a high Q (~30000) superconducting tank circuit tuned to the ion's frequency. The coil in the circuit is a transformer with the primary side (about 3000 turns) attached to the trap and the secondary (only a few turns) going to the SQUID. This transfers the energy from the ion most efficiently into the detector; the resultant damping time for the ion is only a few seconds.

The SQUID is made of a superconducting loop with a "weak link". Such a loop can be considered to lie somewhere between a perfect superconducting loop, which maintains its internal flux by setting up supercurrents to oppose any external field change, and a conducting loop, which allows the flux to change after the eddy currents die from resistive losses. The SQUID loop has coherent continuity of the wave function across the link, which only allows the flux threading the loop to be integral multiples of the fundamental flux quantum $\Phi_0 = \frac{hc}{2e}$, but allows jumps between the number of quanta as the external field changes. By operating the field near such a transition, the SQUID can be used as a sensitive magnetometer. An input coil converts our current signal into a magnetic flux that is thereby detected.

We can vary the strength of the coupling between the ion and the detector by changing the number of turns in the secondary of the coil. For optimal operation, we adjust the coupling so that there is minimal noise coupling back from the SQUID and the ion's axial motion is mostly in equilibrium with the 4.2 K Johnson noise from the effective resistor in the resonant circuit. The resultant signal to noise ratio is now good enough that the current from a single ion (about 10^{-14} A p-p when excited to 20% of the trap) has a peak Fourier transform amplitude 5 times higher than the noise level.

The coupling to the detector has two effects on the axial mode. The real part of the detector impedance gives a width (or damping) to the mode while the imaginary part changes the axial frequency slightly. This is analogous to resonant coupling between a damped oscillator (corresponding to the tuned circuit) and an undamped one (the ion's axial mode). The coupling is defined to be weak when the induced damping for the ion is much smaller than the coil damping constant, which is true for ions heavier than mass 10 u, but is marginal at mass 3. In this limit, the damping constant for the ion on resonance is given by [WEI88] :

$$\gamma = \frac{1}{m}\left(\frac{qB_1}{2z_0}\right)^2 \omega_0 L Q, \qquad (1\text{-}13)$$

where B_1 is a trap dependent constant (≈ 0.8), ω_0 is the tuned circuit resonant frequency (and the ion's axial frequency since we are on resonance), L is the coil inductance, and Q is the quality factor of the detector resonance. The damping time for a mass 28 ion with our present detector is about 4 seconds, while the coil damps in 30 ms. In this limit, the effect of frequency pulling can be neglected.

If, as I have stated, we only detect the axial motion, how do we make a precision measurement of the cyclotron frequency? This brings us to the subject of the next section which reviews our method of coupling the axial and radial modes.

Mode coupling

The techniques for using RF fields to give mode mixing in a Penning trap were pioneered by Dehmelt's group in Washington [WID75]. We have developed this into an elegant phase sensitive scheme for measuring the radial modes, described in detail in [WEI88] and [CWB90]. As we will see, this also allows us to cool the radial modes by

using a single exchange pulse with the axial mode (which is coupled to the thermal bath by the detector).

The radial modes are nominally undamped (have zero linewidth) since the trap is azimuthally symmetric and radiation damping at our frequencies should take hundreds of thousands of years! The azimuthal symmetry is only broken by the split guard ring electrodes. By applying an RF voltage at a frequency ω_p across the two halves of the upper guard ring, we can produce a time varying, diagonal quadrupole potential ($\sim zx\cos(\omega_p t)$). To an ion in, for instance, a large cyclotron orbit, such a field gives kicks in the axial direction and couples the two modes.

These kicks are in phase if $\omega_p = \omega_c' - \omega_z$. Under such resonant coupling, the classical action ($\left|\oint p_{canon} \cdot dq\right|$) swaps back and forth between the two modes at a rate determined by the strength of the coupling. In an analogous two-level atomic system coupled by a laser field, this would be called the Rabi oscillation of population in the two states. Hence, we can develop an analog of the π-pulse which causes a complete population exchange or, for our classical system, an exchange of the action between the modes.

We can carry this analogy further to the level anti-crossing diagram (shown in Fig. 1-3 for an Ar^{++} ion). When the cyclotron and axial mode are coupled by the RF field, the new normal modes in the trap represent a superposition of the two modes. Sufficiently close to resonance, both states can be excited and detected through the axial component of their motions. As the coupling frequency is tuned through the resonance, the two states (corresponding to the axial mode and the cyclotron mode minus one RF photon, but "dressed" by the coupling field) repel each other. On resonance, the splitting is exactly given by the Rabi frequency. We plot this avoided crossing carefully both to obtain the Rabi frequency and to make a preliminary determination of the cyclotron frequency (to about 0.1 Hz). Once we know the Rabi frequency for a given coupling field strength, we know the exact time-amplitude product needed to apply a π-pulse.

The π-pulse technique also allows us to do a one-shot cooling of the cyclotron mode to its sideband cooling limit. For CW sideband cooling, we would leave the coupling drive on until the cyclotron mode cools by coupling to the 4.2 K axial detector bath. The π-pulse method quickly exchanges the actions between an initially hot cyclotron mode and a precooled axial mode. The resultant amplitude in the axial can then damp into the

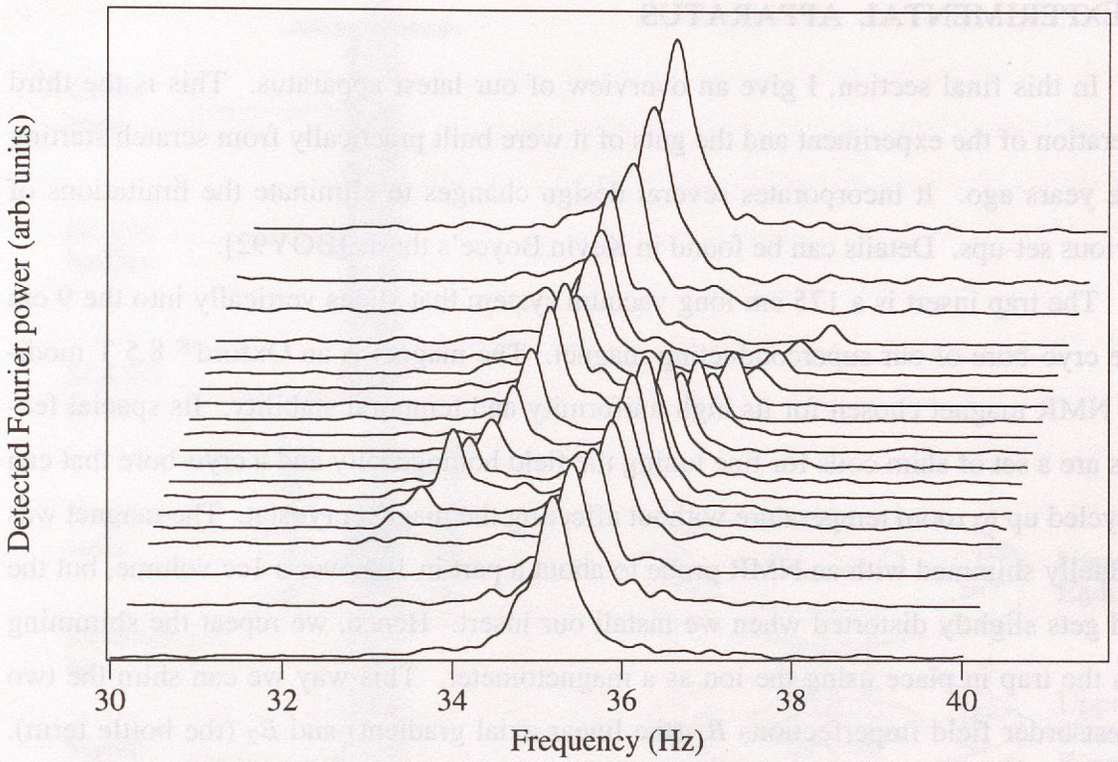

Fig. 1-3 Cyclotron avoided crossing for Ar^{++}. Each horizontal scan is the Fourier power spectrum of the detected axial signal for a fixed coupling frequency. The axial motion is excited with a short pulse with the coupling drive on. The total change in coupling frequency as it is tuned through the resonance is 15 Hz.

detector. In both cases, the cooling limit is obtained from a thermodynamic argument as follows. The entropy change associated with the emission of one RF coupling photon is

$$\Delta S = \frac{\hbar\omega_z}{T_z} - \frac{\hbar\omega_c'}{T_c}, \tag{1-14}$$

where we have defined an equivalent temperature for the modes. This process continues until, at equilibrium, we have a reversible process with no net change in entropy, so that

$$\frac{\hbar\omega_z}{T_z} = \frac{\hbar\omega_c'}{T_c} \Rightarrow T_c = \frac{\omega_c'}{\omega_z} T_z. \tag{1-15}$$

The same argument holds for the magnetron mode except that, because it is at the top of a potential hill, its energy is positive and its "temperature" negative. An ion in a large magnetron orbit is "cooled" to the center of the trap with a coupling field at $\omega_z + \omega_m$. We use the CW cooling scheme for this mode since we cannot get the drive strength high enough to have a short π-pulse without perturbing the detector; the coupling frequency is just too close (a few kHz) to the coil frequency.

4 EXPERIMENTAL APPARATUS

In this final section, I give an overview of our latest apparatus. This is the third generation of the experiment and the guts of it were built practically from scratch starting three years ago. It incorporates several design changes to eliminate the limitations of previous set-ups. Details can be found in Kevin Boyce's thesis [BOY92].

The trap insert is a 175 cm long vacuum system that slides vertically into the 9 cm wide cryo-bore of our superconducting magnet. The magnet is an Oxford® 8.5 T modified NMR magnet chosen for its high uniformity and temporal stability. Its special features are a set of shim coils for fine tuning the field homogeneity and a cryo-bore that can be cycled up to room temperature without affecting the magnet cryostat. The magnet was originally shimmed with an NMR probe to about a part in 10^8 over a 1cc volume, but the field gets slightly distorted when we install our insert. Hence, we repeat the shimming with the trap in place using the ion as a magnetometer. This way we can shim the two lowest order field imperfections B_1 (the linear axial gradient) and B_2 (the bottle term). Later on, we will study the effect of any residual imperfections.

The insert is suspended from the top flange of the magnet as shown in Fig. 1-4. The copper can housing the trap is near the bottom of a central 3/4 inch tube; the tube is of stainless steel most of the way to the can to reduce thermal conductivity into the He bath. A needle tube feeds into the top of the insert from a gas handling manifold to let neutral gas atoms down the 3/4" tube. There is a line of sight path for the particles all the way down to the bottom of our trap, where we have a field emission tip. The central tube also has einzel lenses for guiding ions when we perfect an external ion source. The wires for DC and AC connections to the trap are in a separate 3/16" tube also going into the copper can. The signal from the upper endcap comes out through a twisted pair via a homemade feedthrough and goes to the detector box.

Our detector is a commercial thin film RF SQUID operating at 190 MHz made by Quantum Design, Inc., which also supplies the RF head and control electronics. The SQUID and a homemade toroidal superconducting coil, forming the resonant circuit, are housed in a copper box that is clamped to the central tube. It has to be placed well above the magnet center since the SQUID cannot operate in high magnetic fields. The fringing field at the detector location is about 200 G.

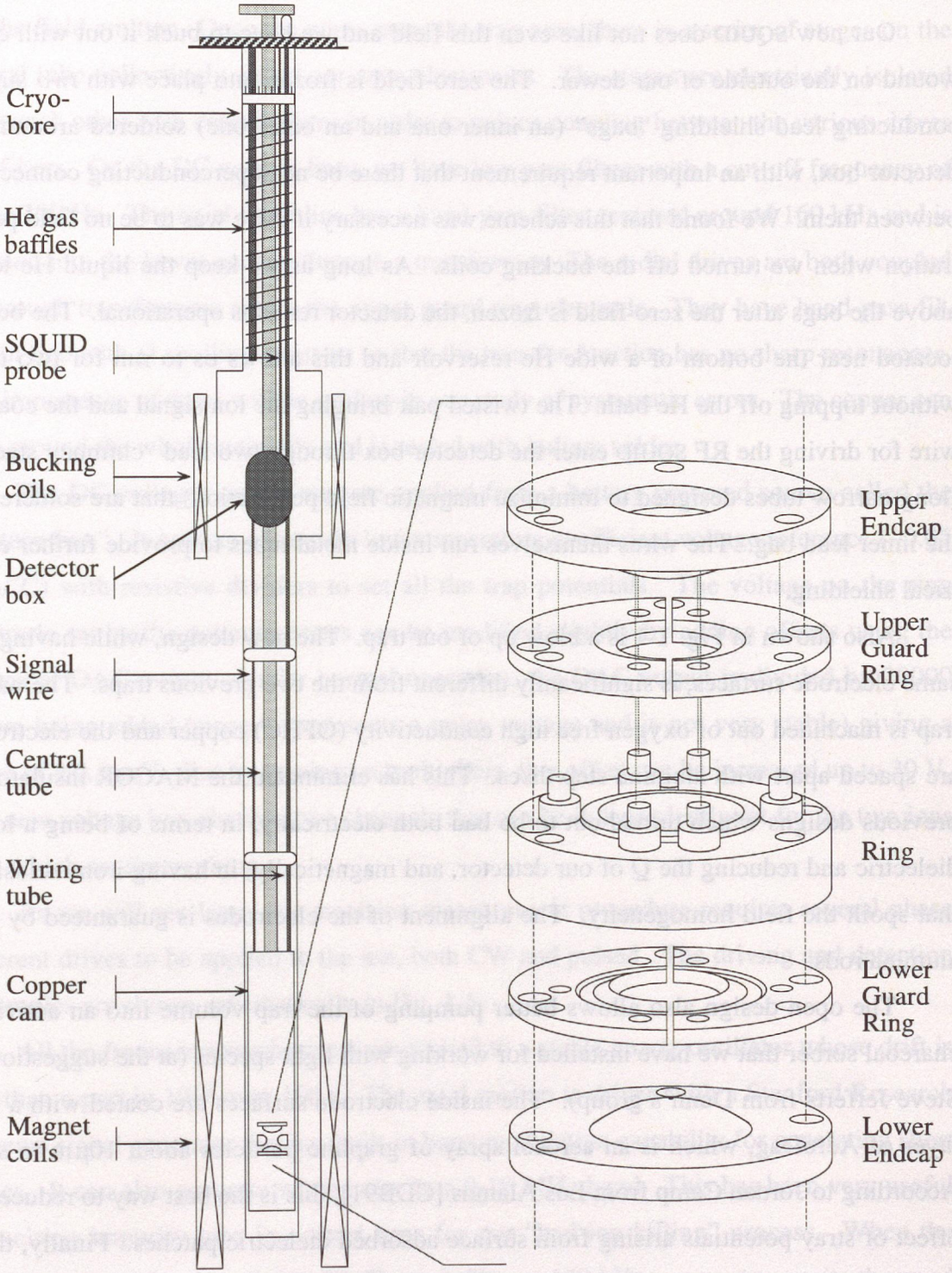

Fig. 1-4 Experimental insert and trap. Shown in the figure is a 1:10 scale version of the experimental insert that goes into the cryo-bore of the magnet. The insert is positioned within the bore by two teflon spacers. Also shown is a blow up of the new trap. The six alumina step discs for spacing the electrodes on the upper side of the ring are shown, there are six more on the lower side (not shown).

Our new SQUID does not like even this field and we have to buck it out with coils wound on the outside of our dewar. The zero-field is frozen into place with *two* superconducting lead shielding "bags" (an inner one and an outer one) soldered around the detector box, with an important requirement that there be no superconducting connection between them. We found that this scheme was necessary if there was to be no field penetration when we turned off the bucking coils. As long as we keep the liquid He level above the bags after the zero-field is frozen, the detector remains operational. The box is located near the bottom of a wide He reservoir and this allows us to run for two days without topping off the He bath. The twisted pair bringing the ion signal and the coaxial wire for driving the RF SQUID enter the detector box through two lead "chimney stacks" (long narrow tubes designed to minimize magnetic field penetration) that are soldered to the inner lead bag. The wires themselves run inside metal tubes to provide further electrical shielding.

Also shown in Fig. 1-4 is a blow up of our trap. The new design, while having the same electrode surfaces, is significantly different from the two previous traps. The whole trap is machined out of oxygen free high conductivity (OFHC) copper and the electrodes are spaced apart with alumina step discs. This has eliminated the MACOR insulator in previous designs which turned out to be bad both electrically, in terms of being a lossy dielectric and reducing the Q of our detector, and magnetically, in having iron inclusions that spoilt the field homogeneity. The alignment of the electrodes is guaranteed by two alumina rods.

The open design also allows better pumping of the trap volume into an activated charcoal sorber that we have installed for working with light species (at the suggestion of Steve Jefferts from Dunn's group). The inside electrode surfaces are coated with a thin layer of AeroDag, which is an aerosol spray of graphite particles about 10μm in size. According to Jordan Camp from Los Alamos [CDB91], this is the best way to reduce the effect of stray potentials arising from surface adsorbed dielectric patches. Finally, there is a field emission tip located just below the lower endcap that allows an ionizing beam of electrons to enter the trap. The trap is aligned by ensuring that we can see the tip from the top of the insert through the holes in the endcaps.

The electrical inputs into the trap are fed via a multi-pin feedthrough (for DC) and BNC coaxial feedthroughs (for AC drives). There is a separate high voltage feedthrough

for the field emitter. Once the wires enter the trap area, there is a series of stages on the central tube collectively called our cryo-electronics. The stages are electrically isolated from each other with copper plates in order to reduce coupling between the various drives and filters. On the DC voltage lines, we have low pass filters with a cut-off frequency of about 300 Hz. The axial drive line has a band-pass filter centered around 160 kHz and is coupled into the lower endcap through a transformer. The radial drives are both coupled in through transformers across the upper guard ring electrode. They have band-pass filters in line with Q spoiling resistors so that the transfer function has no sharp resonances. The importance of these will be evident in our study of systematic errors. The copper can goes around the whole assembly and is sealed with indium solder.

The DC voltages on the trap are applied from a battery powered source called the "voltage box". It uses an extremely low temperature coefficient voltage reference (~0.05 ppm/°C) with resistive dividers to set all the trap potentials. The voltage on the ring electrode set by the potentiometers can be modified slightly by adding offsets using the computer DAC output. Under normal operation, the DAC output is divided by 20000 before being added (since it represents a noisy voltage and is not very stable) giving a range of ±0.5 mV. But by turning on multipliers, this offset can be increased up to 30 V. Our new voltage box also has two channels that can be independently set for the two ions with which we are working.

As we will see later, our precision measurement procedure requires several phase coherent drives to be applied to the ion, both CW and pulsed. The driving and detection electronics are shown schematically in Fig. 1-5.

All the frequency synthesizers are locked to a stable quartz oscillator whose drift is less than a part in 10^{12} over 100 s. The axial motion is driven with a Stanford Research Systems signal generator that has built-in burst modulation capability for generating short pulses. It can also generate white noise in a 0-10 MHz band. This has been very useful in exciting impurity ions in a short time for our "bad ion killing" process. When the noise is on, we bring into line a -30 dB notch filter at 160 kHz so as not to excite the good ion. The radial modes have both to be driven and coupled to the axial mode. For this we use two Hewlett Packard synthesizers that can go up to 60 MHz. Short pulses are generated with a high speed switch in the microsecond pulser box, and a coaxial relay chooses between excitation and coupling pulses.

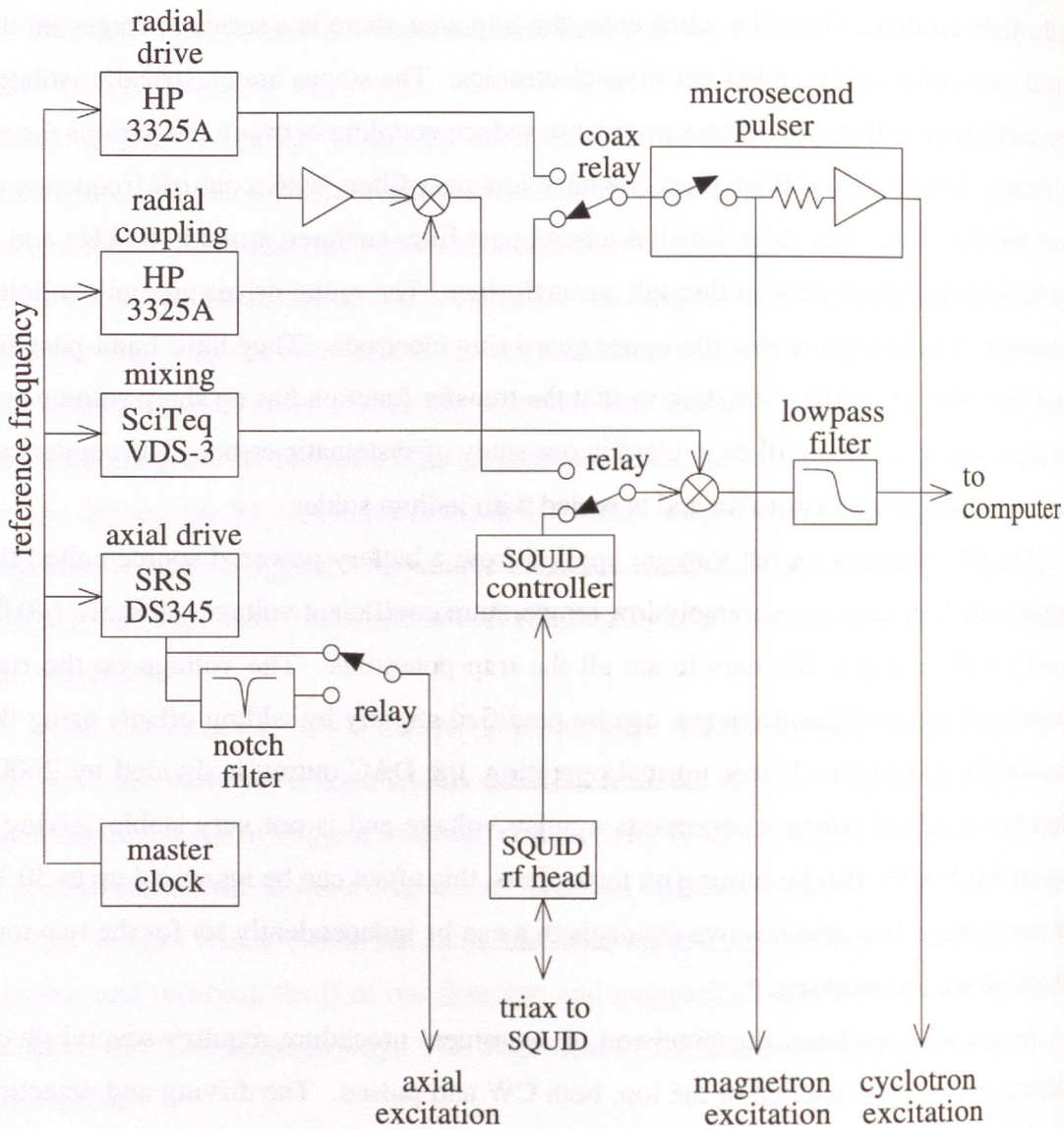

Fig. 1-5 The driving and detecting electronics. The relays are all controlled by the computer, as are all the signal generators except the SciTeq.

All these generators and relays are under the control of a new Macintosh IIci computer. It uses LabView data acquisition and control software to talk to the various instruments. The advantages of a Macintosh over the old PDP-11 should be clear to anyone who has worked with both computers!

2 TECHNIQUES

When I first started on this experiment, a precision of 0.4 ppb had been achieved for the $M[CO^+]/M[N_2{}^+]$ ratio. Any attempt to improve this precision had to begin by understanding the major limitations of the techniques used for this measurement. In this chapter, I will review the old techniques and then discuss in turn our solutions to each limitation. Some of these solutions have not been implemented and remain as proposals for the future.

One of the main improvements has been in the technique for loading a single ion so that we can cycle from an empty trap to having a cooled ion in only a few minutes, compared to half an hour before. A new data analysis algorithm that I will present has reduced our phase estimation error by a factor of three. It gives errors close to the theoretical lowest limits and allows us to make a 0.1 ppb cyclotron resonance measurement in only a minute or less. I will also analyze how magnetic field noise manifests itself in the mass ratio data. This has helped us optimize our measurement process for the *1/f* spectral density that appears to characterize our noise.

1 OLD TECHNIQUES AND THEIR LIMITATIONS

The entire process of making precision mass comparisons using our old trap has been discussed in detail in [COR90] and [CWB89]. It typically consisted of loading the trap with a single ion of type 1, measuring its cyclotron frequency, repeating with a single ion of type 2, and then going back to an ion of type 1. The precision was limited by fluctuations in the magnetic field while switching between the ions. It was therefore im-

portant to avoid doing anything that might correlate the field changes with the ion switching, which would lead to systematic errors not easily detectable from the data.

Loading one ion

The basic technique for making ions in ye olde days was similar in principle to what we use today. A small amount of neutral gas (~ 50 mT-cc) was introduced from the gas handling manifold and ionized in the trapping volume with an electron beam (~10 nA). Since the valves in the manifold were manually operated, this required the operator* to enter the magnet room, with the risk of accidentally moving something that would change the magnetic field slightly.

After the new ions were made, there remained the task of thinning the cloud to one and "killing" any ions of undesired species. This we achieved by applying offset potentials on the lower endcap electrode, which "dipped" the equilibrium position of the ions (i.e. the electrical center of the trap) towards this endcap. If some ions in the trapped cloud had larger amplitudes than others, these would get neutralized on the endcap and leave the trap. After removing the offset, we judged the number of ions left from the strength of the axial signal (directly proportional to the oscillating charge and hence the number of ions) and its width in frequency domain (inversely proportional to the damping time which decreases linearly with the number of ions).

Killing "bad" ions was a more involved process. When we were convinced there was only one good ion left, the above process of thinning was repeated but now the entire cloud was excited with white noise (since different ionic species have different axial frequencies) before dipping. Any excitation of the good ion was cooled on the detector. The white noise was produced around a center frequency using computer generated random numbers input into the amplitude modulation port of a frequency synthesizer. The speed of the output DAC limited us to about 50 kHz wide bands. Therefore, to cover the frequencies of all potential bad ions, the excitation process took 15 minutes covering a range of 30-800 kHz. Occasionally, after dipping, we found that the good ion was gone too. A turn around time of 20-30 minutes was therefore typical for loading the trap with a single good ion.

---

* graduate student

This meant that in a single night of data taking, lasting a few hours, we rarely got more than two switches between the species (i.e. a measurement sequence of 1-2-1). The drift in the magnetic field during the night could not be taken out very accurately and it was not possible to reduce our errors by averaging several measurements in one run.

Data processing

The axial signal from an excited ion in resonance with the detector is, to a very good approximation, given by a decaying sinusoid

$$y(t) = ae^{-\alpha t}\cos(\omega t + \phi) \tag{2-1}$$

This signal is characterized completely by its amplitude a, damping constant α, frequency ω, and initial phase ϕ. The damping constant depends on the real part of the detector impedance at the ion's frequency, and is known for any given ion as long as we can measure the frequency and Q of the detector (Eq. 1-13). However, in order to measure the cyclotron frequency, we have to estimate the frequency and phase from this signal.

In the previous incarnations of this experiment, the axial signal was first digitized by sampling for approximately one damping time (~ 4 s) and then the frequency and phase were estimated by performing a Fast Fourier Transform (FFT). The bin resolution for an FFT is given by the inverse of the total sampling time, and therefore was typically 250 mHz. In order to determine the frequency to higher precision, Eric Cornell [COR90] had implemented a scheme where the signal from the two peak bins was combined in an analytic manner to interpolate between the bin frequencies.

This technique has a problem when most of the signal in centered on one bin [KRB92]. The interpolation now heavily weights the neighbouring bin with its almost pure noise content to allow the frequency to be pulled away from the correct value. Similarly, the phase is also pulled towards the phase of the noise in the neighbouring bin. In the terminology of signal processing, the estimator would be called "biased", i.e. if the same signal were analyzed in the presence of different noise sets, the estimates would not necessarily have a mean given by the correct values.

This estimator not only gave much higher errors for the parameters than the signal to noise ratio warranted, the biased estimates also had non-Gaussian errors. Therefore standard error analysis techniques could not be applied to the data.

Measuring the cyclotron frequency

The method of measuring the cyclotron frequency developed by Robert Weisskoff and Eric Cornell is still the primary technique we use now (see Chapter 3 for details on this, and Chapter 4 to see a new technique for non-doublets). The frequency is measured by measuring the phase accumulated in the cyclotron mode in a given length of time. The phase is read out by applying a π-pulse to swap the cyclotron motion into the axial, and detecting the axial signal. Therefore, the above data analysis scheme implied a large error (about 25°) in reading the cyclotron phase.

This has two effects on the cyclotron frequency measurement. First, for an individual measurement with a given integration time, T, the precision is lower. Secondly, in order to unwrap the phase unambiguously, the value of T is progressively increased from small values. With the large phase error, the integration time could only be increased by a factor of 1.5 to 2. Both these factors combined to make the measurement time on each ion about 20 minutes long.

2 New Ion Making

When we started to try and improve the precision in the summer of 1990, we made several changes to our apparatus that are presented in detail in Kevin Boyce's thesis [BOY92]. In this section I will briefly discuss the changes that helped us to go from 2 to 20 switches in one night of data taking.

Automated gas handler

We completely rebuilt the gas handling manifold with welded fittings to improve its vacuum properties and reduce gas contamination. We use high purity stainless steel valves that are semiconductor manufacturing grade and now have pneumatic actuators on them. The air flow to the actuators is regulated by computer controlled solenoid valves (though there is a manual option). The computer uses a Baratron capacitance manometer to read the gas pressure in the injection chamber and also has control over the field emission voltage. This has allowed us to completely automate the ion making process, from evacuating the injection volume to introducing a small amount of gas while the field emitter is on, with the push of a button and without entering the magnet room.

Another improvement in our technique is to make the ions in a weak trap and adiabatically ramp the trap voltage so that the ions are "cooled" towards the trap center. When the ions are first made, some of them have large axial amplitudes which shifts them out of resonance with our detector (due to anharmonicities in the trapping potential). These ions therefore do not cool and are lost in the dipping process. With our adiabatic compression, the ions couple to the detector more efficiently and thereby cool rapidly. This improvement has reduced our gas load for making one or two *detectable* ions from 50 mTorr-cc to 10 mTorr-cc or less. This may prove to be vital when working with volatile species such as ^{3}He which do not cryo-pump and contaminate our vacuum at high gas loads.

New killing

Perhaps the most important improvement in our loading technique is the bad ion killing process. The basic idea of heating the bad ions with white noise remains the same but now, instead of computer generating the white noise in narrow bands, we use the noise output from the SRS signal generator. This produces almost flat Gaussian noise in a 0-10 MHz band. To prevent excitation of the good ion, we use a notch filter centered at the ion's resonance.

In practice, we find that we can excite the bad ions successfully using 2V (632 $\mu V/\sqrt{Hz}$) of noise power for 4 seconds. The residual excitation of the good ion is very little; nevertheless, we cool it on the detector for about one damping time before dipping the cloud. Our typical offset voltage on the lower endcap for dipping is 90% of the trapping voltage. The total 10 s that we spend before dipping is to be contrasted with the 15 minutes previously. If we accidentally lose the ion after the killing process, it only takes a few seconds to make a new batch again.

The ability of the signal generator to generate band-limited noise also helps us get rid of specific impurity ions quickly. For several of the measurements reported in this thesis, we worked with an ionic species that was not the main fragment of the ionization process. For instance, when we produce Ar^{++} from neutral Ar, the primary species is Ar^+. Similarly, for CD_3^+ from CD_4 or N^+ from N_2, we have to get rid of a large cloud of primary ions that are produced during ionization. The advantage in these cases is that we know the frequency of the unwanted fragment quite precisely. Therefore we pump a lot

of power selectively into these ions by modulating a carrier at their center frequency with noise. The 100 Hz wide noise is necessary since the frequencies of the ions shift as they increase in amplitude.

Improved electronics and computer control

The improvements in the electronics end of the experiment consist, among other things, of a new Macintosh IIci computer with LabView® data acquisition and control software (giving added computing power and the visual advantages of a Mac), a quieter RF SQUID with higher RF frequency of operation (increasing our signal to noise ratio), and a new ultra-stable voltage box.

The most attractive feature of the voltage box, apart from its low thermal drift coefficient, is that it has two identical but independent channels. The two voltages can be set once for the two species that we are working with and then do not have to be touched for the rest of the experiment. As we will see later, this also proved to be our downfall as we were accidentally setting the guard rings on the two channels differently. The two ions therefore had different C_4 shifts and a big advantage of working with a doublet was lost. Fortunately, we caught this error in our study of systematics through measurements on non-doublets.

The changes described in this section allow us to make a single, well-killed ion in a few minutes for most species. In the case of N_2^+, we could even teach the software to determine the number of ions from the power of the signal in the frequency domain. For other species, this was a judgement call best left to the operator, especially when we had to get rid of another fragment before seeing any signal. Still, for most of the measurements in this thesis, we were able to maintain an average of 15-20 switches per nightly run, usually lasting 4 hours.

Part of this success was due to a better data analysis technique that allowed us to make faster and more reliable cyclotron frequency measurements. With our greater computing power, we could implement the new algorithm in a few seconds even though it was slightly more computationally intensive. This is the improvement we consider next.

3 MAXIMUM LIKELIHOOD ESTIMATION

Maximum likelihood analysis is a standard signal processing technique* that can be adapted quite well to solve our problem of parameter estimation [KUT82]. The estimates are obtained by picking a parametric model for the data and performing a least squares fit to determine these parameters. In this section, we will see how this gives unbiased estimates with lower errors than our previous method. In addition, I will show that this technique is optimal since it approaches theoretical lower bounds for the uncertainty in the parameters (Cramer-Rao bounds).

The least squares solution

As mentioned before, the axial signal of the ion is a damped sinusoid when the coupling to the detector is weak (and the trap has no anharmonicities). The actual signal that we store in the computer is mixed down to a frequency of 30 Hz from the original 160 kHz. We use a low pass filter after the mixer to prevent serious aliasing of the noise from high frequencies, at least around the signal frequency. The signal is digitized by sampling at a rate f_{samp}. If f_{samp} is greater than twice the signal frequency, then it satisfies the Nyquist criterion and the signal can be completely reconstructed from the samples.

We can then model the data stream in the time domain as:

$$y_k = \left[a_1 \sin(\omega kh) + a_2 \cos(\omega kh)\right] e^{-\alpha kh} + w(kh) \tag{2-2}$$

where α is the damping time (which we know *a priori*, see Eq. 1-13), k is the index which runs from 0 to $N-1$, $h = 1/f_{samp}$ is the time step (so kh is the time at which the kth sample was taken), and w is Gaussian white noise. We can write this in matrix form:

$$\mathbf{Y} = \mathbf{SA} + \mathbf{W} \tag{2-3}$$

where $\mathbf{Y}$ is a column vector and

$$\mathbf{S} = \begin{pmatrix} 0 & 1 \\ e^{-\alpha h}\sin(\omega h) & e^{-\alpha h}\cos(\omega h) \\ \vdots & \vdots \\ e^{-(N-1)\alpha h}\sin\big((N-1)\omega h\big) & e^{-(N-1)\alpha h}\cos\big((N-1)\omega h\big) \end{pmatrix}, \quad \mathbf{A} = \begin{pmatrix} a_1 \\ a_2 \end{pmatrix}. \tag{2-4}$$

---

* For an excellent review of modern spectrum estimation techniques, see [KAM81].

We denote the estimated values of these parameters by a circumflex, *e.g.*

$$\hat{\mathbf{Y}} = \hat{\mathbf{S}}\hat{\mathbf{A}}, \tag{2-5}$$

so our problem is to find $\hat{\mathbf{S}}$ and $\hat{\mathbf{A}}$ which minimize the squared error

$$E = \sum_{k=0}^{N-1} |\hat{y}_k - y_k|^2 = \left|\hat{\mathbf{Y}} - \mathbf{Y}\right|^2. \tag{2-6}$$

Since we know α already, finding $\hat{\mathbf{S}}$ requires only finding a frequency estimate $\hat{\omega}$. Thus we are looking for three parameters: amplitude, phase, and frequency. For a given $\hat{\omega}$, $\hat{\mathbf{A}}$ is given by the standard least-squares solution [KUT82]

$$\hat{\mathbf{A}} = \left(\hat{\mathbf{S}}^{\mathrm{T}}\hat{\mathbf{S}}\right)^{-1}\hat{\mathbf{S}}^{\mathrm{T}}\mathbf{Y}. \tag{2-7}$$

Using this solution in Eq. 2-5, we find

$$\hat{\mathbf{Y}} = \hat{\mathbf{S}}\left(\hat{\mathbf{S}}^{\mathrm{T}}\hat{\mathbf{S}}\right)^{-1}\hat{\mathbf{S}}^{\mathrm{T}}\mathbf{Y} \tag{2-8}$$

so

$$\begin{aligned}\hat{\mathbf{Y}}^{\mathrm{T}}\hat{\mathbf{Y}} &= \mathbf{Y}^{\mathrm{T}}\hat{\mathbf{S}}\left(\left(\hat{\mathbf{S}}^{\mathrm{T}}\hat{\mathbf{S}}\right)^{-1}\right)^{\mathrm{T}}\hat{\mathbf{S}}^{\mathrm{T}}\,\hat{\mathbf{S}}\left(\hat{\mathbf{S}}^{\mathrm{T}}\hat{\mathbf{S}}\right)^{-1}\hat{\mathbf{S}}^{\mathrm{T}}\mathbf{Y} \\ &= \mathbf{Y}^{\mathrm{T}}\hat{\mathbf{S}}\left(\hat{\mathbf{S}}^{\mathrm{T}}\hat{\mathbf{S}}\right)^{-1}\hat{\mathbf{S}}^{\mathrm{T}}\mathbf{Y} \\ &= \mathbf{Y}^{\mathrm{T}}\hat{\mathbf{Y}}\,.\end{aligned} \tag{2-9}$$

We can now use Eqs. 2-9 and 2-6 to find the error. Since $\mathbf{Y}$ and $\hat{\mathbf{Y}}$ are just column vectors, we have

$$\begin{aligned}E &= \left(\hat{\mathbf{Y}} - \mathbf{Y}\right)^{\mathrm{T}}\left(\hat{\mathbf{Y}} - \mathbf{Y}\right) \\ &= \hat{\mathbf{Y}}^{\mathrm{T}}\hat{\mathbf{Y}} + \mathbf{Y}^{\mathrm{T}}\mathbf{Y} - 2\mathbf{Y}^{\mathrm{T}}\hat{\mathbf{Y}} \\ &= \mathbf{Y}^{\mathrm{T}}\mathbf{Y} - \mathbf{Y}^{\mathrm{T}}\hat{\mathbf{Y}}\,.\end{aligned} \tag{2-10}$$

Our three dimensional minimization problem thus reduces to a problem in one dimension as we want to minimize E with respect to $\hat{\omega}$. Since $\mathbf{Y}$ is fixed, and E and $\mathbf{Y}^{\mathrm{T}}\mathbf{Y} = |\mathbf{Y}|^2$ are both nonnegative, this is equivalent to maximizing the quantity

$$E_2 = \mathbf{Y}^{\mathrm{T}}\hat{\mathbf{Y}} = \mathbf{Y}^{\mathrm{T}}\hat{\mathbf{S}}\left(\hat{\mathbf{S}}^{\mathrm{T}}\hat{\mathbf{S}}\right)^{-1}\hat{\mathbf{S}}^{\mathrm{T}}\mathbf{Y}\,. \tag{2-11}$$

For a given guess of $\hat{\omega}$, the middle factor in the above expression is

$$\hat{\mathbf{S}}^{\mathrm{T}}\hat{\mathbf{S}} = \begin{pmatrix} \sum_{k=0}^{N-1} e^{-2\alpha kh}\sin^2(\hat{\omega}kh) & \sum_{k=0}^{N-1} e^{-2\alpha kh}\tfrac{1}{2}\sin(2\hat{\omega}kh) \\ \sum_{k=0}^{N-1} e^{-2\alpha kh}\tfrac{1}{2}\sin(2\hat{\omega}kh) & \sum_{k=0}^{N-1} e^{-2\alpha kh}\cos^2(\hat{\omega}kh) \end{pmatrix}. \tag{2-12}$$

We can simplify the terms of this matrix by considering the following successive cases.

No damping

We first assume that $\alpha = 0$. The off diagonal terms then represent the sum of regular samples of a sine wave and should average to 0, at least in the limit of infinite samples. Using an integral to estimate the sum, we find that they satisfy

$$\left|\sum_{k=0}^{N-1}\tfrac{1}{2}\sin(2\hat{\omega}kh)\right| \lesssim \frac{1}{2\hat{\omega}h} = \frac{f_{samp}}{2\hat{\omega}}, \tag{2-13}$$

which is about 0.6 for typical values of $f_{samp} = 250$ Hz and $\hat{\omega} \approx 200$. The diagonal elements satisfy

$$\left|\sum_{k=0}^{N-1}\sin^2(\hat{\omega}kh)\right| = \left|\tfrac{1}{2}\sum_{k=0}^{N-1}(1-\cos(2\hat{\omega}kh))\right| \lesssim \frac{N}{2} + \frac{f_{samp}}{2\hat{\omega}}. \tag{2-14}$$

The second term is again about 0.6, and we typically use $N = 1024$, so we can safely make the approximation

$$\hat{\mathbf{S}}^{\mathrm{T}}\hat{\mathbf{S}} = \frac{N}{2}\begin{pmatrix} 1 & 0 \\ 0 & 1 \end{pmatrix}, \tag{2-15}$$

and Eq. 2-11 becomes

$$E_2 = \frac{2}{N}\mathbf{Y}^{\mathrm{T}}\hat{\mathbf{S}}\hat{\mathbf{S}}^{\mathrm{T}}\mathbf{Y} = \frac{2}{N}\left|\hat{\mathbf{S}}^{\mathrm{T}}\mathbf{Y}\right|^2. \tag{2-16}$$

Therefore, the matrix whose norm we need to maximize is given by

$$\hat{\mathbf{S}}^{\mathrm{T}}\mathbf{Y} = \begin{pmatrix} \sum_{k=0}^{N-1} y_k \sin(\hat{\omega}kh) \\ \sum_{k=0}^{N-1} y_k \cos(\hat{\omega}kh) \end{pmatrix}, \tag{2-17}$$

which is just the Digital or Discrete-Time Fourier Transform of our data sample at $\hat{\omega}$ (the DTFT is discrete in time, but continuous in frequency). Hence, the frequency estimate for the case of no damping is given by the frequency at which the DTFT has maximum amplitude.

Actually this result is not very surprising. A signal with no damping is a single tone with zero linewidth. If there are no aliasing problems, the tone can be reconstructed from the sampled data. The only width in frequency domain it gets is because of the finiteness of the data set. But this gives rise to a symmetric sinc^2 broadening and the Fourier power is spread symmetrically around the correct center frequency.

Taking a simple FFT of the data, as we were doing before, gives the digital Fourier transform but with one significant difference, the transform is only calculated in discrete frequency bins. Therefore, an interpolation between the bins was necessary. One way to improve the "resolution" or decrease the bin spacing is to zero pad the data, i.e. append any number of 0's to the data set, before taking the FFT. Since we are adding no new information but just taking the FFT with a larger number of points, this is an effective way of interpolation. Actually, we use this trick when looking at the signal in real time to get a smoother frequency spectrum. This allows us both to better center the ion on the detector and more easily determine if there is more than one ion. If our signal were truly undamped, we could actually estimate the parameters with this technique except that it is computationally inefficient to perform FFT's with many more points. This is because the FFT calculates the entire spectrum with closer bin spacing while we are only interested in higher resolution around the signal frequency.

With damping

Let us now return to Eq. 2-12 and include the effects of damping. We then have for the off-diagonal terms

$$\sum_{k=0}^{N-1} e^{-2\alpha kh} \frac{1}{2}\sin(2\hat{\omega}kh). \tag{2-18}$$

Again, we suspect that this should average to 0 if the amplitude is not decaying "too rapidly" in one cycle. Let us check our intuition by approximating the sum with an integral as before:

$$\int_0^\infty e^{-\alpha t}\sin(\hat{\omega}t)dt = \frac{\hat{\omega}}{\alpha^2+\hat{\omega}^2} \approx \frac{1}{\hat{\omega}} \quad \text{for } \hat{\omega} >> \alpha \ , \tag{2-19}$$

which quantifies our condition "not too rapidly". This gives

$$\left|\sum_{k=0}^{N-1} e^{-2\alpha kh}\tfrac{1}{2}\sin(2\hat{\omega}kh)\right| \lesssim \frac{1}{4\hat{\omega}h} \ , \tag{2-20}$$

which is half the maximum value from the undamped formula Eq. 2-13, so we're in good shape. Also, the cosine terms from the diagonal elements (as in Eq. 2-14) are even smaller, since the integral for them works out to $\alpha/\omega^2 \approx 10^{-5}$. Thus we can simply take the exponential term out front, so that

$$\hat{\mathbf{S}}^{\mathrm{T}}\hat{\mathbf{S}} = C\begin{pmatrix} 1 & 0 \\ 0 & 1 \end{pmatrix} \tag{2-21}$$

where

$$C = \frac{1}{2}\sum_{k=0}^{N-1} e^{-2\alpha kh} . \tag{2-22}$$

Therefore, in the presence of damping, the quantity we wish to maximize is similar to Eq. 2-16 except that the error is now given as (*c.f.* Eq. 2-17)

$$E_2 \propto \left(\sum_{k=0}^{N-1} y_k e^{-\alpha kh}\sin(\omega kh)\right)^2 + \left(\sum_{k=0}^{N-1} y_k e^{-\alpha kh}\cos(\omega kh)\right)^2 , \tag{2-23}$$

which is just the magnitude squared of the DTFT of $y_k e^{-\alpha kh}$. This rather simple result tells us that, instead of taking the digital Fourier transform of the data, we should take something closer to the digital Laplace transform in the case of a damped sinusoid. Again, the result makes intuitive sense if we realize that our signal, instead of being a single tone in Fourier space, is actually a delta function in complex ω space.

Our procedure for parameter estimation is therefore as follows. We calculate the Laplace transform of the data set by multiplying it by $e^{-\alpha kh}$ and then taking its digital Fourier transform. The frequency which maximizes the amplitude of the transform is then the best estimate for the signal frequency. We use this frequency in Eq. 2-7 to find the best fit vector $\hat{\mathbf{A}}$, which gives the estimates for the amplitude and phase.

We have actually implemented the peak search routine using the "Brent" algorithm [PFT88], which is a standard triangular algorithm for finding an extremum when it can be

bracketed. We know the ion's frequency to better than 0.5 Hz by just taking the FFT of the data. Brent's method then zeroes in on the peak frequency in a 0.5 Hz band around this first guess.

Cramer-Rao Bounds

While the maximum likelihood technique presented above provides a convenient and fast method for estimating the ion's parameters, it is important to determine whether there are other techniques that might perform better. One way to achieve this is to find theoretical lower bounds on the variance in the estimated parameters given our signal to noise ratio. The Cramer-Rao (C-R) bounds give exactly this, assuming that the estimator is unbiased. The following detailed analysis for finding the C-R bounds [see *e.g.* RIB74] is presented to enable future adaptations of the estimation technique to signals from two ions.

Consider, as before, a data sample in the time domain

$$y_k = a e^{-\alpha t_k} \cos(\omega t_k + \phi) + w(t_k) \tag{2-24}$$

where ω, a, and ϕ are the unknown parameters, and w is white noise that is Gaussian distributed with 0 mean and variance σ^2. In the presence of the noise, the parameters have a probability distribution such that the joint probability density function (PDF) for the data set $\mathbf{Y}$ and the set of unknown parameters $\boldsymbol{\Theta}$ is

$$\mathrm{f}(\mathbf{Y},\boldsymbol{\Theta}) = \frac{1}{\left(2\pi\sigma^2\right)^N} \exp\left[-\frac{1}{2\sigma^2}\sum_{k=0}^{N-1}\left(y_k - \mu_k\right)^2\right] \tag{2-25}$$

where $\boldsymbol{\Theta} = \begin{pmatrix}\omega & a & \phi\end{pmatrix}^{\mathrm{T}}$ and $\mu_k = a e^{-\alpha t_k}\cos(\omega t_k + \phi)$. For an unbiased estimator, the mean signal μ_k should have the correct parameters.

The C-R bounds are derived from the Fisher information matrix, $\mathbf{J}$, which is defined, not surprisingly, by the logarithm of the PDF and taking partial derivatives with respect to each parameter. Thus,

$$J_{ij} = \mathrm{E}\left[H_{\theta_i} H_{\theta_j}\right] = -\mathrm{E}\left[H_{\theta_i\theta_j}\right] \tag{2-26}$$

where E[ ] denotes expectation and

$$H_{\theta_i} = \frac{\partial}{\partial\theta_i}\log[\mathrm{f}(\mathbf{Y},\boldsymbol{\Theta})]. \tag{2-27}$$

The lower bound on the variance in each estimated parameter is then given by $\mathrm{var}\left[\hat{\theta}_i\right] \geq \left(\mathbf{J}^{-1}\right)_{ii}$. We can derive the elements of $\mathbf{J}$ as follows:

$$H_{\theta_i} = -\frac{1}{2\sigma^2}\sum_{k=0}^{N-1} 2(y_k - \mu_k)\left(-\frac{\partial \mu_k}{\partial \theta_i}\right),$$
$$\text{and } H_{\theta_i\theta_j} = -\frac{1}{\sigma^2}\sum_{k=0}^{N-1}\frac{\partial \mu_k}{\partial \theta_i}\frac{\partial \mu_k}{\partial \theta_i} = -J_{ij} \tag{2-28}$$

where the expectation becomes unnecessary since the elements are independent of y_k. Partial differentiation then yields

$$\frac{\partial \mu_k}{\partial \theta_1} = -at_k e^{-\alpha t_k}\sin(\omega t_k + \phi),$$
$$\frac{\partial \mu_k}{\partial \theta_2} = e^{-\alpha t_k}\cos(\omega t_k + \phi), \tag{2-29}$$
$$\text{and } \frac{\partial \mu_k}{\partial \theta_3} = -ae^{-\alpha t_k}\sin(\omega t_k + \phi),$$

from which we obtain $\mathbf{J}$ as

$$\mathbf{J} = \frac{1}{\sigma^2}\sum_{k=0}^{N-1}\begin{pmatrix} a^2 t_k^2 e^{-2\alpha t_k}\sin^2() & -at_k e^{-2\alpha t_k}\sin()\cos() & a^2 t_k e^{-2\alpha t_k}\sin^2() \\ -at_k e^{-2\alpha t_k}\sin()\cos() & e^{-2\alpha t_k}\cos^2() & -ae^{-2\alpha t_k}\sin()\cos() \\ a^2 t_k e^{-2\alpha t_k}\sin^2() & -ae^{-2\alpha t_k}\sin()\cos() & a^2 e^{-2\alpha t_k}\sin^2() \end{pmatrix}. \tag{2-30}$$

When this matrix is evaluated for a given number of data points N and inverted, its diagonal elements give the C-R lower bounds on estimation error.

The relevant quantities for our case are obtained by setting ω, a and α appropriate for the ion's signal and σ^2 appropriate for the noise level. We can write approximate expressions by performing the summations using integrals as before, but the expressions are quite complicated and do not lead to any new insights. Rather, I have evaluated the matrix numerically for different values of N and plotted the results for the frequency and phase estimates in Fig. 2-1.

Since the ion's signal is decaying exponentially, we would expect that after a certain length of time there is minimal improvement in the estimates and all we are sampling is the noise. This is borne out by the results of our analysis. The figure shows that, as $N \to \infty$, the C-R bounds reach a limiting value. Indeed, this is useful in determining the optimal length of time for which we should take data. From the figure, we see that the

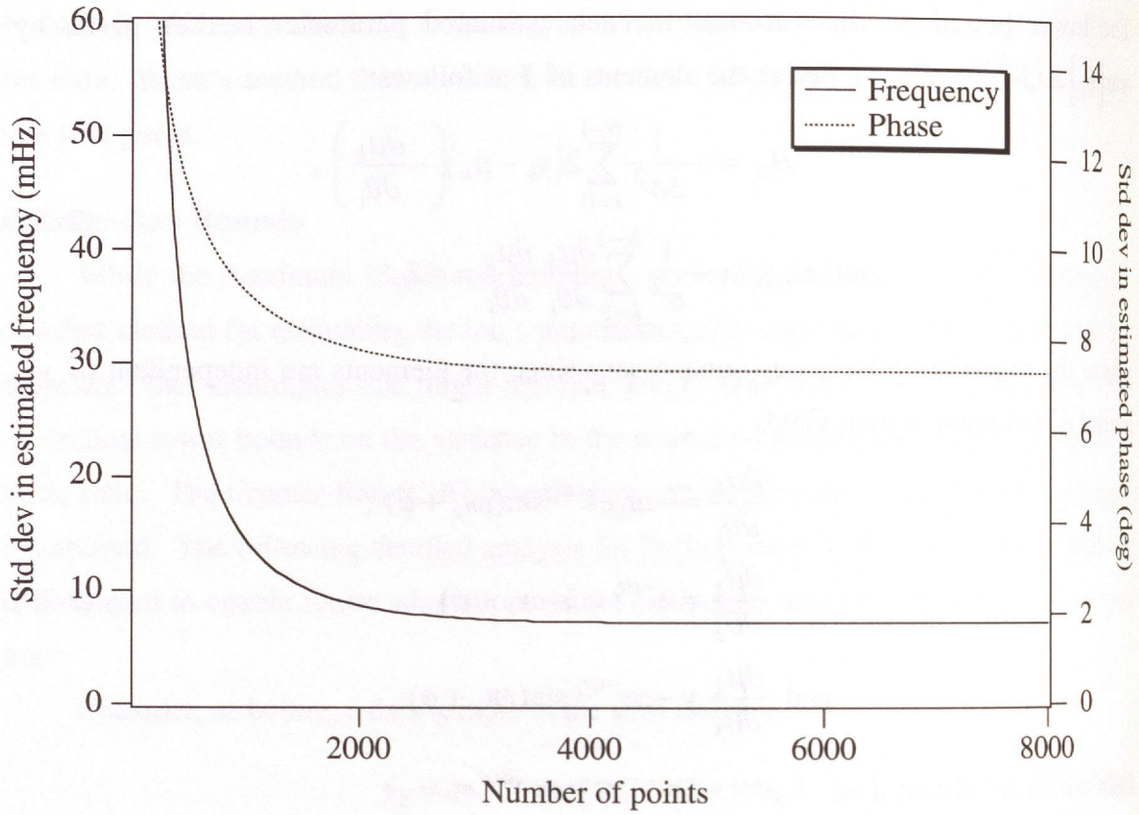

Fig. 2-1 Cramer-Rao bounds for estimation error. The lower bounds on the standard deviation in the estimated frequency and phase are shown as a function of the number of data points, and hence the total sampling time. The damping time was 4 s, the sampling rate was 250 Hz, and the signal to noise was adjusted for our current levels.

uncertainties in the parameters almost reach their limiting values after two damping times, and this has been the data length for most of the results presented in this thesis. For our previous FFT technique, we were sampling for just one damping time since that seemed to give optimal results.

Results and analysis

In Table 2-1, I present a comparison of the different analysis techniques. The standard deviation in the frequency, amplitude and phase are presented from 400 sets of data generated for the same signal parameters. From the results we see that maximizing the Fourier transform gives up to 3 times larger error than maximum likelihood but there is no serious bias in the estimates. Recall that our old technique did essentially this but with a biased scheme for interpolating between bin frequencies. Thus the error would have been larger and non-Gaussian.

Table 2-1. Comparison of different analysis schemes. The average bias and standard deviations in the frequency, amplitude and phase estimates obtained from: (i) maximization of the Fourier transform, (ii) maximum likelihood analysis with the approximation that it is the Laplace transform, and (iii) full maximum likelihood analysis with minimization of the squared error. The uncertainties are obtained from an analysis of 400 computer generated data sets each containing 1024 points. The sampling rate was 250 Hz and the ion frequency 30 Hz. All the data sets had the same signal parameters but different noise simulations. The Cramer-Rao bounds are also presented for these conditions.

Analysis Technique	Error ± Std dev.		
	Freq (mHz)	Amp (arb)	Phase (deg)
Fourier transform	- 3.3 ± 30	-1.7 ± 80	-1.2 ± 11
Maximum likelihood (approx.)	0.3 ± 9	4.9 ± 61	-0.2 ± 7
Maximum likelihood (exact)	0.3 ± 9	4.9 ± 61	-0.2 ± 7
Cramer-Rao bounds	0.0 ± 8	0.0 ± 60	0.0 ± 7

With the approximations we made earlier, maximum likelihood analysis was found to be equivalent to maximizing the Laplace transform. The table shows the validity of these approximations as there is very little difference between this and actually minimizing the squared error. This technique also gives results close to the C-R bounds and therefore forms an ideal analysis tool.

Before finishing this section, I will consider the effects of some of our assumptions being invalid. The analysis above assumed that we know the value of α exactly. In reality, we only know the damping time of the ion approximately and it can change over the course of a run if the Q of our superconducting circuit varies (typically by about 10% over the night). We already know from the table what happens if we assume that the damping time is infinite (or $\alpha = 0$) - our errors increase significantly. Therefore, we get a larger error if we underestimate α, with a limiting factor of three increase as we approach $\alpha = 0$. There is a similar increase in the error if we overestimate α slightly. Of course, in the limit that we assume α is infinite, we get infinite errors. In practice, our knowledge of α has less than 20% uncertainty and our error is close to being optimal.

Another potential problem arises because we modeled the signal as a damped sinusoid. This assumption is not entirely valid because, as with any real oscillator, the ion's

motion has anharmonic components. However, one would expect this not to cause a serious problem in the frequency estimate since the frequency is constrained in our analysis by points at long times (with correspondingly small amplitude) when the effect of higher order terms is truly negligible. A similar argument holds for the phase of *this frequency component*. But the initial phase of the *ion's motion* may be off since the frequency of the ion is chirping as it rings down. The phase of the zero-amplitude frequency component is the initial phase of the ion's motion added to any integrated phase built up from the chirped part.

The chirped frequency can be written as

$$\begin{aligned} \omega(t) &= \omega_0 + \alpha_2 a^2(t) \\ &= \omega_0 + \alpha_2 a^2 \exp(-2\alpha t) \end{aligned} \tag{2-31}$$

where α_2 is a second order correction to the frequency. The phase is then

$$\begin{aligned} \phi(t) &= \phi_0 + \int_0^t \omega(t')dt' \\ &= \phi_0 + \omega_0 t + \alpha_2 a^2 \int_0^t e^{-2\alpha t'}\, dt' \,. \end{aligned} \tag{2-32}$$

Therefore, at long times, the estimated initial phase (of the ω_0 component) is

$$\phi_0(\text{est}) = \phi_0 + \alpha_2 a^2 \int_0^\infty e^{-2\alpha t'} dt' = \phi_0 + \frac{\alpha_2 a^2}{2\alpha} \,. \tag{2-33}$$

This offset in the initial phase is not a problem for our pulse and phase measurement technique where such phase shifts are eliminated when determining the frequency from the slope. However, since the estimated phase is now also amplitude dependent, thermal fluctuations in the amplitude show up as increased phase noise (in practice, this is only about 5° and adds in quadrature with the estimation noise).

The above expectations for the effects of a small anharmonicity term in the trapping potential are confirmed with computer simulated data. The lowest order electrostatic anharmonicity in the trap is usually designated by the dimensionless quantity C_4 (see Chapter 3, § 4). The second order correction introduced above is related to C_4 as $\alpha_2 = 3\omega_0 C_4 / 4d^2$. In Fig. 2-2, I show the results of the effect of anharmonicity from one set of computer simulations. The errors in the estimated frequency and phase are plotted as a function of C_4. The data length was 8 seconds while the damping time was 4

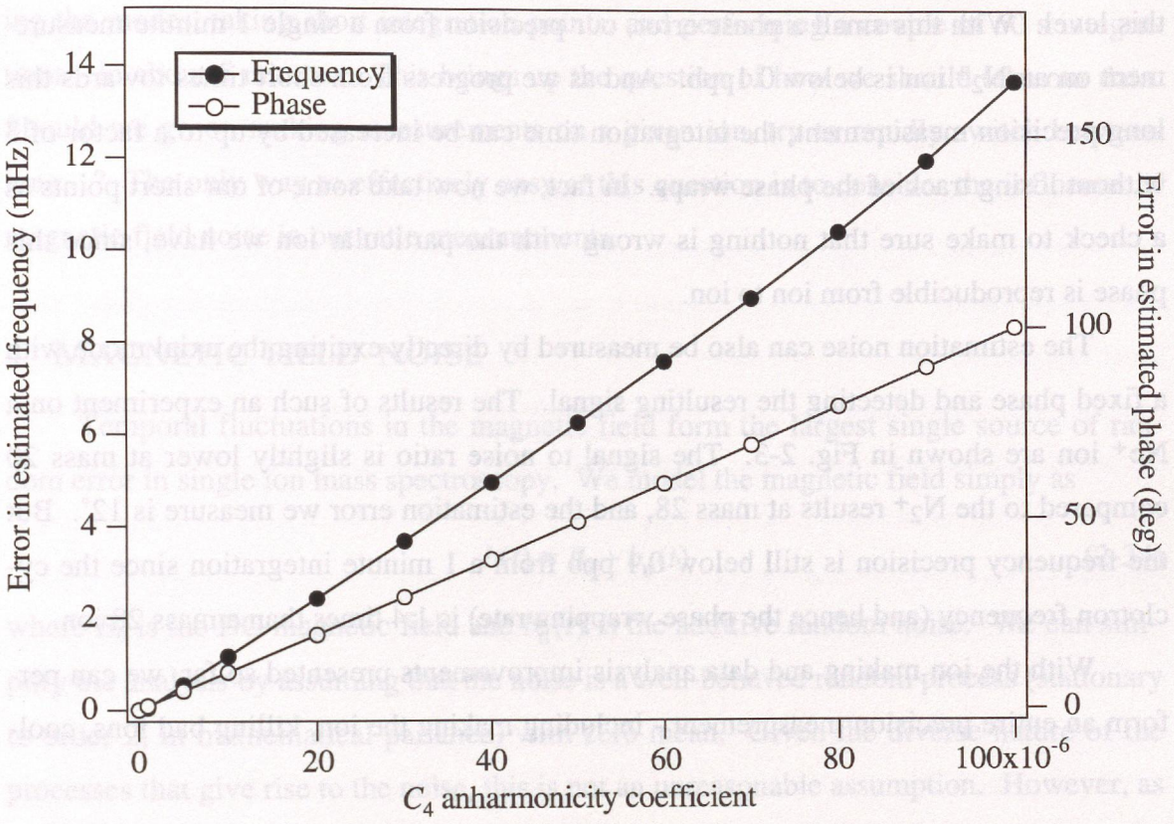

Fig. 2-2 The effect of small anharmonicity on estimated parameters. The errors in the estimated frequency and phase are shown as a function of C_4 (see text). The data consisted of 2048 points sampled at 250 Hz with a damping time of 4 s.

seconds. The phase error remains linear with C_4 as expected from the simple expression in Eq. 2-33, but is a factor of smaller in magnitude. The frequency error is not zero but indeed much smaller than the maximum shift $\alpha_2 a^2$.

Of course, the acid test of our new analysis scheme comes from working on real signals. We have studied the estimation error by exciting the cyclotron mode of a single N_2^+ ion with a fixed phase and applying a π-pulse after 75 ms. The time during which the cyclotron motion evolves freely is now so short that even with a part in 10^8 change in the magnetic field, there should only be a 1.3° phase change (at 4.6 MHz). The RMS fluctuations in the field during the day are usually below this. Therefore, the detected phase should be a constant except for estimation error.

From this we found that the phase error was about 10° and the frequency error was 15 mHz. The frequency error was slightly larger than we expected and we attribute at least some of it to actual changes in the trap voltage since our voltage box is not stable at

this level. With this small a phase error, our precision from a single 1 minute measurement on an N_2^+ ion is below 0.1ppb. And as we progress from short times towards this long precision measurement, the integration time can be increased by up to a factor of 3 without losing track of the phase wraps. In fact, we now take some of our short points as a check to make sure that nothing is wrong with the particular ion we have, since this phase is reproducible from ion to ion.

The estimation noise can also be measured by directly exciting the axial mode with a fixed phase and detecting the resulting signal. The results of such an experiment on a Ne^+ ion are shown in Fig. 2-3. The signal to noise ratio is slightly lower at mass 20 compared to the N_2^+ results at mass 28, and the estimation error we measure is 12°. But the frequency precision is still below 0.1 ppb from a 1 minute integration since the cyclotron frequency (and hence the phase wrapping rate) is 1.4 times than a mass 28 ion.

With the ion making and data analysis improvements presented so far, we can perform an entire precision measurement - including making the ion, killing bad ions, cool-

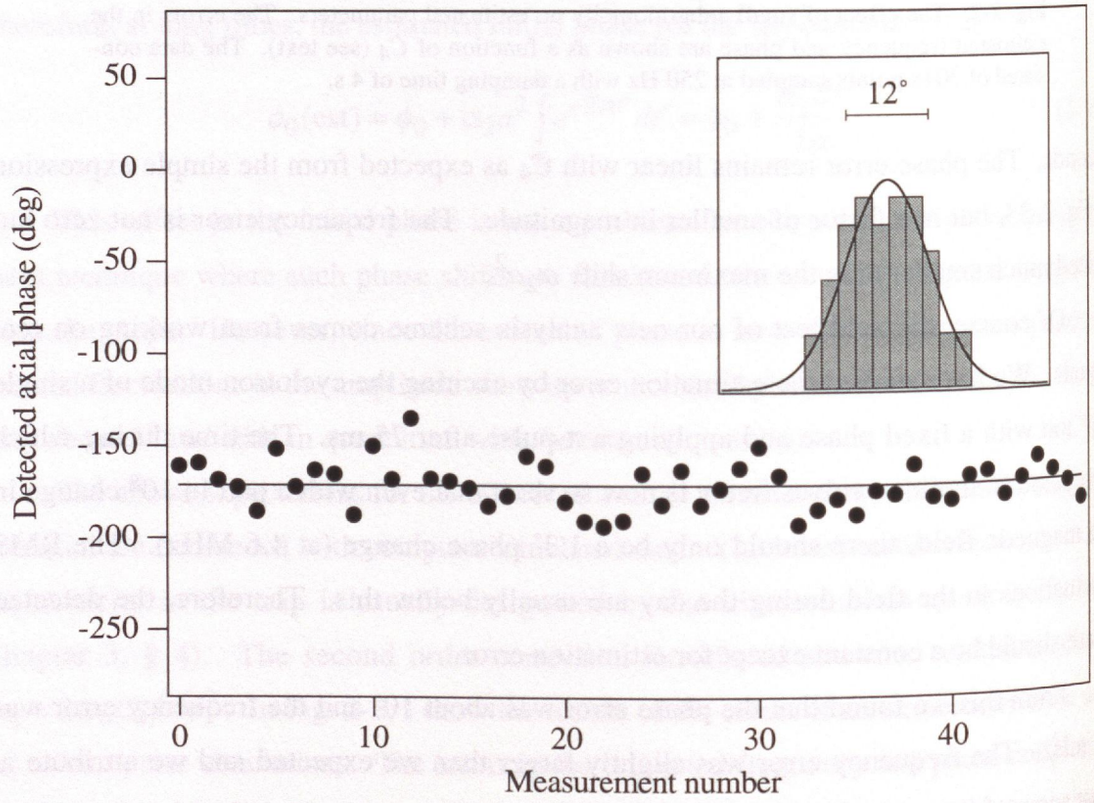

Fig. 2-3 Phase estimation noise for Ne^+. The axial phase is measured after exciting the cyclotron mode with a fixed phase and applying a π-pulse after 100 ms.

ing the modes, taking short integration points, and performing a couple of 50 s integrations - in about 5 minutes. This brings up the question of how we should take our data. Should we go on making measurements on a given ion, try to rapidly switch between ions...? The only way to effectively answer this question is to consider the influence of magnetic field noise in our ratio measurements.

4 MAGNETIC FIELD NOISE

Temporal fluctuations in the magnetic field form the largest single source of random error in single ion mass spectroscopy. We model the magnetic field simply as

$$b(t) = B_0 + b_n(t) \tag{2-34}$$

where B_0 is the DC magnetic field and $b_n(t)$ is the additive random noise. We can simplify the analysis by assuming that the noise is a well-behaved random process (stationary to order 2, in mathematical parlance) with zero mean. Given the diverse nature of the processes that give rise to the noise, this is not an unreasonable assumption. However, as we will see later, the correlation time for some of the low frequency Fourier components is longer than the time scale of the experiment. These then appear as slow drifts of the magnetic field over the duration of the experiment. Finally, over really long time scales, there is creep in the magnetic field due to relaxation of the superconducting coils in the magnet. However, such steady changes do not show up over the time scale of a nightly run.

In practice, it is difficult to determine the power spectral density of this noise, $B_n(f)$, especially at low frequencies. But we can go a long way towards understanding the variance in our data by assuming two common spectral forms for $B_n(f)$ - white and $1/f$. The problem we therefore want to analyze is that, given a certain form for $B_n(f)$, what is the variance that appears in our final mass ratio data. This would help in optimizing the measurement process for best results.

In order to do this, we need to represent the measurement process as a linear filter with transfer function $H(f)$. We can consider our entire measurement process as a measurement of the magnetic field (rather than the mass ratio) and ask the equivalent question - what is the variance in the magnetic field at the output of the process? Then,

$$\mathrm{E}\left[B^2\right] = \mathrm{var}(B) = \int_{-\infty}^{\infty} B(f)|\mathrm{H}(f)|^2 df \tag{2-35}$$

We will limit our discussion to the case of doublets, where the mass ratio measurement can be equivalently thought of as a mass difference measurement.

To write the equivalent transfer function, consider how we perform a mass comparison measurement. We first get down to a single ion of type 1, measure the phase after short integration times (to prevent errors of 2π when we unwrap the phase), and finally integrate the cyclotron phase for a time T which sets the precision (in conjunction with the phase estimation error, which we will not include explicitly in our present analysis). We then repeat the whole process with an ion of type 2. If the total time for a single measurement is t_0, from introducing the gas to dumping the trap, t_0-T represents a dead time t_d which we can hope to minimize as much as possible. But given a certain dead time, we want to find the optimal values of T and the number of measurements (in a single night experiment of total quiet magnetic time t_e) in order to minimize the error. It must be noted parenthetically that the dead time is not totally independent of T since the number of short integration time measurements to be made depends on the total phase that needs to be unwrapped.

Transfer Function

When we measure the cyclotron frequency of an ion of mass m by measuring the accumulated phase over a time T, we are effectively taking a time average of the B field:

$$\omega_c = \frac{1}{T}\int_{t-T}^{t} \frac{eb(\tau)}{mc} d\tau = \frac{e}{mc}\left[\frac{1}{T}\int_{t-T}^{t} b(\tau)d\tau\right] = \frac{e\overline{B}}{mc}. \tag{2-36}$$

The integration for time T can be represented by a filter with impulse response given by a rectangular function of length T,

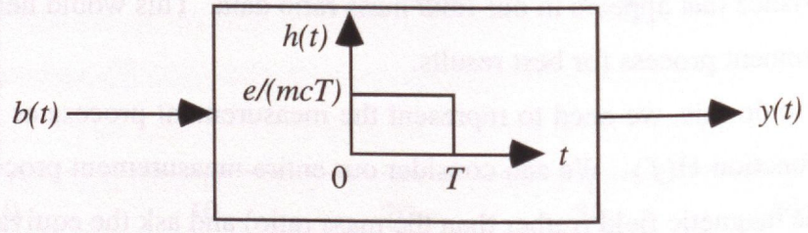

$$y(t) = \int_{-\infty}^{\infty} b(\tau)\mathrm{h}(t-\tau)d\tau = \frac{e}{mcT}\int_{t-T}^{t} b(\tau)d\tau = \frac{e\overline{B}}{mc}. \tag{2-37}$$

Therefore one mass *difference* measurement on two ions would be represented by a filter with response

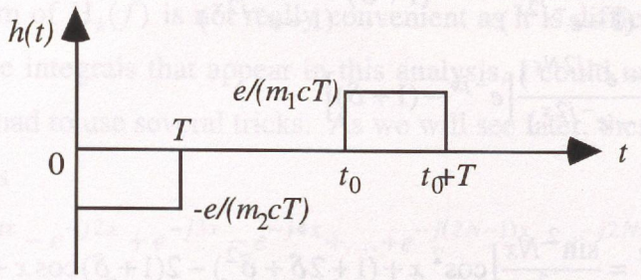

$$y(t) = -\frac{e}{m_2 cT}\int_{t-T}^{t} b(\tau)d\tau + \frac{e}{m_1 cT}\int_{t-t_0-T}^{t-t_0} b(\tau)d\tau = \omega_{c1} - \omega_{c2}. \tag{2-38}$$

We can simplify the notation by normalizing the cyclotron frequency difference to ω_{c1} and calling it δ, i.e. $\omega_{c2} = \omega_{c1}(1+\delta)$. Then we can suppress the constant $e/m_1 c$ from the transfer function.

In this notation we generalize this to N sets of measurements in the following manner.

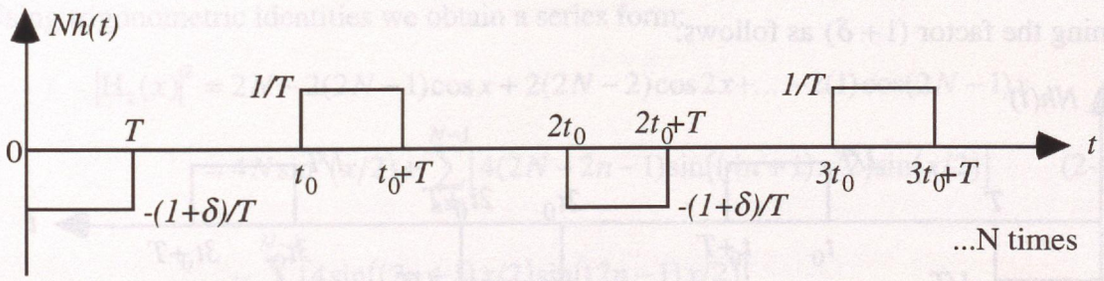

Since the various boxes in the figure just represent time shifted versions of the single rectangular function, the transfer function for N measurements is

$$\begin{aligned} \mathrm{H}(f) &= \frac{1}{N}\mathrm{H}_1(f)\sum_{n=1}^{N}\left[-(1+\delta)e^{-j2\pi(2n-2)ft_0} + e^{-j2\pi(2n-1)ft_0}\right] \\ &\equiv \frac{1}{N}\mathrm{H}_1(f)\mathrm{H}_2(f) \end{aligned} \tag{2-39}$$

where

$$\mathrm{H}_1(f) = e^{-j\pi fT}\frac{\sin(\pi fT)}{\pi fT} \tag{2-40}$$

is the Fourier transform of the rectangular function from 0 to T with amplitude $\frac{1}{T}$. Let $2\pi ft_0 = x$. Then,

$$H_2(x) = e^{-jx} + e^{-j3x} + \ldots + e^{-j(2N-1)x} - (1+\delta)\left[1 + e^{-j2x} + \ldots + e^{-j(2N-2)x}\right]$$
$$= \frac{e^{-jx}(1-e^{-j2Nx})}{(1-e^{-j2x})} - (1+\delta)\frac{(1-e^{-j2Nx})}{(1-e^{-j2x})} \qquad (2\text{-}41)$$
$$= \frac{(1-e^{-j2Nx})}{(1-e^{-j2x})}\left[e^{-jx} - (1+\delta)\right]$$

so that

$$|H_2(x)|^2 = \frac{\sin^2 Nx}{\sin^2 x}\left[\cos^2 x + (1+2\delta+\delta^2) - 2(1+\delta)\cos x + \sin^2 x\right]$$
$$= \frac{\sin^2 Nx}{\sin^2 x}\left[2(1+\delta) + \delta^2 - 2(1+\delta)\cos x\right]$$
$$\approx \frac{\sin^2 Nx}{\sin^2 x} 4(1+\delta)\sin^2(x/2), \qquad \text{if } \delta^2 << \delta << 1 \qquad (2\text{-}42)$$
$$= \frac{\sin^2 Nx}{\cos^2(x/2)}(1+\delta) .$$

The approximation $\delta^2 << \delta << 1$ is valid for mass doublets which typically have δ below 10^{-3}. The above expression allows us to redefine the impulse response after subsuming the factor $(1+\delta)$ as follows:

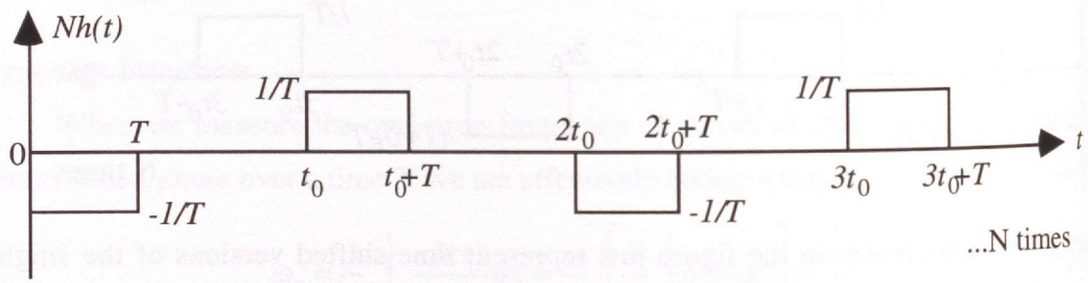

$$H_2(x) = -1 + e^{-jx} - e^{-j2x} + e^{-j3x} - \ldots - e^{-j(2N-2)x} + e^{-j(2N-1)x}$$
$$= \frac{-1(1-e^{-j2Nx})}{(1+e^{-jx})} = -\frac{e^{-jNx} j\sin Nx}{e^{-jx/2}\cos(x/2)} \qquad (2\text{-}43)$$

We obtain the same transfer function as in Eq. 2-42,

$$|H_2(x)|^2 = \frac{\sin^2 Nx}{\cos^2(x/2)}, \qquad (2\text{-}44)$$

without the factor $(1+\delta)$, which, for the purposes of this analysis, is just a scale factor (while in reality it is the quantity we are actually trying to measure). Notice that the

transfer function has effectively become the difference in the average magnetic field between successive measurements.

The above form of $H_2(f)$ is not really convenient as it is difficult to integrate. In fact, for many of the integrals that appear in this analysis, I could not find solutions in standard tables and had to use several tricks. As we will see later, these are facilitated by rewriting Eq. 2-43 as

$$\begin{aligned} -e^{jx}H_2(x) &= e^{-jx} - e^{-j2x} + e^{-j3x} - e^{-j4x} + \ldots + e^{-j(2N-1)x} - e^{-j2Nx} \\ &= \cos x - \cos 2x + \cos 3x - \cos 4x + \ldots + \cos(2N-1)x - \cos 2Nx \\ &\quad - j[\sin x - \sin 2x + \sin 3x - \sin 4x + \ldots + \sin(2N-1)x - \sin 2Nx] \end{aligned} \tag{2-45}$$

so that

$$\begin{aligned} |H_2(x)|^2 &= \cos^2 x + \cos^2 2x + \cos^2 3x + \ldots + \cos^2(2N-1)x + \cos^2 2Nx \\ &\quad - 2\cos x\cos 2x + \ldots + 2\cos x\cos(2N-1)x - 2\cos x\cos 2Nx \\ &\quad \vdots \\ &\quad - 2\cos(2N-1)x\cos 2Nx \\ &\quad + \text{corresponding sin terms} \end{aligned} \tag{2-46}$$

Using trigonometric identities we obtain a series form:

$$\begin{aligned} |H_2(x)|^2 &= 2N - 2(2N-1)\cos x + 2(2N-2)\cos 2x + \ldots - 2(1)\cos(2N-1)x \\ &= 4N\sin^2(x/2) + \sum_{n=1}^{N-1}\left[4(2N-2n-1)\sin\left((4n+1)x/2\right)\sin(x/2)\right] \\ &\quad - \sum_{n=1}^{N-1}\left[4\sin\left((2n+1)x/2\right)\sin\left((2n-1)x/2\right)\right] \end{aligned} \tag{2-47}$$

We use this result in Eq. 2-39 for the overall transfer function.

$$\begin{aligned} |H(f)|^2 &= \frac{1}{N^2}\frac{\sin^2(\pi fT)}{(\pi fT)^2}|H_2(f)|^2 \\ &= \frac{4}{N}\frac{\sin^2(\pi fT)}{(\pi fT)^2}\sin^2(\pi ft_0) \\ &\quad + \frac{4}{N^2}\sum_{n=1}^{N-1}\left[(2N-2n-1)\frac{\sin^2(\pi fT)}{(\pi fT)^2}\sin(4n+1)\pi ft_0\sin\pi ft_0\right] \\ &\quad - \frac{4}{N^2}\sum_{n=1}^{N-1}\left[\frac{\sin^2(\pi fT)}{(\pi fT)^2}\sin(2n+1)\pi ft_0\sin(2n-1)\pi ft_0\right] \end{aligned} \tag{2-48}$$

White noise

For our first analysis, we will assume that the spectrum of B field noise is white. Then $B(f)$ is just a constant, say A, so that,

$$\mathrm{var}(B) = \int_{-\infty}^{\infty} A|\mathrm{H}(f)|^2 df \tag{2-49}$$

which is a series of standard integrals of the form [GRR80]

$$\mathrm{I} = A\int_{-\infty}^{\infty} \frac{\sin^2(\pi f T)}{(\pi f T)^2}\sin(n\pi f t_0)\sin(m\pi f t_0)df \quad , n \geq m \geq 1 \text{ and } t_0 > T. \tag{2-50}$$

It has solutions given by

$$\int_0^{\infty} \frac{\sin^2(ax)}{x^2}\sin(bx)\sin(cx)dx = \frac{\pi}{16}\left(|b-2a-c|-|2a-b-c|+2c\right) \quad , [a,b,c>0].$$

Our integrals therefore reduce to

$$\begin{aligned}\mathrm{I} &= \frac{A}{(\pi T)^2}\frac{\pi}{8}\left(|n\pi t_0 - 2\pi T - m\pi t_0| - |2\pi T - n\pi t_0 - m\pi t_0| + 2m\pi t_0\right) \\ &= \begin{cases} 0 & \text{if } n-m \geq 2 \\ \dfrac{A}{2T} & \text{if } n-m = 0 \end{cases}\end{aligned} \tag{2-51}$$

which gives the result we are seeking:

$$\mathrm{var}(B) = \frac{2A}{NT} = \frac{2A(T+t_d)}{t_e T} = 2A\left(\frac{1}{t_e} + \frac{t_d}{t_e T}\right). \tag{2-52}$$

This expression is not unexpected if we realize that for white noise, by definition, the values of the B field are uncorrelated over all time scales. Therefore, the variance improves inversely with the product NT, which is the total time of precision measurement on each ion. It does not matter whether we perform a large number of measurements with short T or just a few with large T since the noise is completely uncorrelated. For a fixed t_e and t_d the above result shows that we want to increase the integration time as much as possible. Of course, after some point, it is not going to be worthwhile because noise sources that we have neglected for the present analysis will become important. These conclusions can be understood better from a surface plot of the variance as a function of T and t_d for a fixed t_e, shown in Fig. 2-4.

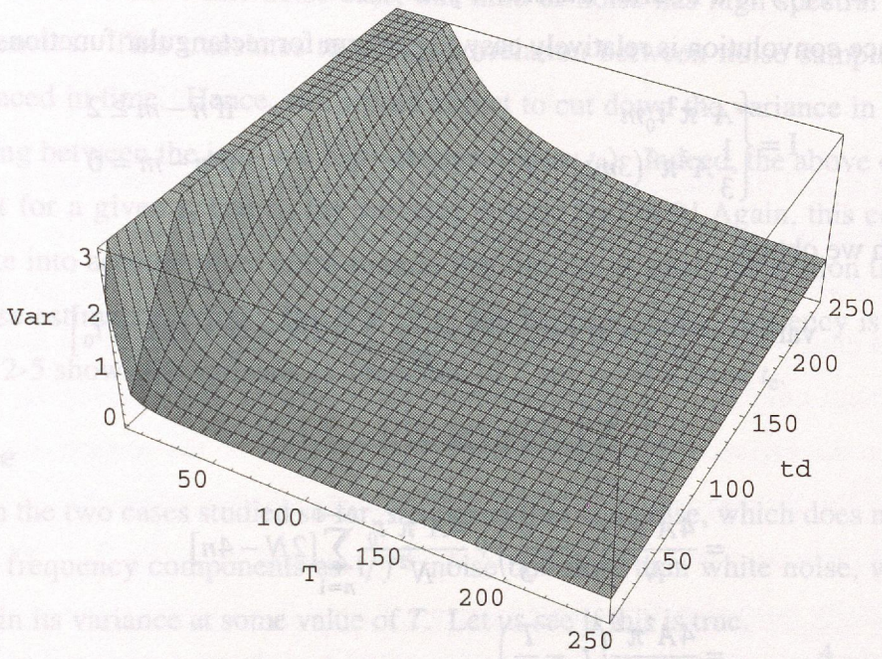

Fig. 2-4 Surface plot of the variance for white noise. The variance (arbitrarily normalized) is shown as a function of the integration time and dead time assuming the total time for the experiment remains a constant.

$1/f^2$ Noise

Before we analyze $1/f$ noise, we will consider the mathematically simpler case of $1/f^2$ noise. This should enable us to qualitatively understand the behaviour for noise spectra with a high density of low frequency components. For this case, $B(f)=\frac{A^2}{f^2}$. Now we need to evaluate integrals of the form,

$$\mathrm{I}=A^2\pi^2{t_0}^2\int_{-\infty}^{\infty}\frac{\sin^2(\pi fT)}{(\pi fT)^2}\frac{\sin(n\pi ft_0)}{(\pi ft_0)}\frac{\sin(m\pi ft_0)}{(\pi ft_0)}df \quad , n\geq m\geq 1 \text{ and } t_0>T. \qquad (2\text{-}53)$$

These integrals are not found in standard tables and I have evaluated them using the convolution theorem, i.e. the product of the functions in frequency domain is equal to their convolution in time domain. In the form above, each of the sinc functions in the integrand has a simple Fourier transform which is just the rectangular function. From the convolution theorem we derive the following:

$$\int_{-\infty}^{\infty}\mathrm{f}_1(\tau)\mathrm{f}_2(-\tau)d\tau=\int_{-\infty}^{\infty}\mathrm{F}_1(f)\mathrm{F}_2(f)df$$

where $f(t) \Leftrightarrow F(f)$ is a Fourier transform pair. This result can be used to evaluate the integral since convolution is relatively easy to perform for rectangular functions:

$$I = \begin{cases} A^2\pi^2 t_0 m & \text{if } n-m \geq 2 \\ \frac{1}{3}A^2\pi^2(3mt_0 - T) & \text{if } n-m = 0 \end{cases} \tag{2-54}$$

from which we obtain,

$$\begin{aligned} \text{var}(B) &= \frac{4}{N}\frac{1}{3}A^2\pi^2(3t_0 - T) + \frac{4}{N^2}\sum_{n=1}^{N-1}\left[(2N-2n-1)A^2\pi^2 t_0\right] \\ &\quad - \frac{4}{N^2}\sum_{n=1}^{N-1}\left[A^2\pi^2 t_0(2n-1)\right] \\ &= \frac{4A^2\pi^2}{N}\left(t_0 - \frac{T}{3}\right) + \frac{4A^2\pi^2 t_0}{N^2}\sum_{n=1}^{N-1}[2N-4n] \\ &= \frac{4A^2\pi^2}{N}\left(t_0 - \frac{T}{3}\right). \end{aligned} \tag{2-55}$$

Therefore, for $1/f^2$ noise, we have the simple result,

$$\text{var}(B) = \frac{4A^2\pi^2}{N}\left(t_0 - \frac{T}{3}\right) = \frac{4A^2\pi^2}{t_e}\left(t_d + T\right)\left(t_d + \frac{2T}{3}\right). \tag{2-56}$$

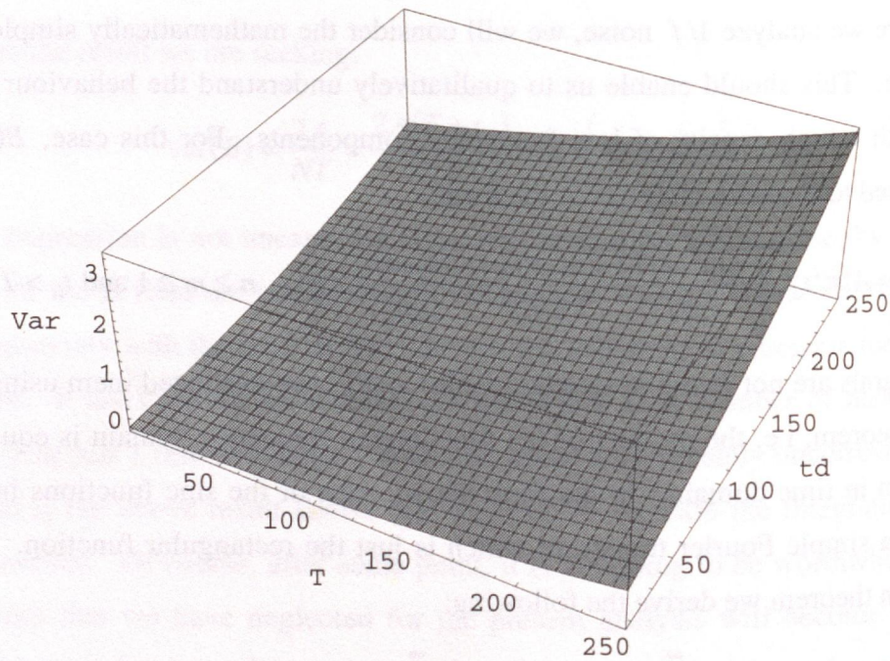

Fig. 2-5 Surface plot of the variance for $1/f^2$ noise. The variance (arbitrarily normalized) is shown as a function of the integration time and dead time assuming the total time for the experiment remains a constant.

In contrast to the white noise case, this kind of noise has high spectral density at low frequencies. This translates to a high correlation between noise samples that are closely spaced in time. Hence, one would expect to cut down the variance in the output by switching between the ions at a high frequency (low t_0). Indeed, the above expression shows that for a given t_e and t_d, the variance is least for $T = 0$! Again, this conclusion fails to take into account other noise sources that limit us at small integration times (such as the phase estimation error). But it is clear that high switching frequency is an advantage. Fig. 2-5 shows the variance as a function of T and t_d for a fixed t_e.

$1/f$ Noise

From the two cases studied so far, we expect that $1/f$ noise, which does not have as much low frequency components as $1/f^2$ noise but more than white noise, will have a minimum in its variance at some value of T. Let us see if this is true.

Now the power spectrum of the magnetic field is given by $B(f) = \dfrac{A}{f}$ and we have to evaluate integrals of the form,

$$\mathrm{I} = A\pi t_0 \int_{-\infty}^{\infty} \frac{\sin^2(\pi fT)}{(\pi fT)^2} \frac{\sin(m\pi ft_0)}{(\pi ft_0)} \sin(n\pi ft_0)\,\mathrm{sgn}(f)\,df \quad , n \geq m \geq 1 \text{ and } t_0 > T. \tag{2-57}$$

$$= \frac{At_0}{2} \int_{-\infty}^{\infty} \frac{\sin^2(\pi fT)}{(\pi fT)^2} \frac{\sin(m\pi ft_0)}{(\pi ft_0)} 2j\sin(n\pi ft_0)(-j\pi)\,\mathrm{sgn}(f)\,df$$

The signum function is necessary in order to make $B(f)$ an even function of frequency. We can use the convolution technique of integration by noting that

$$\text{F.T.}[-j\pi\,\mathrm{sgn}(f)] = \frac{1}{t} \quad \text{and} \quad \text{F.T.}[2j\sin(m\pi ft_0)] = \delta\left(t + \frac{mt_0}{2}\right) - \delta\left(t - \frac{mt_0}{2}\right)$$

The convolution integrals are complicated by the log terms introduced when we integrate $1/t$. Nevertheless, we can perform the integrals and obtain

$$\left(\frac{A}{T^2}\right)^{-1} \mathrm{I} = [b(n-m)]^2 \ln[b(n-m)] - \frac{1}{2}[b(n-m)-T]^2 \ln[b(n-m)-T]$$

$$-\frac{1}{2}[b(n-m)+T]^2 \ln[b(n-m)+T] - [b(n+m)]^2 \ln[b(n+m)] \tag{2-58}$$

$$+\frac{1}{2}[b(n+m)-T]^2 \ln[b(n+m)-T] + \frac{1}{2}[b(n+m)+T]^2 \ln[b(n+m)+T]$$

where $b = t_0/2$ and $n - m \geq 2$. For $n = m = 1$, we obtain a similar result,

$$\left(\frac{A}{T^2}\right)^{-1} \mathrm{I} = -T^2 \ln[T] - (2b)^2 \ln[2b] + \frac{1}{2}(2b-T)^2 \ln[2b-T] + \frac{1}{2}(2b+T)^2 \ln[2b+T] \tag{2-59}$$

Using Eqs. 2-58 and 2-59, we obtain the variance in B as a series involving T, t_d and t_e. Rather than list the lengthy expressions, I just show a surface plot of the variance as a function of T and t_d for a fixed t_e in Fig. 2-6. From the figure, we see that along the t_d direction, it is clearly advantageous to have as small a value as possible since this dead time limits the total number of measurements we can perform. For a given t_d, we have a minimum in the variance at approximately $t_d/2$. The steps on the surface occur because the value of N is discrete and smaller values of T do not take full advantage of the total t_e.

The differences among these three cases are apparent from Fig. 2-7. The variance in B (arbitrarily normalized) is plotted against T for a fixed t_d and t_e, i.e. it is a section through the three surface plots shown earlier. The optimal integration time can now be determined if we know the spectrum of the magnetic field fluctuations.

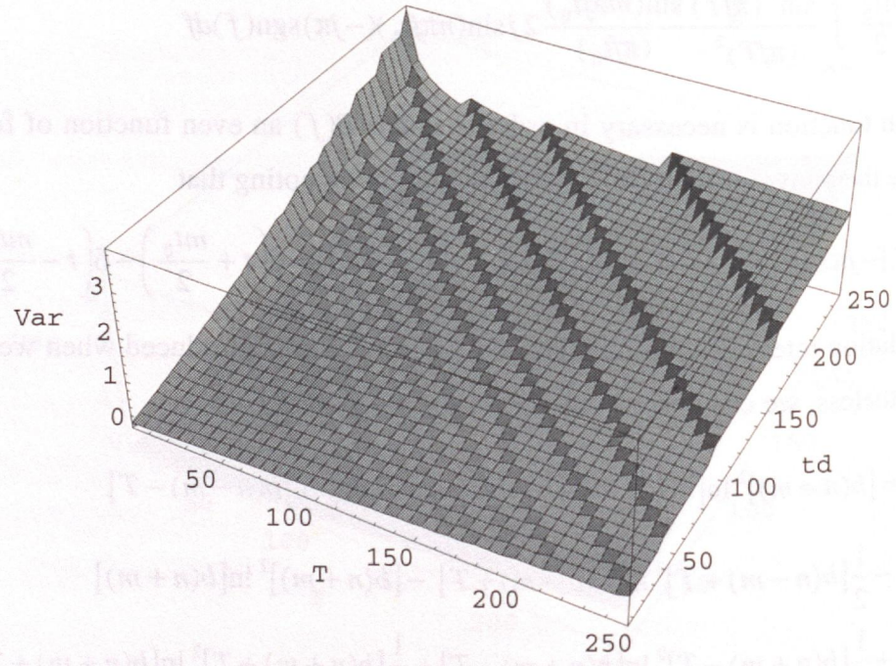

Fig. 2-6 Surface plot of the variance for $1/f$ noise. The variance (arbitrarily normalized) is shown as a function of the integration time and dead time assuming the total time for the experiment remains a constant.

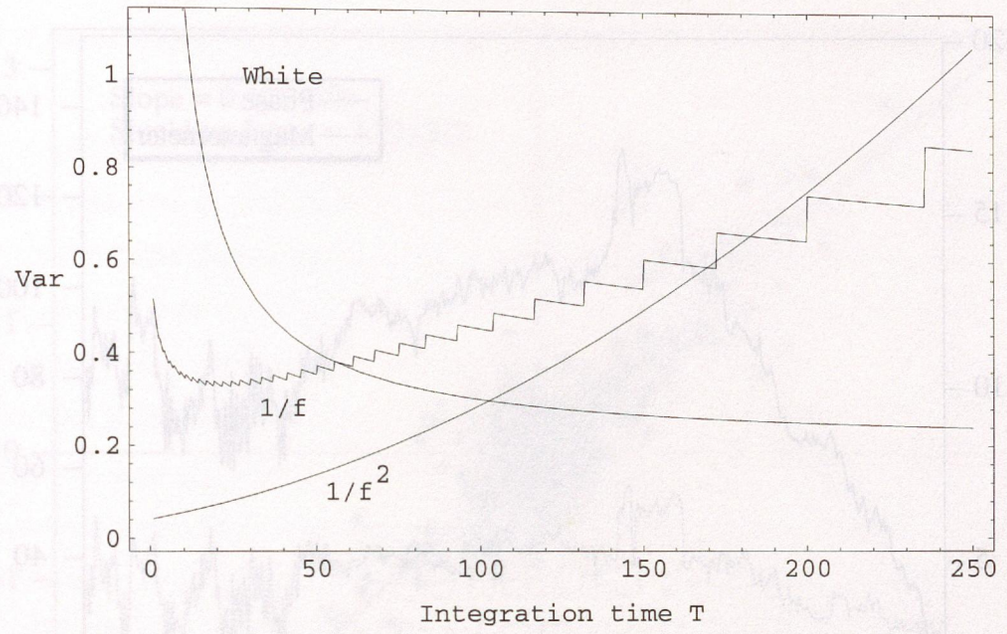

Fig. 2-7 Comparison of the output variance for three different kinds of magnetic field noise. The variances have been arbitrarily scaled and only their variations are significant. The dead time for each ion and the total time of the experiment are assumed constant.

So what is the actual spectral density of our magnetic noise? We have measured this by monitoring the cyclotron phase from a single N^+ ion (evolved in 30.2 s) over the course of a night, as shown in Fig. 2-8. We also monitor the external field with a flux gate magnetometer. The drift in the magnetometer reading is dominated by changes in the bucking field necessary to null the fringing field from the magnet at the magnetometer location. Therefore, the drift is independent of the external field seen by the ion. But as seen from Fig. 2-9, the *changes* in the magnetometer reading are well correlated with the changes in the ion's accumulated phase during the noisy time when the subway is running (after 6:00 AM). During this time, the shielding factor from the superconducting coils of the magnet is about 8. During the quiet time, the correlation disappears. This could be either because the magnetometer is not sensitive enough or that the noise is now entirely due to internal processes.

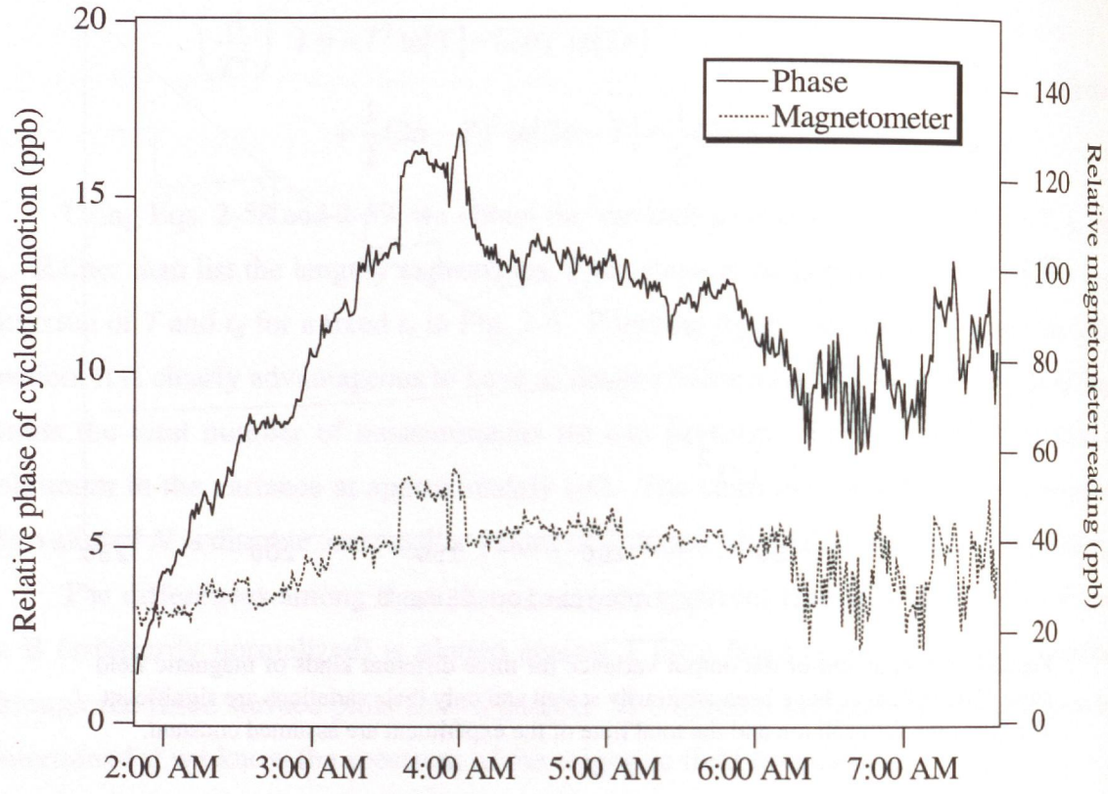

Fig. 2-8 Variation in the magnetic field over a night. The field in the trap was monitored by measuring the phase accumulated in the cyclotron mode of an N^+ ion in 30.2 s. The external field was monitored with a flux gate magnetometer. The jump in the middle is due to the movement of the elevator. The drift of the magnetometer reading is uncorrelated with the actual external field changes.

Spectral analysis on the quiet time data appears to show a $1/f$ type spectrum. We do not have enough data to fit the shape exactly, but there is clearly a high density of low frequency components. From our earlier analysis, the optimal integration time should be about half the dead time. In practice, we find that our dead time, including the time for the short integrations, is about 3 minutes for most ions. We therefore use an integration time of 1 minute for all our data. When combined with the phase estimation error, this gives us a precision below 0.1 ppb per measurement. The high frequency tail of the magnetic noise spectrum where it is almost flat (for frequencies greater than about 0.04 Hz) has an RMS amplitude of 0.2-0.4 ppb. Therefore, the phase noise does not contribute significantly to the statistical errors in the mass ratios.

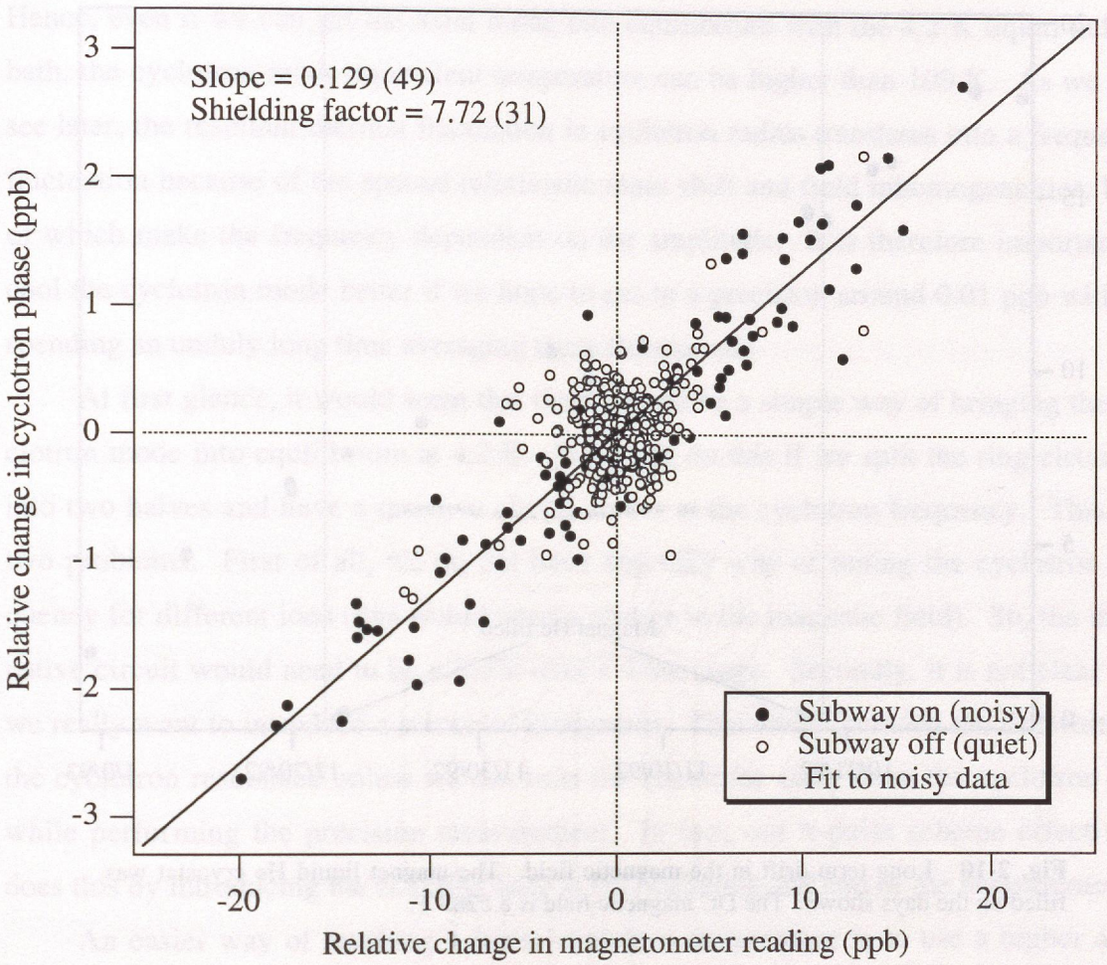

Fig. 2-9 A comparison of the output variance for three different kinds of magnetic field noise. The variances have been arbitrarily scaled and only their variations are significant. The dead time for each ion and the total time of the experiment are assumed constant.

As can be seen from Fig. 2-8, the low frequency noise components appear as slow drifts over these time scales. We can take out these drifts quite well with a polynomial fit. The residual fluctuations around the fit (corresponding to the high frequency Fourier components) are then mostly white and can be averaged. We have verified the validity of assuming that the residual fluctuations are random by studying the histograms of measured ratios. We will study the effects on the mass ratio of different ways of removing the magnetic noise in Chapter 3.

Finally, as mentioned earlier, there is a steady decrease in the magnetic field over time scales of a few months, probably due to creep in the superconducting coils. This is shown in Fig. 2-10, where all the mass ratio measurements that were used in this study have been converted into measurements of the magnetic field. The drift appears linear

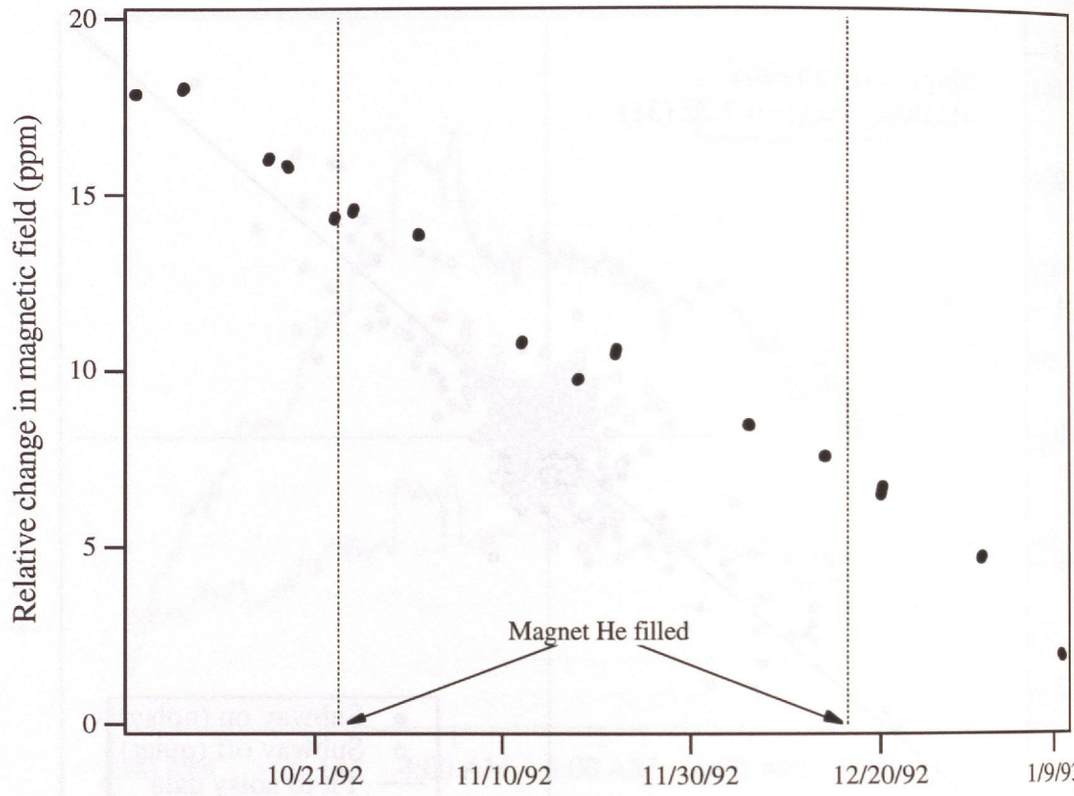

Fig. 2-10 Long term drift in the magnetic field. The magnet liquid He cryostat was filled on the days shown. The DC magnetic field is 8.5285 T.

and does not seem to be affected by filling of the magnet He cryostat. The deviations from a pure linear drift are probably determined by the exact location of dewars and other metallic objects in our lab. This drift is steadily downward; by contrast, the drifts during a night can go up or down indicating that they are low frequency noise components.

5 OTHER PROPOSED IMPROVEMENTS

I conclude this chapter with some of the other improvements to our apparatus that are in various stages of implementation.

High frequency cooling

We saw in the last chapter that our sideband cooling scheme for the cyclotron mode has a temperature limit given by

$$T_c = \left(\frac{\omega_c'}{\omega_z}\right) T_z. \tag{2-60}$$

Hence, even if we can get the axial mode into equilibrium with the 4.2 K liquid helium bath, the cyclotron mode equivalent temperature can be higher than 100 K. As we will see later, the resultant thermal fluctuation in cyclotron radius translates into a frequency fluctuation because of the special relativistic mass shift and field inhomogeneities, both of which make the frequency dependent on the amplitude. It is therefore important to cool the cyclotron mode better if we hope to get to a precision around 0.01 ppb without spending an unduly long time averaging these fluctuations.

At first glance, it would seem that there should be a simple way of bringing the cyclotron mode into equilibrium at 4.2 K. We could do this if we split the ring electrode into two halves and have a resistive circuit across at the cyclotron frequency. This has two problems. First of all, we do not have any easy way of tuning the cyclotron frequency for different ions (this would need a change in the magnetic field). So, the dissipative circuit would need to be tunable over a wide range. Secondly, it is not clear that we really want to introduce a source of dissipation. This would broaden the linewidth of the cyclotron resonance unless we can tune the circuit far away from the cyclotron line while performing the precision measurement. In fact, our π-pulse scheme effectively does this by introducing the coupling only at the beginning and end of the measurement.

An easier way of reaching a lower cyclotron temperature is to use a higher axial frequency, as seen from Eq. 2-60. We use a frequency of 160 kHz because that is close to the limit for operation of our SQUID detector. But this is a limit only if we want to detect the ion. We could use a higher axial frequency by increasing the trap voltage if all we wanted was a resistive bath at this frequency without actually seeing the ion. A tuned circuit operating at 1 MHz with an inductance of 1mH and a Q of 2000 would damp an N_2^+ ion in 65 sec. This is not a small damping time but it has some advantages. The coil width of 500 Hz means that we do not have to get the voltage on the trap exactly right for the ion to be cooled. And we have to do this cooling only for the long integration point that takes several minutes, so the added cooling time is not significant.

We thought that making a resonant circuit at 1 MHz with a Q of 2000 should be no problem with an inductor made with (resistive) copper wires. It turns out that the skin effect in the copper wire is enhanced by interactions between neighbouring loops in the coil and the increased resistance limits the Q to 200 even at helium temperatures. By carefully spacing the loops away from each other we could get a Q as high as 800. We also

added to the voltage box the capability to put up to 200V on the trap. But in the configuration we had designed, the high frequency coil was coupling too much noise into the detector and had to be removed.

We have since come to believe that the coil should really be built with superconducting wire. It is then easier to get the inductance and Q we desire. This means that it will have to be housed in the detector box away from the high field region. With proper design, we think it can be placed in series with the detector coil without affecting operation at 160 kHz.

Magnetic shielding

As mentioned earlier, the superconducting coils of the magnet have an intrinsic shielding factor for external noise of about 8. Gabrielse and Tan have shown that a cleverly designed magnet can have a shielding factor as high as 150. We can potentially improve this factor by simply using a superconducting loop around the trap. However, since the loop maintains flux rather than field, it is important to keep it dimensionally stable. This may not be as easy as it sounds, since a small change in temperature or pressure of the helium bath can change the size of the loop unacceptably.

We have not put too much effort into shielding at this stage since the exact source of our magnetic field noise is not clear. If the noise is predominantly due to motion of the trap with respect to the magnet coils, as we believe it is at least during the quiet time, then external shielding is not the problem. We need to figure out a way of fixing our loop with respect to the trap either by putting it right on the trap or on the copper can surrounding it. But we think that a more elegant solution is to measure the cyclotron frequencies of two ions simultaneously (see Chapter 6).

External ion source

The capabilities of our apparatus will be really improved if we are able to load ions made externally. It will allow us to work with species such as H_2O^+ and NH_3^+ which are difficult to handle in our gas handler since they rapidly adsorb on the walls. In fact, we have found it almost impossible to introduce these neutrals with our current set-up since they do not make it through the needle tubing leading to our insert. Ultimately, we may be able to work with exotic ions produced at reactors or with an EBIT.

An external ion loader also solves bad ion problems since a simple mass filter with 0.1 resolution can filter out our primary sources of contamination. We have built an ion source based on a commercial ion gun with an ExB mass filter that proves adequate for selecting ions such as N^+ and N_2^+. We can detect the ions successfully at the end of a drift tube which enters the top of our insert. We have installed Einzel lenses in the insert to steer the ions into the high field region. Once there, they should just spiral along the field lines into the trap. We do not anticipate any serious problems getting this to work and this will probably be the next major improvement in our apparatus.

The ion source also reduces our gas load by several orders of magnitude and could prove vital to successfully doing the mass 3 measurement. It can probably reduce our ion switching time by another factor of 2, giving us a $\sqrt{2}$ statistical improvement in overall accuracy. But we do not really consider this as a necessary improvement to achieve our ultimate goal in precision.

3 DOUBLET MEASUREMENTS

Precision mass comparison in general has traditionally been done on two ions with nominally the same mass to charge ratio, referred to as doublets. In a Penning trap, the ratio of the cyclotron frequencies of the two ions is then close to unity. A typical example would be O^+ and $CH_4{}^+$, which we refer to as mass 16 ions since both of them have a mass about 16 u. The difference in their masses arises because the 16 neutrons and protons in their nuclei are bound differently. Nuclear binding energies are of order a few MeV while each nucleon weighs about 1 GeV, so the mass ratio of the two ions typically differs from unity by a few parts in 10^4.

Herein lies the advantage of a doublet comparison. The cyclotron frequency in a trap, as we will see, may be systematically shifted due to a variety of effects, usually scaling as some high power of the mass of the ion. With a doublet, the shift is almost exactly the same for both ions and its effect on the ratio is down by three orders of magnitude. In this chapter, I will review our procedure for making a doublet mass comparison and show how systematic shifts cause negligible error. We have experimentally verified this error budget with different kinds of overdetermined sets (Chapter 5).

1 PROPOSAL TO OBTAIN ABSOLUTE MASSES

When we measure a doublet mass ratio, we are making a precise measurement of a *small* mass difference. Indeed, it is traditional in mass spectrometry to report only these mass differences. Consider a measurement of the ratio $M[CO^+]/M[N_2{}^+]$. Once we

convert the ionic ratio to neutral atom values, this can be thought of as a precision measurement of the difference:

$$M[2N - C - O] = \delta \times M[2N], \tag{3-1}$$

where the right hand side is a small quantity. This leads to a problem when we try to get the absolute masses of the atoms from a set of doublet ratios. By absolute mass, I mean the mass of the atom referred to ^{12}C, whose mass in atomic units (au) is defined to be 12. Thus the mass of an arbitrary atom A in au would be defined as:

$$M[A] = 12\left(\frac{m[A]}{m[^{12}C]}\right). \tag{3-2}$$

Singularity in matrix inversion

At first glance, it would seem that Eq. 3-1 yields one relation between the masses of N and O in terms of C, which we can combine with other measurements to solve for the masses. For instance, the ratios $M[N^+]/M[CH_2^+]$ and $M[O^+]/M[CH_4^+]$ yield two more equations for the three unknown masses of H, N and O:

$$M[C + 2H - N] = \delta' \times M[C + 2H], \tag{3-3}$$

$$M[C + 4H - O] = \delta'' \times M[C + 4H]. \tag{3-4}$$

On closer inspection, we see that there is a problem. When we try to eliminate H by multiplying Eq. 3-3 by 2 and subtracting from Eq. 3-4, we obtain

$$M[2N - C - O] = \delta'' \times M[C + 4H] - 2\delta' \times M[C + 2H], \tag{3-5}$$

which has the same left hand side as Eq. 3-1. Even though the right hand sides are not identical, they are small quantities and have three orders of magnitude larger *relative* error; so we should think of them as constants close to 0 for the purposes of solving this system of equations. Therefore the system of equations has a "singularity", i.e. when we solve for the masses we obtain values with large errors. This is explicit in the following solution for the mass of H:

$$M[H] = \frac{-2\delta(1-\delta') - 2\delta' + \delta''}{4\delta(1-\delta') + 4\delta' - 4\delta''} M[C]. \tag{3-6}$$

If we took all the δ's to be 0, we indeed have a singularity. In reality, the solution has a relative error of about 1×10^{-6}.

The source of this problem is that a measurement of a doublet ratio constrains the difference between the numerator and the denominator much more strongly than it does each one. Indeed, this is precisely the reason we work with doublets: the cyclotron frequency of each ion may be shifted, but their difference is not. And we can see that this singularity in inverting the differences is a general problem. Say we perform a series of measurements on molecules which contain H and D; then all the doublets are formed by replacing two H's with one D (examples would be CH_4 and CD_2, CD_2H_2 and CD_3, C_2H_4 and $C_2D_2H_2$,...). Hence, each one of these is only going to precisely constrain the difference $M[2H - D]$ and we will be left with the same problem.

The way around this is to find doublets that are formed by replacing a given species with carbon alone. One solution is to compare some species to carbon using a multiple charge state - *e.g.* Li^+ vs. C^{++} where we have effectively replaced a Li atom with half a carbon. Or we measure a doublet that involves only one species other than carbon - *e.g.* $C_3D_8^+$ vs $C_4D_2^+$, where 6D's have been replaced by one C. This is a viable alternative in our case because the two species could conceivably be introduced from a gas manifold. But at mass 52, it is right at the limit of our capabilities in terms of precision and applied voltage. The solution I present below is easier to implement.

Overcome with $M[Ar^+]/M[Ar^{++}]$

The basic idea of this solution is that the mass ratio* of the two charge states of Ar - Ar^+ and Ar^{++} - is exactly 2 but for some small corrections which can be calculated to 1 ppt accuracy (see next chapter on non-doublets for details). By comparing different hydrocarbons to these two charge states, we can obtain a linear system of equations that can be solved without the above loss in precision.

The actual scheme uses the three comparisons:

$$\begin{aligned} R_{40} &= M[Ar^+]/M[C_3H_4{}^+] \\ R_{20} &= M[Ar^{++}]/M[CD_4{}^+] \\ R_{18} &= M[CD_3{}^+]/M[CD_2H_2{}^+] \end{aligned} \tag{3-7}$$

at mass 40, 20, and 18, respectively. The first two ratios can be combined with the known ratio $R_{known} = M[Ar^+]/M[Ar^{++}]$ as follows:

---

* I sloppily refer to this as the mass ratio; in reality it is the ratio of the mass to charge ratios for the two species, which is what we measure from the cyclotron frequencies.

$$\frac{M[\mathrm{Ar}^+]}{M[\mathrm{C_3H_4}^+]}\times\frac{M[\mathrm{CD_4}^+]}{M[\mathrm{Ar}^{++}]}\times\frac{M[\mathrm{Ar}^{++}]}{M[\mathrm{Ar}^+]}\times 2=\frac{2R_{40}}{R_{20}R_{known}}$$
$$\Rightarrow\quad \frac{M[2\mathrm{C}+8\mathrm{D}]}{M[3\mathrm{C}+4\mathrm{H}]}=R'_{40} \tag{3-8}$$

where the factor of 2 is introduced just to make the final ratio close to unity. We now effectively have two doublets, at mass 18 with 2H replaced by D, and at mass 40 with (C+4H) replaced by 8D (so that the combination yields C replaced by 6D). The two mass difference equations they yield are

$$\begin{aligned} M[2\mathrm{H}-\mathrm{D}] &= \delta_{18}\times M[\mathrm{C}+2\mathrm{D}+2\mathrm{H}]\ , \\ M[\mathrm{C}+4\mathrm{H}-8\mathrm{D}] &= \delta'_{40}\times M[3\mathrm{C}+4\mathrm{H}]\ , \end{aligned} \tag{3-9}$$

which are precisely the kind of equations we were looking for. Now when we eliminate a variable such as D, we do not cause the left hand side to go to zero; instead, we obtain

$$M[12\mathrm{H}-\mathrm{C}]=8\delta_{18}\times M[\mathrm{C}+2\mathrm{D}+2\mathrm{H}]-\delta'_{40}\times M[3\mathrm{C}+4\mathrm{H}] \tag{3-10}$$

where I have not bothered to eliminate the D in the right hand side because it needs to be known with much lower precision. The solution for the mass of H is then:

$$M[\mathrm{H}]=\frac{1}{12}M[C]+\frac{2}{3}\delta_{18}\times M[\mathrm{C}+2\mathrm{D}+2\mathrm{H}]-\frac{1}{12}\delta'_{40}\times M[3\mathrm{C}+4\mathrm{H}]. \tag{3-11}$$

The dominant term is the mass of C divided by 12, and the others represent small corrections to it. Therefore the final relative error is of the same order as the relative errors in the ratios.

The three ratios discussed here form part of the set of ratios that we have measured in this study using our standard doublet procedure presented in the following section.

2 MEASUREMENT PROCEDURE

A typical measurement run means more than just spending a sleepless night in the lab. From filling the experiment with He in the morning to making sure that there is no problem with holding the freight elevator on our floor for a few hours, there is a lengthy check list we have to go through before the run. In this section, I will briefly describe the procedure to get the trap ready for a run, our "pulse and phase" (PNP) technique for measuring the cyclotron frequency, and finally a typical measurement cycle.

Tuning the trap

Before starting a run, we have to adjust the guard ring voltage to make sure that the trap is "tuned", i.e. the axial electrostatic potential is as harmonic as possible. The tuned guard ring setting usually changes by a mV or so over a few days, leading us to believe that this is caused by charged patches adsorbed on the surfaces of the electrodes. Occasionally, we see the trap get progressively mistuned over the course of a run, especially if we are field emitting a lot. We will consider the effect of these patches in more detail later.

The trap is tuned using the two-drive scheme described in Weisskoff's thesis [WEI88]. One drive (~161 kHz, exactly 1 kHz above the detector resonance) is applied between the endcaps while the second drive (exactly 1 kHz) is applied to the ring. The ring drive FM modulates the ion's signal and produces characteristic sidebands every 1 kHz. When the first upper sideband is resonant with the 161 kHz axial drive, we get a resonant excitation of the axial mode which induces a large signal into the detector. We improve the signal to noise by using a lock-in detection scheme. We plot the shape of the ion's response in the frequency domain by sweeping the ring voltage (using the computer supplied offset to the voltage box setting). As shown in Fig. 3-1, if the trap is anharmonic we get an asymmetric lineshape with hysteretic dependence on the sweep direction. A tuned response has the same shape and amplitude in both directions.

When we first started working with the new voltage box, we were tuning the two channels independently for the two ions, quite foolishly as it turned out. The guard ring potential has a mass dependence that is almost exactly half the value for the ring potential (see the section on patch effects for the exact dependence). Therefore, the difference in the guard ring settings for the two ions should be half the difference in ring settings. When we looked at our old data, we found that this was off by 1-2 mV in a few cases, which means that we were measuring the cyclotron frequencies of the two ions with different C_4 coefficients. This also means that our technique for trap tuning is good only to perhaps 1 mV or so, much larger than the 0.1 mV that we believed we could tune to. One possible reason is that it takes us 10 minutes or more to carefully plot the resonance lineshape in both directions, allowing noise and voltage drifts to distort it. A quicker method relying on a transient response might be necessary before we can reduce C_4 significantly.

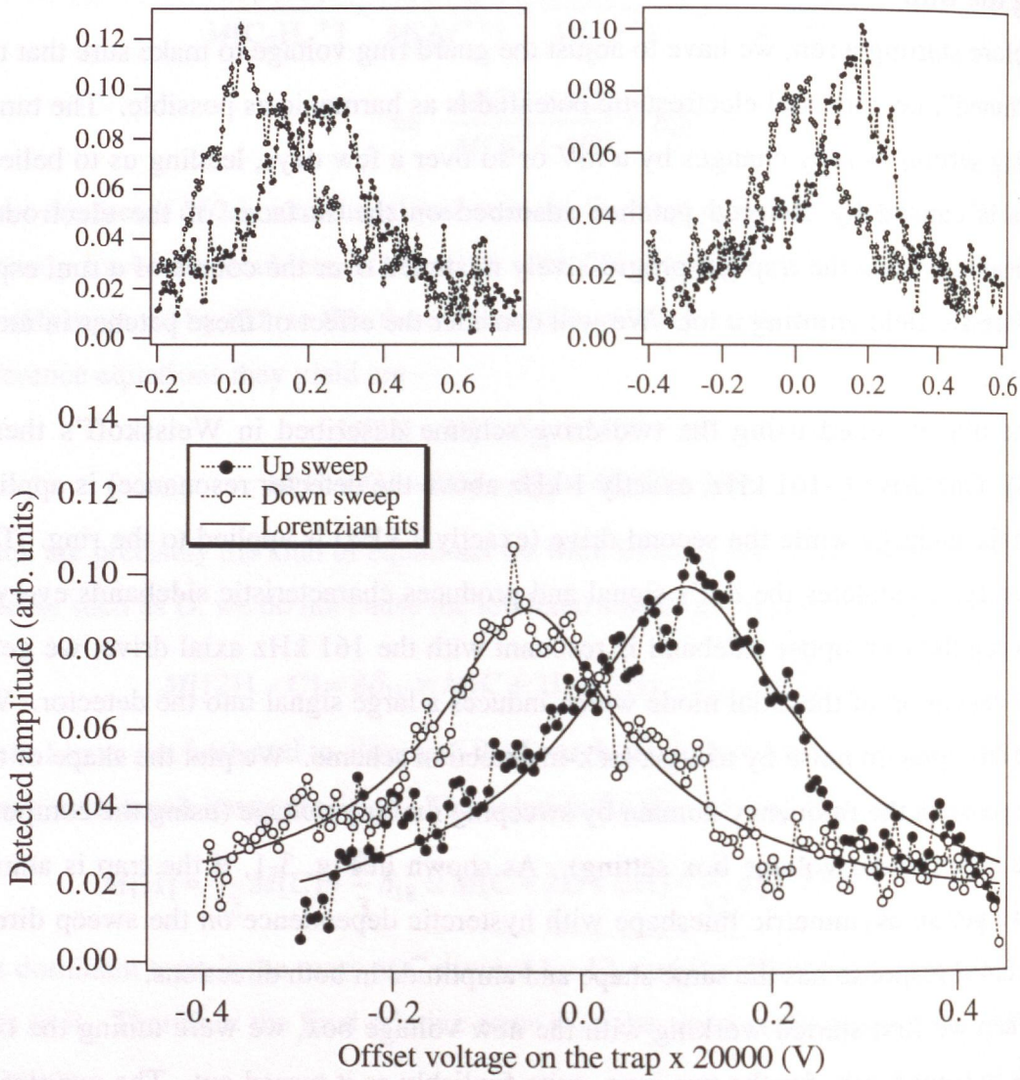

Fig. 3-1 Tuning the trap with a $C_3H_4^+$ ion. The ion's response in the frequency domain is obtained by sweeping the ring voltage in a small range and detecting the axial signal with a two drive scheme. The upper responses are for a trap with the guard ring 0.4 mV too negative (left) and 0.1 mV too positive (right) and show hysteretic dependence on the sweep direction. The lower response is obtained when the trap is well tuned; the separation between the peaks is from the time constant of the lock-in detector. The voltage scale as shown is such that 1 V corresponds to 0.314 Hz. The ion's damping time from the tuned response is 5.3 seconds.

PNP method for the cyclotron frequency

With the trap tuned, we are ready to start the run if we know the resonant coupling frequency for the cyclotron-to-axial π-pulse. This we obtain from the cyclotron avoided crossing as shown in Fig. 3-2. For each ion, we map the avoided crossing very carefully

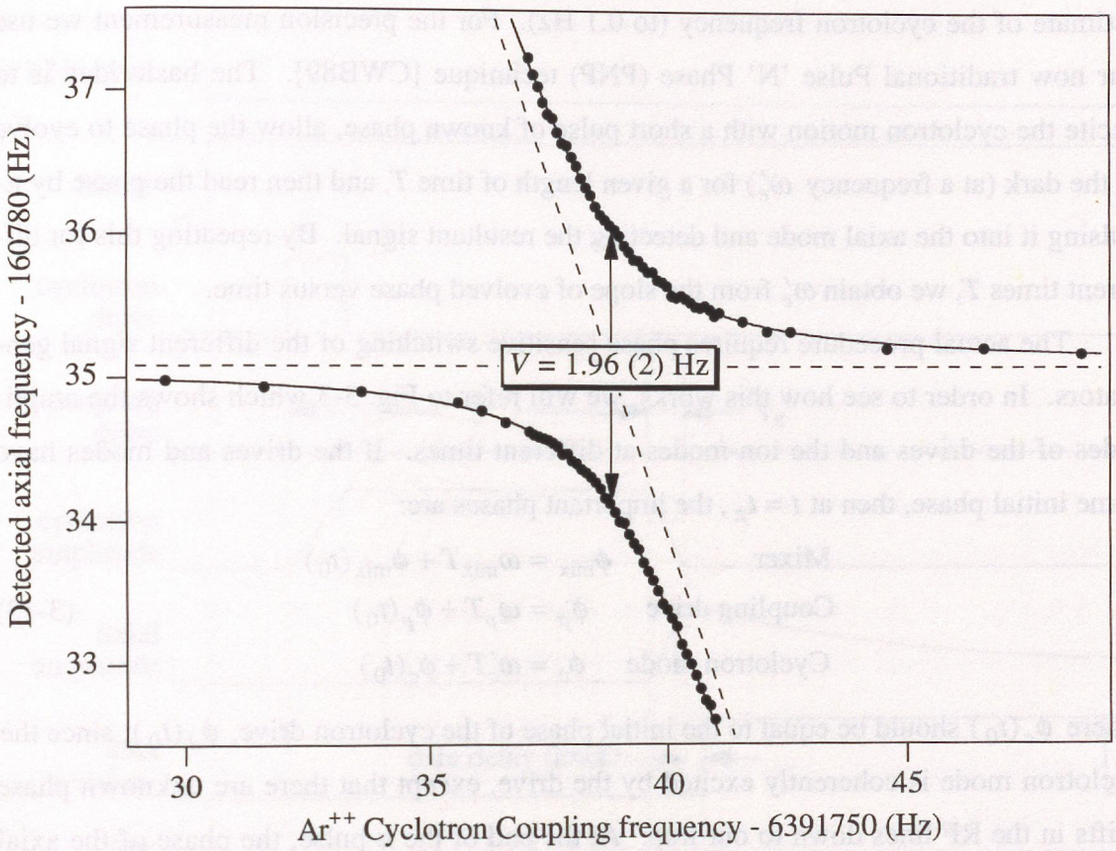

Fig. 3-2 Cyclotron avoided crossing for Ar^{++}. The frequencies of the two states that appear near the detector are plotted as the coupling frequency is scanned through the resonance. The actual detected signals from which the frequencies were extracted are shown in Fig. 1-3.

once to determine the strength of the drive at the ion's location. If the splitting on resonance is V Hz, then the π-pulse duration τ_π (in s) is given by:

$$2\pi V\tau_\pi = \pi \;\Rightarrow\; \tau_\pi = \frac{1}{2V}. \tag{3-12}$$

The RF field strength at the ion's location depends not only on the drive generator output but also on the transfer function of all the cables, amplifiers and filters in line. We are careful not to change the cables or move them too much since we have seen unexpected resonances that change the π-pulse duration. We also worry about nonlinearities in the transfer function; therefore we measure the avoided crossing splitting with a given drive voltage and then adjust the time duration (rather than the amplitude) to obtain a π-pulse.

A quick eyeballing of the avoided crossing with an FFT of the ion's axial response is enough for everyday use. From this we get both the coupling frequency and a rough

estimate of the cyclotron frequency (to 0.1 Hz). For the precision measurement we use our now traditional Pulse 'N' Phase (PNP) technique [CWB89]. The basic idea is to excite the cyclotron motion with a short pulse of known phase, allow the phase to evolve in the dark (at a frequency ω_c') for a given length of time T, and then read the phase by π-pulsing it into the axial mode and detecting the resultant signal. By repeating this for different times T, we obtain ω_c' from the slope of evolved phase versus time.

The actual procedure requires phase sensitive switching of the different signal generators. In order to see how this works, we will refer to Fig. 3-3 which shows the amplitudes of the drives and the ion modes at different times. If the drives and modes have some initial phase, then at $t = t_\pi$, the important phases are:

$$\begin{aligned} &\text{Mixer} && \phi_{\text{mix}} = \omega_{\text{mix}} T + \phi_{\text{mix}}(t_0) \\ &\text{Coupling drive} && \phi_p = \omega_p T + \phi_p(t_0) \\ &\text{Cyclotron mode} && \phi_c = \omega_c' T + \phi_c(t_0) \end{aligned} \tag{3-13}$$

where $\phi_c(t_0)$ should be equal to the initial phase of the cyclotron drive, $\phi_d(t_0)$, since the cyclotron mode is coherently excited by the drive, except that there are unknown phase shifts in the RF lines down to our trap. At the end of the π-pulse, the phase of the axial motion is given by the phase difference between the cyclotron mode and the coupling drive at the beginning of the π-pulse [COR90]. Again, the phase of the coupling field that the ion sees is not simply the phase at the drive source but depends on the shifts from the transfer function.

The transfer function phase shifts should remain constant as long as we do not disturb the cable lengths. Also, since the cyclotron drive (at $\sim\omega_c'$) and the coupling drive (at $\omega_c' - \omega_z$) differ only by 160 kHz out of a few MHz, we expect that their phase shifts are the same (as it is very unlikely that we have high Q resonances in the filters) and should cancel. Therefore, I just use the drive generator phases in the following and leave the transfer function phase as an unknown constant ϕ_{tf}. As we will see, fixed phases are anyway not important in this technique since we only look at the slope of the evolved phase. Then the phase of the axial mode after the π-pulse at $t = t_\pi + \tau_\pi$ is:

$$\begin{aligned} \text{Axial mode} \quad \phi_z &= \omega_c' T + \phi_d(t_0) - \omega_p T - \phi_p(t_0) + \phi_{\text{tf}} \\ &= (\omega_c' - \omega_p) T + \phi_d(t_0) - \phi_p(t_0) + \phi_{\text{tf}} \ . \end{aligned} \tag{3-14}$$

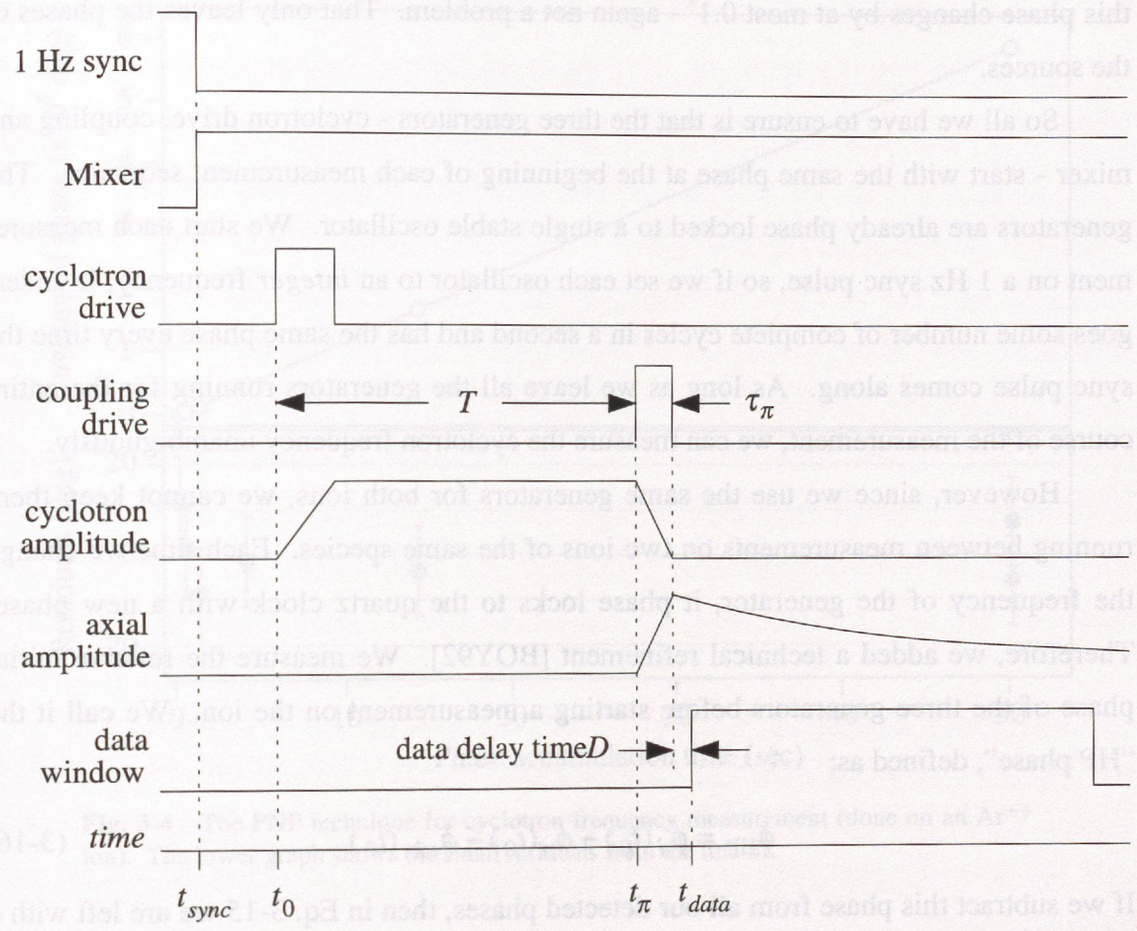

Fig. 3-3 Timing of the drives for a PNP measurement (not to scale). T is the phase integration time. D is a typical delay of 2 ms before recording the data.

When we start detecting the axial signal at $t = t_{data}$, we multiply it with the mixer and take the difference frequency component. Therefore the phase we actually detect is the difference between the phase of the axial motion and the mixer. If we denote the mixed down axial frequency as ω_z' (usually about 30 Hz), then the detected phase at $t = t_{data}$ is:

$$\begin{aligned}\phi_{\text{det}} &= (\omega_c' - \omega_p)T + \phi_d(t_0) - \phi_p(t_0) + \phi_{\text{tf}} - \omega_{\text{mix}}(T + \tau_\pi) - \phi_{\text{mix}}(t_0) + \omega_z' D \\ &= \left[\omega_c' - (\omega_p + \omega_{\text{mix}})\right]T + \phi_{\text{tf}} - \omega_{\text{mix}}\tau_\pi + \omega_z' D + \phi_d(t_0) - \phi_p(t_0) - \phi_{\text{mix}}(t_0)\ .\end{aligned} \tag{3-15}$$

This expression contains all the information necessary for our PNP measurement. We see that the slope of the detected phase versus T gives us the *offset* of the cyclotron frequency from the sum of the mixer and coupling drives. This is true as long as the other phases remain constant. We never change τ_π or ω_{mix}, therefore that term poses no problem. The D we use is 2 ms, and our axial frequency is stable to better than 0.1 Hz, so

this phase changes by at most 0.1° - again not a problem. That only leaves the phases of the sources.

So all we have to ensure is that the three generators - cyclotron drive, coupling and mixer - start with the same phase at the beginning of each measurement sequence. The generators are already phase locked to a single stable oscillator. We start each measurement on a 1 Hz sync pulse, so if we set each oscillator to an *integer* frequency, it undergoes some number of complete cycles in a second and has the same phase every time the sync pulse comes along. As long as we leave all the generators running for the entire course of the measurement, we can measure the cyclotron frequency unambiguously.

However, since we use the same generators for both ions, we cannot keep them running between measurements on two ions of the same species. Each time we change the frequency of the generator, it phase locks to the quartz clock with a new phase. Therefore, we added a technical refinement [BOY92]. We measure the relative initial phase of the three generators before starting a measurement on the ion. We call it the "HP phase", defined as:

$$\phi_{\mathrm{HP}} = \phi_d(t_0) - \phi_p(t_0) - \phi_{\mathrm{mix}}(t_0) \tag{3-16}$$

If we subtract this phase from all our detected phases, then in Eq. 3-15 we are left with a phase that is only dependent on $\omega_c' T$ and should be reproducible from ion to ion of a given species. This is particularly true for the short integration points, when fluctuations in ω_c' (of about 0.3 ppb arising from field variations) do not have enough time to build up phase. Indeed, we originally intended to use the HP phase to take fewer measurements on each ion since there is not much point in repeating the reproducible short integrations. But now we feel that the time spent on short integrations is useful since these points are valuable in judging if there is anything wrong with a particular ion.

There is one last step before converting the detected phase into a cyclotron frequency. The estimation routine only gives us the phase modulo 360°. We have to keep track of the phase wraps and add that many multiples of 360° before plotting the evolved phase versus T. We do this by increasing our integration time from about 0.2 s to 50.2 s in 6 steps. With each longer integration our precision in the frequency increases correspondingly and we can integrate 3.5 times longer the next time.

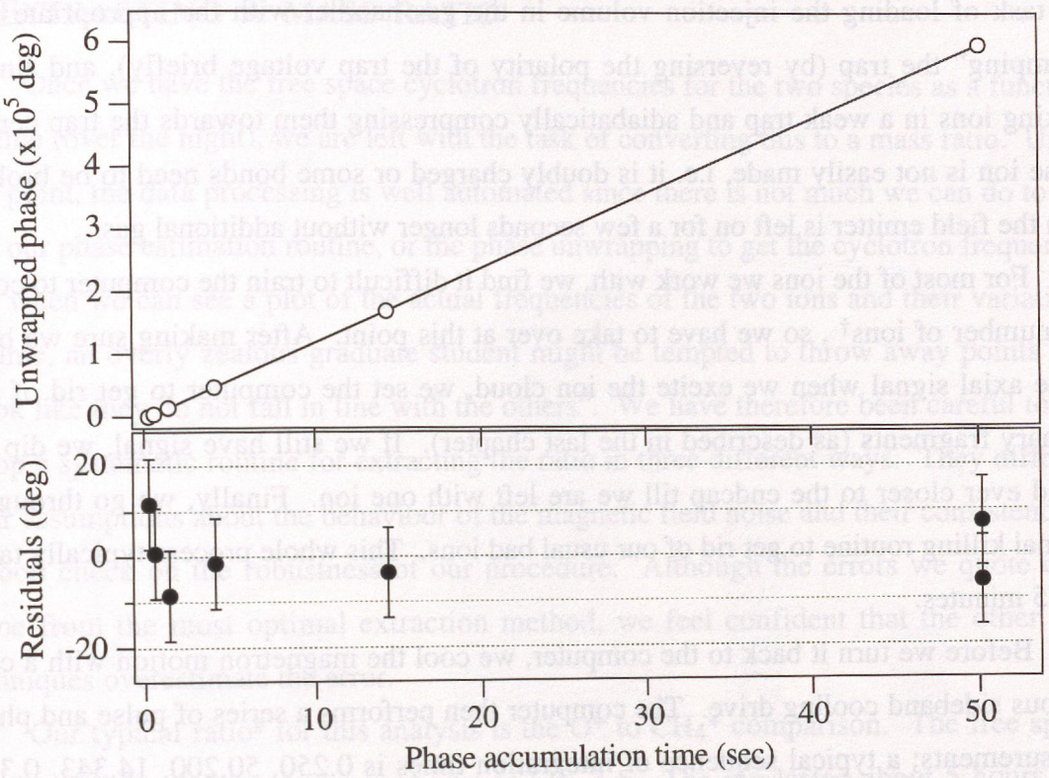

Fig. 3-4 The PNP technique for cyclotron frequency measurement (done on an Ar^{++} ion). The lower graph shows the small residuals from the line fit.

A typical measurement of the cyclotron frequency with this technique is shown in Fig. 3-4. We start off the automatic phase unwrapping algorithm around the frequency we measure from the avoided crossing. After that it should not stray, and a good indicator of this is the small residuals from the line fit. These should only be due to phase estimation noise (the effect due to field drift is negligible) and are about 10° from the figure, consistent with our earlier analysis.

A typical run

The preparatory steps for starting a run are to make sure that the experiment is well filled with He, the trap is tuned and that there is enough gas of each species in the bottles to last the night. We then find the magnetron and cyclotron cooling frequencies for the two ions by avoided crossing and store these frequencies in the appropriate signal generators.

The making of a single ion during the run proceeds as follows. We first set the voltage on the trap to center the ion on the detector coil. The computer then takes over

the task of loading the injection volume in the gas handler with the appropriate gas, "dumping" the trap (by reversing the polarity of the trap voltage briefly), and finally making ions in a weak trap and adiabatically compressing them towards the trap center. If the ion is not easily made, i.e. it is doubly charged or some bonds need to be broken, then the field emitter is left on for a few seconds longer without additional gas.

For most of the ions we work with, we find it difficult to train the computer to count the number of ions† , so we have to take over at this point. After making sure we have some axial signal when we excite the ion cloud, we set the computer to get rid of any primary fragments (as described in the last chapter). If we still have signal, we dip the cloud ever closer to the endcap till we are left with one ion. Finally, we go through a normal killing routine to get rid of our usual bad ions. This whole process typically takes 3 to 5 minutes.

Before we turn it back to the computer, we cool the magnetron motion with a continuous sideband cooling drive. The computer then performs a series of pulse and phase measurements; a typical sequence of integration times is 0.250, 50.200, 14.343, 0.314, 50.200, 0.585, 1.421, 4.098 and 50.200. The raw data at the output of the mixer is sampled and stored for later analysis. Once the computer is done, we repeat the process with the other species.

All the data sets from one night are then analyzed to get the initial phase and axial frequency. For each ion, we unwrap the phase and convert it into a trap cyclotron frequency and, using the average axial frequency, into a free space cyclotron frequency (recall from the last chapter that we do not really need the magnetron frequency).

† See Kevin Boyce's thesis [BOY92] to see how we were able to do this for N_2^+ and CO^+.

3 EXTRACTING A MASS RATIO

Once we have the free space cyclotron frequencies for the two species as a function of time (over the night), we are left with the task of converting this to a mass ratio. Up to this point, the data processing is well automated since there is not much we can do to adjust our phase estimation routine, or the phase unwrapping to get the cyclotron frequency. But when we can see a plot of the actual frequencies of the two ions and their variations in time, an overly zealous graduate student might be tempted to throw away points that "look like they do not fall in line with the others". We have therefore been careful to develop a systematic routine for extracting the ratio in three different ways. They differ in their assumptions about the behaviour of the magnetic field noise and their consistency is a good check on the robustness of our procedure. Although the errors we quote only come from the most optimal extraction method, we feel confident that the other two techniques overestimate the error.

Our typical ratio[#] for this analysis is the O^+ to CH_4^+ comparison. The free space frequencies for the two ions are shown in Fig. 3-5. The run lasted about 5 hours and there were 8 or 9 single ions of each kind measured. On each ion, we made three precise measurements of the cyclotron frequency (with $T = 50.2$ s), at the beginning, middle and end of the measurement cycle.

Switches without removing drift

For our analysis of magnetic field noise in the last chapter, we assumed that the mass ratio was obtained by taking the ratio of two neighbouring cyclotron frequencies. We refer to these as "switches" - corresponding, in our example, to a measurement of the cyclotron frequency of O^+ followed by one on CH_4^+, or vice versa. From Fig. 3-5 we see that there were 16 switches in this particular run. The figure also shows a fair amount of temporal variation that is common to both ions. These are the low frequency Fourier components that I referred to in the last chapter. However, for our first analysis, we will ignore this drift and simply take each ratio of neighbouring frequencies as an independent measure of the mass ratio.

[#] It just happens to be our best measurement to date!

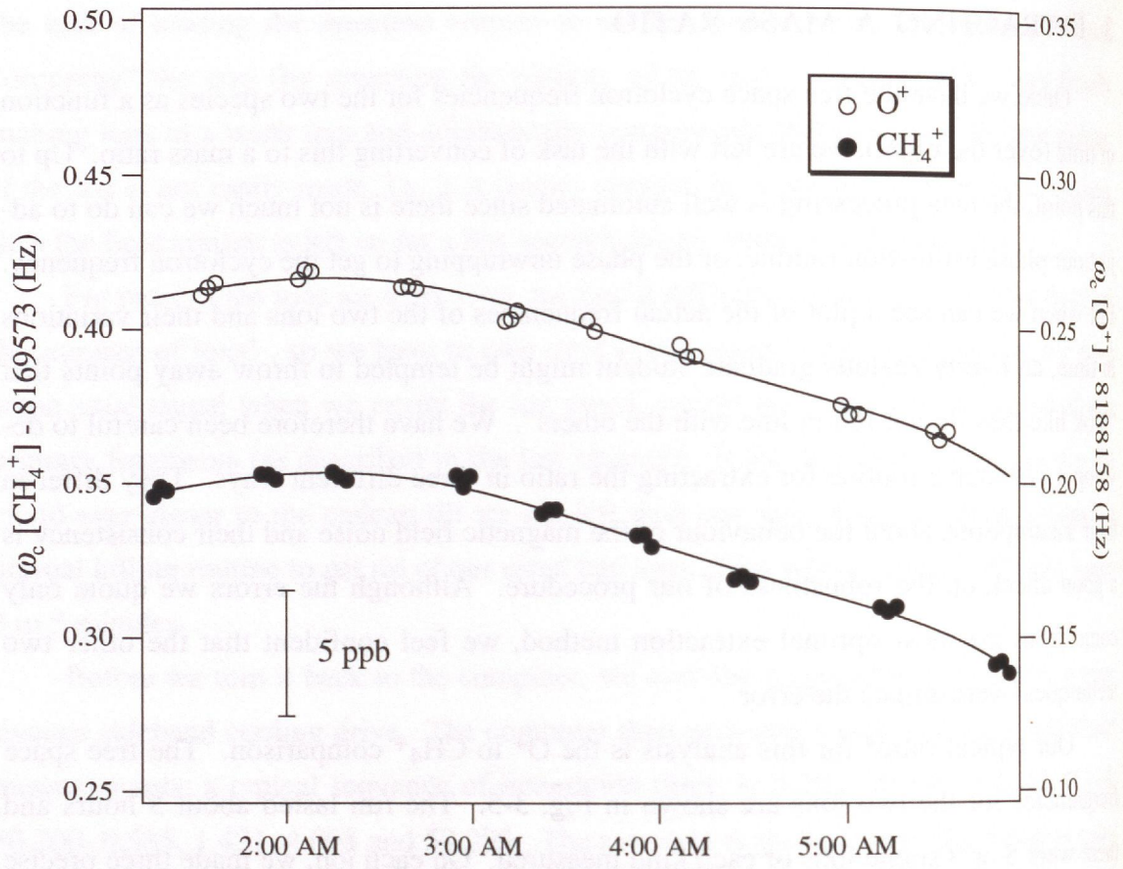

Fig. 3-5 O^+ vs. CH_4^+ comparison. The free space cyclotron frequencies for the two ions are plotted as a function of time. The solid lines are a polynomial fit to the magnetic field variation.

This is equivalent to assuming that the switches are close enough in time that the magnetic field has not had time to drift significantly. Indeed, this is the reason we take our precision measurements at the beginning and end of the measurement cycle; it minimizes the dead time between measurements on neighbouring ions. By taking at least two precision measurements on each ion, we get two switches from each cycle, one going up in frequency and the other down. This maximizes the number of switches but has another advantage as well. If there is a local linear drift in the field, our switches would give a low ratio followed by a high one (or the other way around depending on the sign of the slope). However, as long as the measurements on the two ions are spaced about equally apart, we expect that the mean ratio is not affected by this bimodal distribution.

We usually obtain such a bimodal distribution of ratios when we do not remove the drift. Since the distribution is non-Gaussian, the standard deviation overestimates the

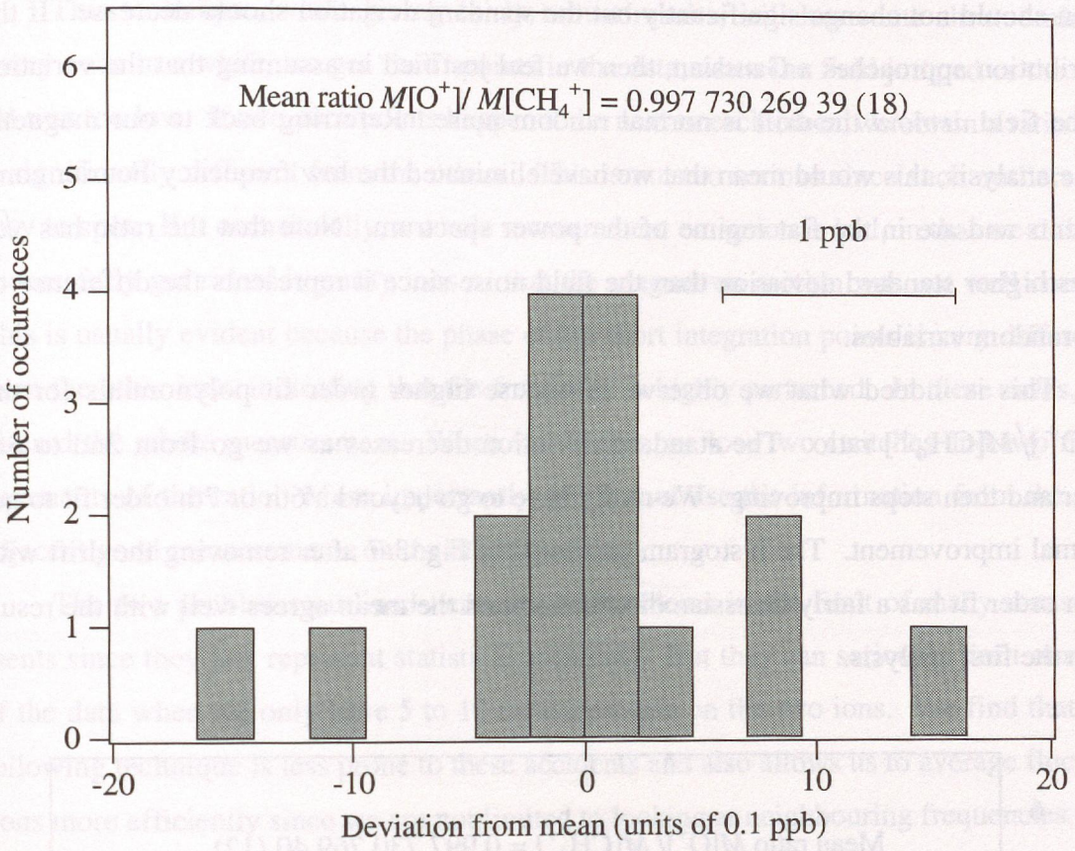

Fig. 3-6 Histogram of ratios without removing drift. Each switch is taken to be an independent ratio measurement. Note that the distribution is significantly non-Gaussian but quite symmetric about 0 deviation (bimodal).

normal error. But this analysis is very valuable since it requires minimal data massaging before it gives us a fair estimate of at least the mean mass ratio. In Fig. 3-6, I show a histogram of the $M[O^+]/M[CH_4^+]$ ratios obtained from the raw switches.

Switches after removing drift

We can do better if we fit the frequencies to a polynomial variation in the magnetic field, but still work under the assumption that there is correlation left between the nearest neighbour measurements. In other words, we would like to keep the ratio not very dependent on how well we extract the drift. Hence, for this analysis, we remove the field drift from the cyclotron frequencies, but, as before, take each switch as an independent measurement of the ratio.

Again we obtain a series of independent ratios for statistical analysis. Now we expect that, as we fit the drift better (using successively higher order polynomials), the

mean should not change significantly but the standard deviation should decrease. If the distribution approaches a Gaussian, then we feel justified in assuming that the variation of the field *around* the drift is normal random noise. Referring back to our magnetic noise analysis, this would mean that we have eliminated the low frequency Fourier components and are in the flat regime of the power spectrum. Note that the ratio has $\sqrt{2}$ times higher standard deviation than the field noise since it represents the difference of two random variables.

This is indeed what we observe as we use higher order fit polynomials for the $M[O^+]/M[CH_4^+]$ ratio. The standard deviation decreases as we go from 2nd to 5th order and then stops improving. We rarely have to go beyond a 6th or 7th order fit to get optimal improvement. The histogram presented in Fig. 3-7 after removing the drift with a 5th order fit has a fairly Gaussian distribution and the mean agrees well with the result from the first analysis.

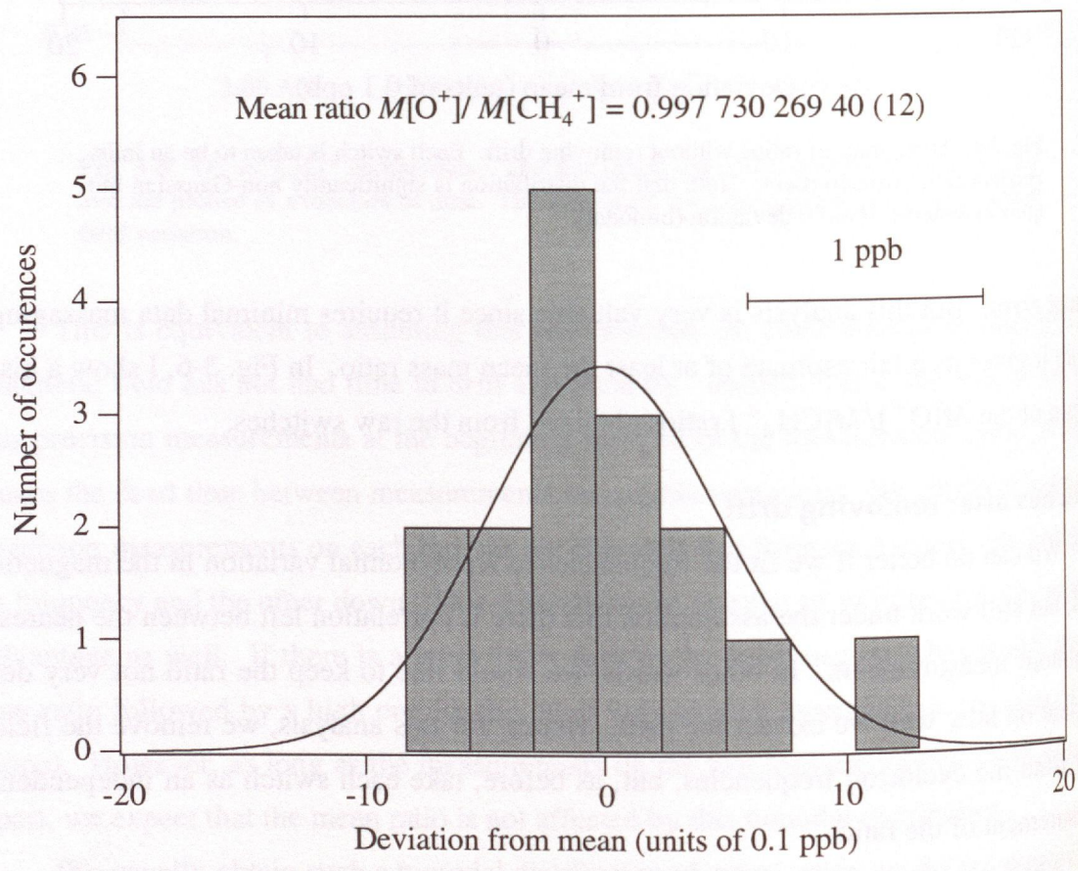

Fig. 3-7 Histogram of measured ratios after removing drift. Each switch is taken to be an independent measure of the ratio. The field drift has been taken out with a 5th order polynomial fit.

This technique, while giving fairly robust results, still has some shortcomings. Every once in a while, we get "bad" points in the data, when the field jumped or the signal was too low. If two such points happen to lie next to each other, we obtain a ratio that is significantly different from the others. This is not too serious since such outliers are easy to spot. But occasionally, a whole measurement on an ion is bad, in that we did not successfully get rid of impurity ions or that the magnetron motion was not well cooled. This is usually evident because the phase of the short integration points is very different* from the other ions, indicating that the frequency is highly perturbed. In these cases, we discard the whole measurement. When we do this, we lose two switches and two measurements of the ratio. More importantly, we do not use the information from the two adjacent good measurements on the other species.

The two problems outlined here are not problems in the limit of many measurements since they just represent statistical accidents. But they can seriously limit our use of the data when we only have 5 to 10 measurements on the two ions. We find that the following technique is less prone to these accidents and also allows us to average fluctuations more efficiently since we are not limited to looking at neighbouring frequencies.

Fit to drift and mass ratio

The most optimal method to extract the mass ratio is to fit the cyclotron frequencies of the two ions to a ratio and a field drift at the same time. This amounts to assuming that the individual frequency measurements are normally distributed around the drift, or equivalently, that the field noise is random after we remove the drift. But now it is harder to predict what should happen to the distribution if we use an overly restrictive fit. Usually it is obvious from looking at the fit that we have a poor fit, and the mean ratio we get is probably deviant. We judge this quantitatively by looking at the χ^2 as we progressively increase the order of the fit polynomial. When we finally have a satisfactory fit, the residuals in the frequencies should have a normal distribution.

In Table 3-1, I summarize the results of this analysis on the $M[O^+]/M[CH_4{}^+]$ ratio. We see that the χ^2 decreases rapidly up to a 5th order fit while the mean remains constant within error. The residuals from the 5th order fit have a Gaussian distribution as shown in Fig. 3-8. The final mean is consistent with the values from the other two

* In fact, the phase is completely random and has no correlation with the other ions.

Table 3-1. Effect on $M[O^+]/M[CH_4{}^+]$ of the order of fit polynomial. The listed values of χ^2 and mass ratio are obtained when the magnetic field drift is removed using a polynomial in time of given order. The improvement in χ^2 beyond 5th order is very small.

Order of polynomial	χ^2	$M[O^+]/M[CH_4{}^+]$
2nd	0.000487	0.997 730 269 38 (12)
3rd	0.000303	0.997 730 269 37 (9)
4th	0.000268	0.997 730 269 41 (9)
5th	0.000238	0.997 730 269 42 (8)
6th	0.000221	0.997 730 269 46 (8)
7th	0.000212	0.997 730 269 45 (8)

analyses, but has smaller error. As mentioned earlier, this method allows us to average fluctuations slightly better since we can take three precision measurements on each ion, all of which contribute to the average, while only the outer two contribute to the average in the previous analyses. Taking more points on each ion does not help as we begin to be limited by local fluctuations in the field.

Finally, this scheme has another advantage in that we can look at the histogram of the residuals for each species independently. Then, if there is some systematic difference in their errors, this will show up as a difference in the widths of the two histograms. In our current example, we found a small difference that may well be within the statistical uncertainty in determining the widths from the number of points we have. We will return to possible sources of this difference in the next section on systematic errors.

Neutral atom masses from ions

The above analysis gives us a mass ratio for the two *ions*. Before we solve for the atomic masses, we have to convert this to a ratio of the masses of neutral constituent atoms. This means that we have to account for the missing electron(s) and binding energies. Here, I will set the notation for the corrections that we have used to obtain the results reported in this thesis.

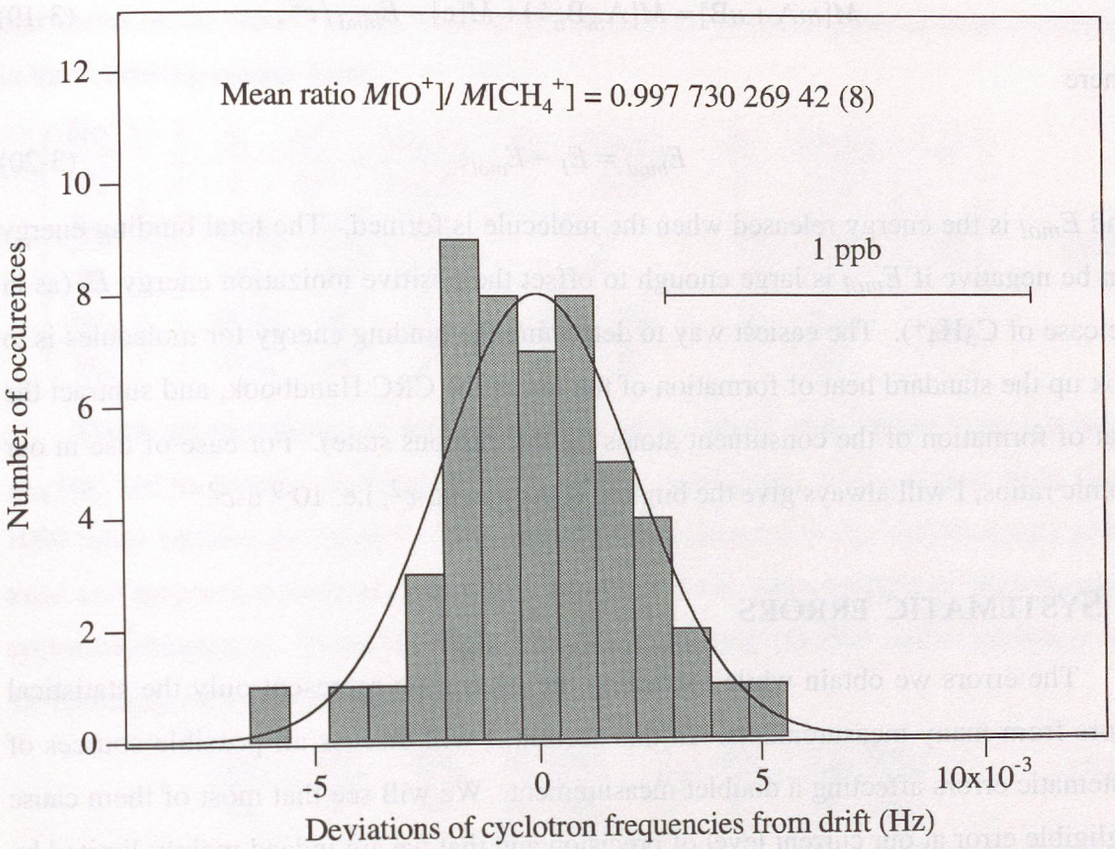

Fig. 3-8 Histogram of frequency deviations around drift. The residuals in the cyclotron frequency of both ions around the drift is accounted for in this histogram.

For a multiply charged atomic species A^{n+}, the only energy correction comes from the energy needed to ionize the atom n times. The mass of the neutral atom can be derived from:

$$M[A] = M[A^{n+}] + M[ne] - E_{bind}/c^2 . \tag{3-17}$$

The binding energy is just the sum of the n ionization energies,

$$E_{bind} = E_I + E_{II} + \ldots + E_n , \tag{3-18}$$

which is always positive. The energies can be looked up in a standard reference such as the CRC Handbook of Physics and Chemistry. We usually work with $n = 1$ and, in some cases, $n = 2$.

For a singly charged molecular ion $A_mB_n^+$, the energy corrections include the ionization energy and the chemical bond energy between the neutral atoms. Now we derive the neutral constituent masses from:

$$M[mA + nB] = M[A_m B_n^+] + M[e] - E_{bind}/c^2, \tag{3-19}$$

where

$$E_{bind} = E_I - E_{mol}, \tag{3-20}$$

and E_{mol} is the energy released when the molecule is formed. The total binding energy can be negative if E_{mol} is large enough to offset the positive ionization energy E_I (as in the case of $C_3H_4^+$). The easiest way to determine the binding energy for molecules is to look up the standard heat of formation of the ion in the CRC Handbook, and subtract the heat of formation of the constituent atoms (in the gaseous state). For ease of use in our atomic ratios, I will always give the binding energy in nu-c^2, i.e. 10^{-9} u-c^2.

4 SYSTEMATIC ERRORS

The errors we obtain while extracting the mass ratio represent only the statistical errors from many measurements. In this section, I will discuss all possible sources of systematic errors affecting a doublet measurement. We will see that most of them cause negligible error at our current level of precision and that we are indeed mainly limited by the random errors that arise from magnetic field fluctuations.

The systematic errors broadly fall into two categories - amplitude dependent and amplitude independent. The amplitude dependent ones are more easily studied because we can vary the strength of our drives to excite the modes to different amplitudes, at least in a narrow range. These are also the more dominant sources of error and we should be able to eliminate them by extrapolating to 0 amplitude. However, for a doublet, they cause few problems if both ions have the same amplitude.

Most of these errors have been studied in detail both in [BRG86] and [WEI88] from their effect on the ion's equations of motion. Here, I just give their results without showing that other similar effects cause much smaller shifts.

The three sources - B_2, C_4 and relativity

The largest sources of amplitude dependent error arise from the special relativistic mass shift, and the second order inhomogeneities in the trapping fields, usually denoted B_2 (magnetic bottle) and C_4 (the electrostatic term). All three effects give rise to a shift

that varies as the square of the mode amplitude. They can be expressed most compactly in the following matrix form:

$$\begin{pmatrix} \frac{\delta\omega_c'}{\omega_c'} \\ \frac{\delta\omega_z}{\omega_z} \\ \frac{\delta\omega_m}{\omega_m} \end{pmatrix} = \begin{pmatrix} -\frac{B_2}{2} - \frac{\omega_c'^2}{2c^2} + \frac{3\omega_m C_4}{2\omega_c' d^2} & \frac{B_2}{2} - \frac{3\omega_m C_4}{\omega_c' d^2} & -\frac{B_2}{2} - \frac{3\omega_m C_4}{\omega_c' d^2} \\ \frac{\omega_c' B_2}{4\omega_m} - \frac{\omega_c'^2}{4c^2} - \frac{3C_4}{2d^2} & \frac{3C_4}{4d^2} & \frac{B_2}{4} - \frac{3C_4}{2d^2} \\ \frac{\omega_c' B_2}{2\omega_m} - \frac{\omega_c'^2}{2c^2} - \frac{3C_4}{d^2} & -\frac{B_2}{2} + \frac{3C_4}{d^2} & \frac{B_2}{2} - \frac{3C_4}{2d^2} \end{pmatrix} \begin{pmatrix} \rho_c^2 \\ a_z^2 \\ \rho_m^2 \end{pmatrix} \tag{3-21}$$

There are two things to note from this matrix. Some of the terms have factors of ω_m/ω_c' (or its inverse) in front of the B_2 and C_4 coefficients which makes them about 1000 times smaller (or larger). Also, we are only interested in the modifications to the axial and magnetron frequency insofar as they affect the determination of the free space cyclotron frequency. From the expression for calculating the free space frequency and the hierarchy of trap frequencies, we obtain:

$$\frac{\delta\omega_c}{\omega_c} \approx \frac{\delta\omega_c'}{\omega_c'}, \quad \frac{\delta\omega_c}{\omega_c} = \frac{\omega_z^2}{\omega_c^2}\frac{\delta\omega_z}{\omega_z}, \text{ and } \frac{\delta\omega_c}{\omega_c} = \frac{\omega_m^2}{\omega_c^2}\frac{\delta\omega_m}{\omega_m}. \tag{3-22}$$

Our typical error in measuring the magnetron frequency is less than 0.05 Hz, which only causes a 0.002 ppb shift in the cyclotron frequency, so we never have to worry about corrections to it. Corrections to the axial frequency, on the other hand, are quite significant.

In order to estimate the magnitude of these shifts in the trap cyclotron frequency, we need to consider the mode amplitudes *during* the measurement. The axial mode is in thermal equilibrium with the detector for the entire duration of the 50 s integration. Hence its average amplitude is very close to the thermal RMS value. The magnetron mode, on the other hand, is cooled once at the beginning of the measurement and then left alone. Its amplitude can lie anywhere on the Boltzmann distribution with corresponding probability, with a mean again given by the thermal RMS value.

The cyclotron radius depends on the RF pulse strength that we use to excite it. We always adjust the drive pulse so that the resultant axial amplitude after a π-pulse maximally utilizes the harmonic region of the trap (in order to maximize our signal to noise ratio). Since the π-pulse exchanges the actions between the modes, the optimal cyclotron amplitude is given by:

$$\rho_{c,\mathrm{opt}} = \left(\frac{\omega_z}{\omega_c'}\right)^{1/2} a_{z,\mathrm{opt}} \,, \tag{3-23}$$

where $a_{z,\mathrm{opt}}$ is the usable axial amplitude independent of the ion and depends only on how well we can tune the trap. We will see later how we can experimentally ensure that $a_{z,\mathrm{opt}}$ is the same for all ions. The drive pulse only determines the average cyclotron radius. The actual radius is the vectorial sum of the drive amplitude ($\rho_{c,0}$) and the residual thermal amplitude ($\rho_{c,th}$) from the last cooling. The resultant thermal fluctuation in the radius, given by $\sqrt{2}\rho_{c,0}\rho_{c,th}$, causes a scatter in the frequency measurements due to the above effects, but the mean shift is determined only by $\rho_{c,0}$.

The shifts in the axial frequency that we are concerned about occur while detecting the signal after a π-pulse. During the axial ring-down into the detector, the cyclotron radius is at its π-pulse cooling limit, as is the magnetron radius, and their effects on the axial frequency are negligible. But what about the large axial amplitude? The above matrix does not really help us understand the dependence of the axial frequency on the axial amplitude; that is determined by the sensitivity of the maximum likelihood analysis to the presence of a small C_4 term. From computer simulations, we estimate that this

Table 3-2. Systematic errors for doublets. The first three expressions in the second column give the effect of the different corrections on ω_c' to lowest order in the cyclotron amplitude. The last row is the effect of the C_4 term on the axial frequency and thereby in calculating ω_c. The magnitude of these shifts (in ppb) is shown in the third column for measurements on an ion of mass 20 u and mass 40 u, for which we use $a_c \approx 0.017$ cm and $a_c \approx 0.024$ during the ω_c' measurement, respectively. The field inhomogeneities were shimmed to $B_2 = 0.4(2)\times10^{-6}$ cm^{-2} and $|C_4| \le 1.0\times10^{-4}$. The last column shows the advantage of working with a doublet. Limits on systematic error (in ppb) are given assuming that the values of a_c for the two species differ by 3%.

Correction	Form of $\Delta\omega_c/\omega_c$	Magnitude of $\Delta\omega_c/\omega_c$ (ppb)		Upper limit on systematic error	
		Mass 20	Mass 40	Mass 20	Mass 40
Magnetic	$-(B_2/2)a_c^2$	0.058	0.116	0.003	0.007
Electric	$\frac{3}{4}(C_4/d^2)(\omega_m/\omega_c')a_c^2$	0.022	0.173	0.001	0.010
Relativity	$-\frac{1}{2}(\omega_c'^2/c^2)a_c^2$	0.272	0.135	0.016	0.008
Electric (axial)	$(\omega_z^2/\omega_c^2)\delta\omega_z/\omega_z$	0.038	0.150	0.002	0.009

error is of the order of 10 mHz (see Chapter 2).

The resultant error budget for doublets is presented in Table 3-2.

Measuring B_2 and C_4 from axial shift

We usually measure the B_2 coefficient from the shift in the axial frequency as a function of cyclotron radius, sometimes called the bottle shift. This has the advantage that we can measure the axial frequency quite well even when the cyclotron radius is so large that we have to apply two or three π-pulses to cool it effectively (the anharmonic shift in the axial response at large amplitudes prevents the π-pulse from resonantly transferring all the energy from the cyclotron mode in one shot).

From the matrix, we see that the shift is actually due to a combination of terms involving B_2 and C_4. When the B_2 coefficient is large, as it is when we first start shimming the magnet after reenergizing it, we can neglect the effect of C_4 in a well tuned trap. But once we have the magnet shimmed, both coefficients might contribute equally and we cannot easily separate the two effects. What we measure then is an effective B_2 for the axial shift given by:

$$B_{2,\mathrm{eff}}(\mathrm{axial}) = B_2 - 6\frac{\omega_m}{\omega_c}\frac{C_4}{d^2}. \tag{3-24}$$

We can define a similar effective B_2 for the cyclotron frequency shift:

$$B_{2,\mathrm{eff}}(\mathrm{cyc}) = B_2 - 3\frac{\omega_m}{\omega_c}\frac{C_4}{d^2}, \tag{3-25}$$

which is unfortunately not the same as for the axial.

Our best method to separate the two coefficients is to measure the axial shift for a low mass ion, such as C^+, where the factor ω_m/ω_c' is 1.08×10^{-4} and makes the C_4 term negligible compared to even a small B_2. From this, we obtain a residual B_2 of about 0.4 G/cm^2, using a certain calibration for the strength of the driving field exciting the ion. Absolute calibration of the amplitude remains a poorly solved problem in our studies because we do not know the transfer functions of the cryo-electronics (after they are cooled) well enough to determine how hard we are driving the ion. Our best estimate is that the maximum usable axial amplitude, $a_{z,\mathrm{opt}}$ (introduced in Eq. 3-23), is 20% of the trap size, and this is the value used in calculating the above numerical estimate of B_2. However,

the calibration cancels when calculating the shift due to the above effects, because we can measure the coefficients only in terms of the applied drive at the source.

Equation 3-24 also allows us to obtain the effect of the guard ring voltage (V_{gr}) on C_4. The slope of $\delta\omega_z/\omega_z$ vs. ${\rho_c}^2$ gives us $B_{2,\text{eff}}$, which we can then study as a function of V_{gr}. Any change in the slope is due to the change in C_4. We characterize this by defining a quantity for our trap (after [BRG86]):

$$D_4 = V_r \frac{\partial C_4}{\partial V_{gr}}, \tag{3-26}$$

where V_r is the voltage on the ring electrode. Again this depends on the absolute amplitude calibration we use; instead we will define a new calibration independent quantity. We earlier defined the optimal axial amplitude independent of the ion's mass as $a_{z,\text{opt}}$ (Eq. 3-23). Then the quantity $D_4' = D_4\, a_{z,\text{opt}}^2 / d^2$ is a dimensionless constant that expresses the strength of our guard ring electrodes in terms of our usable absolute amplitude.

We can measure this quantity by studying the effective bottle shift as a function of V_{gr}. We obtain D_4 from the variation in $B_{2,\text{eff}}$ as follows:

$$\frac{\partial B_{2,\text{eff}}(\text{axial})}{\partial V_{gr}} = 6\frac{\omega_m}{\omega_c'}\frac{1}{d^2}\frac{\partial C_4}{\partial V_{gr}} = 6\frac{\omega_m}{\omega_c'}\frac{1}{d^2}\frac{D_4}{V_r}. \tag{3-27}$$

The axial shift versus the duration of the cyclotron excitation pulse (at a fixed drive amplitude) gives us $B_{2,\text{eff}}$ in $(\text{ms})^{-2}$. If the pulse duration to excite the cyclotron radius to $\rho_{c,\text{opt}}$ lasts t_p ms, then we can convert the measurement in $(\text{ms})^{-2}$ to a measurement in cm^{-2} by multiplying with $t_p^2/\rho_{c,\text{opt}}^2$ to yield:

$$D_4 \frac{a_{z,\text{opt}}^2}{d^2} = \frac{t_p^2}{6}\frac{\omega_c'^2}{\omega_m\omega_z} V_r \frac{\partial B_{2,\text{eff}}(\text{axial})}{\partial V_{gr}}. \tag{3-28}$$

Fig. 3-9 shows a plot of the measured $B_{2,\text{eff}}$ as a function of V_{gr} for a $C_3H_4^+$ ion (mass 40). From this we calculate D_4' to be 0.0056 (3).

Measuring D_4 from cyclotron shift

We can also measure the effect of V_{gr} on C_4 by measuring the shift in the cyclotron frequency (instead of the axial frequency) as we change the guard ring voltage. From the perturbation matrix (Eq. 3-21), we can write the shift when the cyclotron radius is equal to $\rho_{c,\text{opt}}$ as:

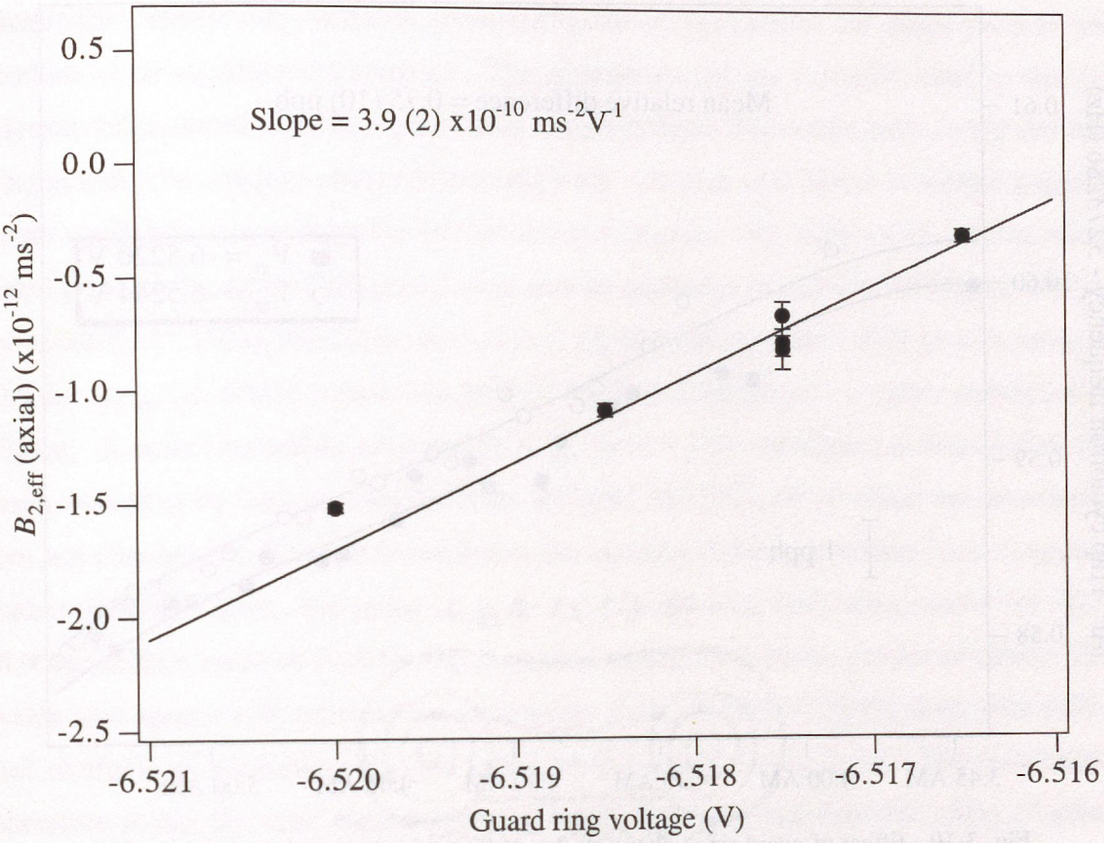

Fig. 3-9 Effect of guard ring on C_4. The axial frequency shift changes as we change the guard ring voltage. The slope gives D_4' of 0.0056 (3) using $t_p = 20$ ms.

$$\delta\omega_c' = \frac{3}{2}\omega_m \frac{C_4}{d^2}\rho_{c,\mathrm{opt}}^2 = \frac{3}{2}\frac{\omega_m\omega_z}{\omega_c'}\frac{C_4}{d^2}a_{z,\mathrm{opt}}^2. \tag{3-29}$$

By measuring the cyclotron frequency at different values of V_{gr}, we obtain:

$$\frac{\partial\omega_c'}{\partial V_{gr}} = \frac{3}{2}\frac{\omega_m\omega_z}{\omega_c'}\frac{\partial C_4}{\partial V_{gr}}\frac{a_{z,\mathrm{opt}}^2}{d^2}, \tag{3-30}$$

so that,

$$D_4\frac{a_{z,\mathrm{opt}}^2}{d^2} = \frac{2}{3}\frac{\omega_c'}{\omega_m\omega_z}V_r\frac{\partial\omega_c'}{\partial V_{gr}}. \tag{3-31}$$

We have measured this shift with both an Ar^+ ion (mass 40) and an Ar^{++} ion (mass 20). Shown in Fig. 3-10 is a plot of the cyclotron frequencies of Ar^+ measured on the same night with guard ring settings that differed by 2.4 mV. From this, we obtain the

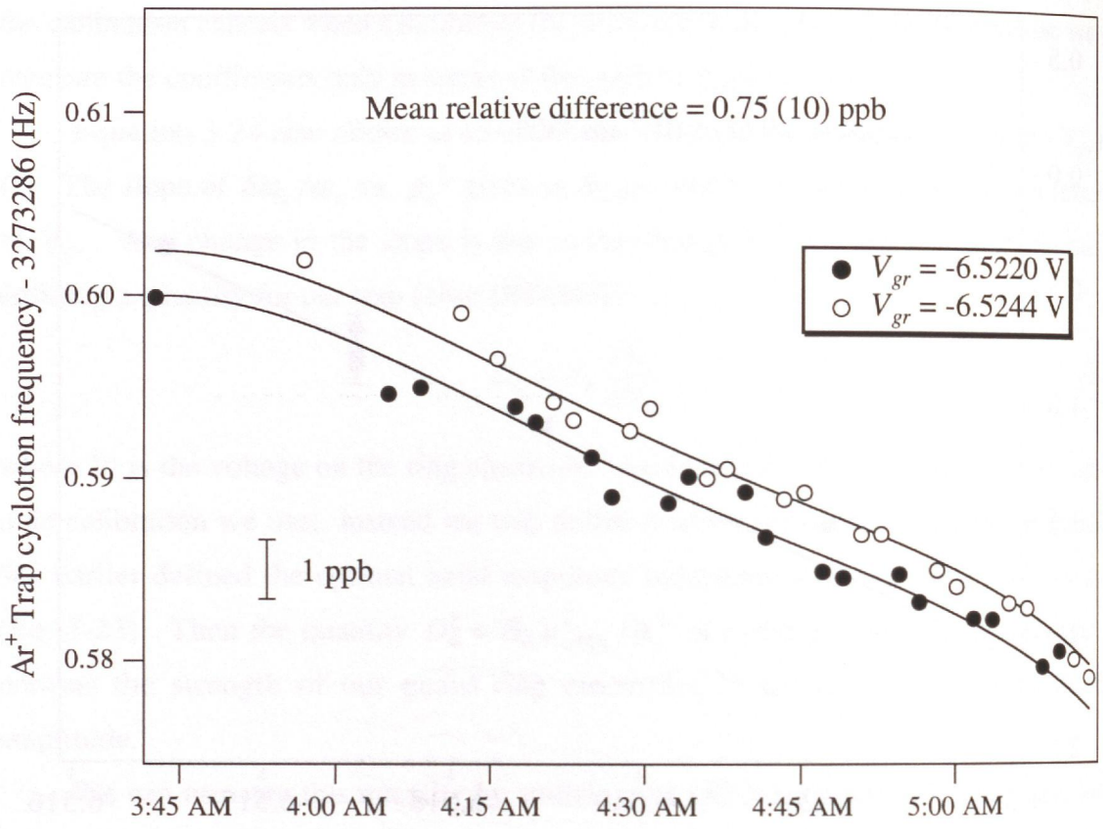

Fig. 3-10 Effect of guard ring voltage on the cyclotron frequency of an Ar^+ ion. The solid line is a 4th order polynomial fit to the field drift.

value of D_4' as 0.045 (6), while the Ar^{++} measurement yields a value of 0.033 (7). This is to be compared with the value of 0.0056 obtained from the axial measurement.

The inconsistency with the axial value could be due to several reasons. The most likely explanation is that the guard ring also changes some higher order electrostatic term (C_6 or C_8) which has different effects on the axial and cyclotron frequencies. Then what we are measuring when we change the guard ring is mostly the change in the higher order coefficient. Another possibility is that the axially measured D_4' is incorrect. The axial measurement is complicated by the fact that shifts in ω_z can be caused by changes in the ring voltage, even though we have been careful to avoid this effect. The value of D_4' measured from the cyclotron shift seems more reliable because it has been measured at different masses (20 and 40) with consistent results. Of course, this is also the value we care about for our cyclotron frequency measurement.

What are the implications of this high value of D_4'? For one thing, it means that we are probably underestimating the size of our electrostatic shifts on the cyclotron

frequency. This is not a problem at our current level of precision, but might become important as we increase the accuracy. The dependence of the cyclotron shift on the cyclotron radius should also be studied more carefully since that would help clarify our suspicion that it is a higher order electrostatic term. A clear clue that it is indeed a higher order correction comes from the following consideration. The value of D_4 can be calculated from the location of the guard rings and the geometry of our trap [WEI88, p 293] to be about 0.11. Using this value, the value of D_4' from the cyclotron shift gives a value of 0.6 for $a_{z,\mathrm{opt}}/d$, which means that 60% of the trap is harmonic - a rather unbelievable figure. A more reasonable estimate for $a_{z,\mathrm{opt}}/d$ is 0.2 (as mentioned earlier) which has been arrived at by various considerations [COR90, BOY92], all of which are convincing but not conclusive. Using this number in the cyclotron shift, we obtain $D_4 = 1$, again a rather unlikely figure. But using $a_{z,\mathrm{opt}}/d = 0.2$ in the axial shift measurement of $D_4' = 0.0056$ yields a value of 0.14 for D_4, in modest agreement with the predicted value. This value also agrees with previous measurements of D_4 [WEI88, COR90] done with different methods of estimating C_4, but using similar values for $a_{z,\mathrm{opt}}/d$. The conclusion therefore is that the axial measurement probably accurately estimates the effect of guard ring voltage on C_4, but the cyclotron shift is caused by a dominant higher order term.

Transfer functions from avoided crossing

As seen from Table 3-2, the shifts produced by the above effects can be as large as 0.2 ppb. We can neglect systematic errors in the ratios calculated from cyclotron frequencies measured at a finite amplitude only if both ions of a doublet have the same amplitude. One way to ensure this is to use the same drive voltage for the two ions and to design the filters and electronics to have a flat transfer function in the range of interest. We can directly measure the strength of the coupling drive at the ion's location for a given source voltage from the avoided crossing splitting. Of course, we are interested in the transfer function at the cyclotron drive frequency which is 160 kHz away. But if the splitting is the same for both ions, it is quite unlikely that the transfer function has a high Q resonance. For example, a 2% difference in the measured coupling drive strengths at the frequencies for a doublet (with $\Delta m/m$ of 1×10^{-3}) translates to a transfer function Q of less than 5.

We can measure the avoided crossing splitting to less than 2%. Within this error, we always find the same value for the two ions. Therefore, we conservatively estimate that the amplitudes for the two ions are the same to 3%, giving the error budget in Table 3-2. We do not care about the absolute amplitude for the B_2 and C_4 shifts because these inhomogeneities are measured only as a function of applied drive. However, this is not true for the relativistic shift which depends on the actual velocity of the ion. Even with a worst case assumption that we are off by a factor of two in our amplitude calibration, special relativity does not pose a systematic problem at the current level of precision for ions with a mass greater than 10 u. Such a large amplitude may however cause an unacceptable relativistic shift for our proposed mass 3 measurement.

We also use the avoided crossing splitting to make sure that the cyclotron radius is close to the optimal value (Eq. 3-23) for all ions. Then we can be certain that the axial amplitude after the π-pulse is the same $a_{z,\mathrm{opt}}$ independent of the ion's mass. The way we achieve this is to first adjust the coupling drive so that the avoided crossing splitting is always close to 2 Hz (this also means that the duration of the π-pulse is close to 250 ms). From [COR90], we see that the quadrupole field strength (E_p)in the trap for a constant splitting (V) scales as:

$$E_p = \frac{2m\sqrt{\omega_z \omega_c'}}{q} V \sim m\sqrt{\omega_z \omega_c'}\,. \tag{3-32}$$

For the same source voltage, the dipole field strength (E_d) at the driving frequency (160 kHz away) should be proportional to E_p with a factor that depends only on the geometry of the guard rings, as long as there is no appreciable change in the RF transfer functions. Using this driving field, if we excite the cyclotron motion with a drive pulse that lasts t_p ms, the resulting radius is given (from the resulting velocity) as:

$$\frac{qE_d t_p}{m} = \omega_c' \rho_c \;\Rightarrow\; \rho_c = \frac{qE_d t_p}{m\omega_c'} \sim t_p \sqrt{\frac{\omega_z}{\omega_c'}}\,. \tag{3-33}$$

Thus, the axial amplitude after the π-pulse (see Eq. 3-23) is independent of mass, as long as we keep t_p constant. In our trap, we obtain the optimal cyclotron radius $\rho_{c,\mathrm{opt}}$ with a 20 ms pulse when the splitting is 2 Hz.

Patch induced shifts in position

The most important source of amplitude independent error arises from shifts in the equilibrium position of the ion as a function of the applied voltage. The mean position of the ion (or the electrical center of the trap) is determined by the point at which the applied field cancels the stray fields due to charged patches adsorbed on the electrodes or work function differences in the leads. The applied field changes as we change the trap voltage and therefore the two ions are not measured at the same location. If there are any linear gradients in the magnetic field, this will cause a systematic difference in the magnetic field at the site of the two ions, giving an error in the measured ratio.

We collectively refer to the sources of stray fields as patch effects since these potentials tend to change with time, which we can best attribute to drifts in the adsorbed patches. We have several ways of measuring the effective size of these patches. They can first of all produce an offset in the ring and guard ring voltages. The ring voltage to make the ion resonant with the fixed detector frequency is linear with respect to the mass of the ion and should pass through the origin as the mass goes to 0. Any offset of the voltage is (probably) due to a symmetric patch on the endcaps combined with a patch on the ring electrode. A similar effective patch on the guard rings can be measured from the tuned guard ring voltage with respect to mass.

Fig. 3-11 shows the tuned voltages obtained on the same day for two ions, Ar^+ and Ne^+. From the offsets, we find that the ring patch (V_{rp}) is only about 0.6 mV while the guard ring has a patch (V_{grp}) of 135 mV. The patch on the ring potential is considerably smaller than it used to be with our earlier traps probably because of our increased care in keeping a clean vacuum. The slopes of the lines in the figure give us further information about the trap. From Chapter 1 (Eq. 1-7), we see that the ring voltage to mass relationship is:

$$V_r - V_{rp} = -\frac{d^2 \omega_z^2}{e} m, \tag{3-34}$$

where the negative sign appears because we want to trap positive ions. From the measured slope, we obtain $d = 0.54958\ (1)$ cm. This value has remained stable to better than a part in 10^4 over a few months, even as the patch effects shift. It is also in good agreement with the value of $d = 0.5490\ (8)$ cm specified for machining, indicating that there

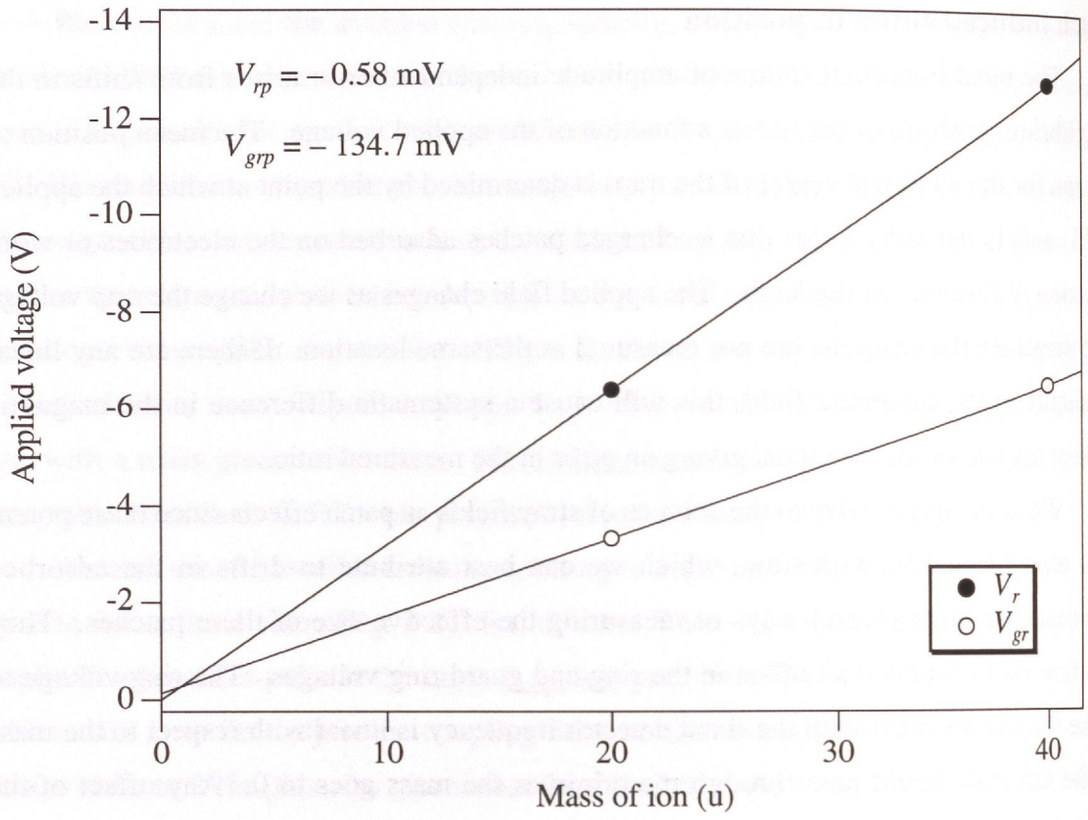

Fig. 3-11 Patch effect offsets in trap voltages. The tuned ring and guard ring settings are shown as a function of the mass of the ion. The intercept with the y axis indicates the patch effect offset. The slopes depend on the trap parameters.

are no serious machining or assembly errors. The location of the guard rings is chosen so that the applied voltage on them is nominally half the ring voltage; i.e. the ratio

$$\alpha = \frac{V_{gr} - V_{grp}}{V_r - V_{rp}} \tag{3-35}$$

should be close to 1/2. The value we measure from the graph is 1/2.0046.

The patches that can cause systematic errors have to be antisymmetric with respect to the endcaps (to produce a shift in the axial position). If the antisymmetric patch is V_{Ap}, the shift in position it produces in our trap is given by [WEI88, p 34],

$$\Delta z = 0.2 \frac{V_{Ap}}{V_r} \text{ cm.} \tag{3-36}$$

We have measured the size of the axial antisymmetric patch to be 22 mV by applying known offsets between the endcaps (section 4-1). This shift is actually not a problem since we can apply an external offset to null it. But there can be similar sized shifts in the

radial plane which we cannot probe or null. We will see in the next chapter that such patches pose a fundamental limitation to measuring non-doublet ratios. However, for doublets, the applied voltage for the two ions is so close to being equal that there is no appreciable error. For example, a 22 mV patch with a 0.1 G/cm field gradient causes only a 2 ppt error in the $M[O^+]/M[CH_4^+]$ ratio (which has a $\Delta m/m$ of $2.3\text{x}10^{-3}$).

Other amplitude independent sources

As mentioned in Chapter 1, the coupling to the detector can pull the axial frequency of the ion. In the weak coupling limit, i.e. when the induced damping time for the ion is much longer than the damping time of the coil, the pulling shows a dispersion relation with the detuning δ between the ion's axial frequency and the coil frequency:

$$\Delta\omega_z = \frac{\gamma_0\gamma_i}{4}\frac{\delta}{\delta^2+\gamma_0^2/4}, \tag{3-37}$$

where γ_0 is the coil damping constant and γ_i is the ion's damping constant. We always operate close to resonance so that the detuning is very small compared to the coil width, under these conditions the shift linearizes to,

$$\Delta\omega_z = \frac{\gamma_i}{\gamma_0}\delta. \tag{3-38}$$

For a worst case detuning of 0.5 Hz, the shift in the axial frequency for a mass 20 ion is only 9 mHz, which produces a shift in the cyclotron frequency of 0.032 ppb. Moreover, though we might be detuned from the coil by 0.5 Hz, we are rarely detuned differentially for one ion and not for the other. So the effect on the ratio is even smaller.

Another potential source of error is the presence of impurity ions during the measurement. In general, we feel fairly confident that we can get rid of all impurity ions since we have been able to keep an ion in the trap for days when we choose to do so. The long lifetime of the ions also shows us that the background pressure is low enough (we estimate 10^5 atoms/cm^3) that there are negligibly few collisions with neutral atoms during a measurement.

It is however possible that the production procedures for the two members of a doublet will have dramatically different probabilities for producing bad ions and the occasional one that slips by will always be for one species. If the perturbation on the cyclotron frequency is not strong enough for us to detect it while analyzing the data, then

the perturbed measurement should still produce a frequency that deviates from the others. In our ratio extraction routine, this will show up as a skewed distribution for one species. This is one advantage of looking at the histogram of residuals for the two ions separately. If one of them is significantly skewed, we would suspect a systematic difference in some source of perturbation. So far, we have never detected any and can safely claim that if any such effect occurs, it is well below our level of precision.

Conclusions

All the sources of systematic error presented so far do not limit us even at the 0.01 ppb level when dealing with doublets. The statistical error in the ratio extracted from the data far exceeds any systematic shifts and comes, we believe, primarily from the magnetic field fluctuations. But it is important to consider other sources of error that might limit us if we can eliminate field fluctuations. Fluctuations in the voltage box, slightly better than a part in 10^7 now, will limit the precision per 1-minute measurement at about 0.03 ppb. More important are the thermal fluctuations in the cyclotron amplitude after sideband cooling. The shot to shot fluctuation in the cyclotron frequency from this will limit us at 0.05 ppb, unless we can find better ways of cooling the cyclotron mode to lower temperatures. We will describe one way of reducing the amplitude fluctuations using a squeezing technique in Chapter 6.

4 MASS COMPARISON OF NON-DOUBLETS

The precision method presented in the last chapter works quite well for doublets. Unfortunately, we cannot experimentally test the reliability of this method because there are no "calibrated" ratios for doublets. Comparing an ion to itself is in some sense a calibrated value of unity, but is not a very strong test of systematic errors since we might be making the same mistake each time.

This shortcoming disappears when we consider a pair of ions whose cyclotron frequency ratio is not close to unity, referred to as non-doublets. There exist several non-doublets whose ratio can be calculated to 1 ppt precision essentially because the mass of the main constituent cancels. Thus, for example, the ratio $M[N_2^+]/M[N^+]$ should be exactly 2 independent of the mass of N, except that we have to correct for the missing electrons and some binding energies. However, these corrections are well known, so we can predict the ratio very precisely.

In this chapter, we will see that the PNP technique fails when we try to measure non-doublet ratios. The largest source of error turns out to be not the type of amplitude dependent effects that we found were dominant for doublet measurements, but the patch induced shift in the equilibrium position. Therefore, we have developed a new resonance technique that allows us to measure the cyclotron frequency of the two ions with the same trap voltage applied. With this improvement, we can test our measurement errors against the known non-doublet ratios and also measure the masses of atoms in atomic units by direct comparison to a C^+ ion.

The error budget for non-doublets is quite different from the one for non-doublets because the trap frequencies of the two ions are so disparate. The error analysis and our

results on non-doublets are summarized in a paper submitted to Physical Review Letters, which I append to this chapter.

1 PREVIOUS ATTEMPTS

We had tried two times in the past to study our systematic errors by measuring the N_2^+ vs. N^+ non-doublet ratio. Both times we obtained a much larger deviation from the predicted result than we had expected. If the source of this error were indeed the shift in equilibrium position of the ion with different applied voltages, then this discrepancy poses no problem for the doublet measurements. But we have to prove this result before drawing such a conclusion.

Predicted value for $M[N_2^+]/M[N^+]$

It is easy to see that the expected value for this ratio is close to 2. As we step through the following brief calculation, we will see that the corrections are known well enough that the final error is of order 1 ppt.

In the notation introduced in Chapter 3, we can write the masses of the atomic and molecular ion as:

$$\begin{aligned} M[N^+] &= M[N] - M[e] + E_{bind,N}/c^2 \ , \\ M[N_2^+] &= M[2N] - M[e] + E_{bind,N_2}/c^2 . \end{aligned} \tag{4-1}$$

Therefore the expected ratio is:

$$\begin{aligned} R_{N_2/N} &= \frac{M[2N] - M[e] + E_{bind,N_2}/c^2}{M[N] - M[e] + E_{bind,N}/c^2} \\ &= 2\left(\frac{1 - M[e]/M[2N] + E_{bind,N_2}/c^2 M[2N]}{1 - M[e]/M[N] + E_{bind,N}/c^2 M[N]}\right) \\ &\approx 2\left(1 + M[e]/M[2N] + \left(E_{bind,N_2} - 2E_{bind,N}\right)/c^2 M[2N]\right) . \end{aligned} \tag{4-2}$$

We see that the leading correction comes from the mass of half an electron relative to the mass of N. The electron mass is known to two parts in 10^8 and the nitrogen atom is 26000 times heavier, therefore the error from this correction is less than 1 ppt. Similarly, the binding energies are known to 0.01 eV while the mass of N is 14 GeV, and

again the error is less than 1 ppt. Using $E_{bind,N}$ = 15.599 nu-c^2 and E_{bind,N_2} = 6.151 nu-c^2, we find that the expected ratio is 2.000 039 175 424 (1).

First attempt

When we first measured this ratio in 1990, we obtained a value that differed from the expected value by 3 ppb. The amplitude dependent errors that we considered for doublets cause, of course, a much more serious error for non-doublets. This is because the frequencies for the two ions are not nearly the same and the shifts do not cancel to first order. Furthermore, the optimal cyclotron amplitudes for the two ions are different and the magnitude of the shifts are not the same. However, when the size of these shifts was measured carefully, we found that they should be much less than 1 ppb; not quite large enough to cause the discrepancy we observed.

Our best guess at the time was that this was due to the change in the magnetic field at the ion's location resulting from the patch induced shift in the position of the ion, as discussed in the last chapter. With this non-doublet, we have to apply about 9 V to bring N_2^+ into axial resonance with the detector, while we only need 4.5 V for N^+. Therefore, the displacement from the geometric center due to surface potentials is twice as large for N^+ as for N_2^+ (see Eq. 3-36). We estimated the size of the antisymmetric patch potential in the axial direction to be about 30 mV, which results in a difference of 5.4 μm between the positions of N^+ and N_2^+. Combined with our linear field gradient of 2×10^{-6} cm^{-1}, this should cause a shift of order 2 ppb, consistent with our measurement.

Nulling axial offset in position

We can actually measure the axial patch offset by studying the shift in the axial frequency as a function of the offset voltage applied to the lower endcap. When we apply a voltage to the lower endcap, we introduce a cubic term in the electrostatic potential which causes a parabolic shift in the axial frequency [WEI88, p 300]. The minimum of this parabola indicates the electrical center of the trap. As shown in Fig. 4-1, we found that the center was 22 mV off from 0 applied potential. We feel confident that this is indeed a patch offset from the fact that it does not scale with the trap voltage; we obtain the same value with both an N^+ ion and an N_2^+ ion. The shape of the parabola depends on the size of our trap and agrees quite well with the predicted value [BOY92].

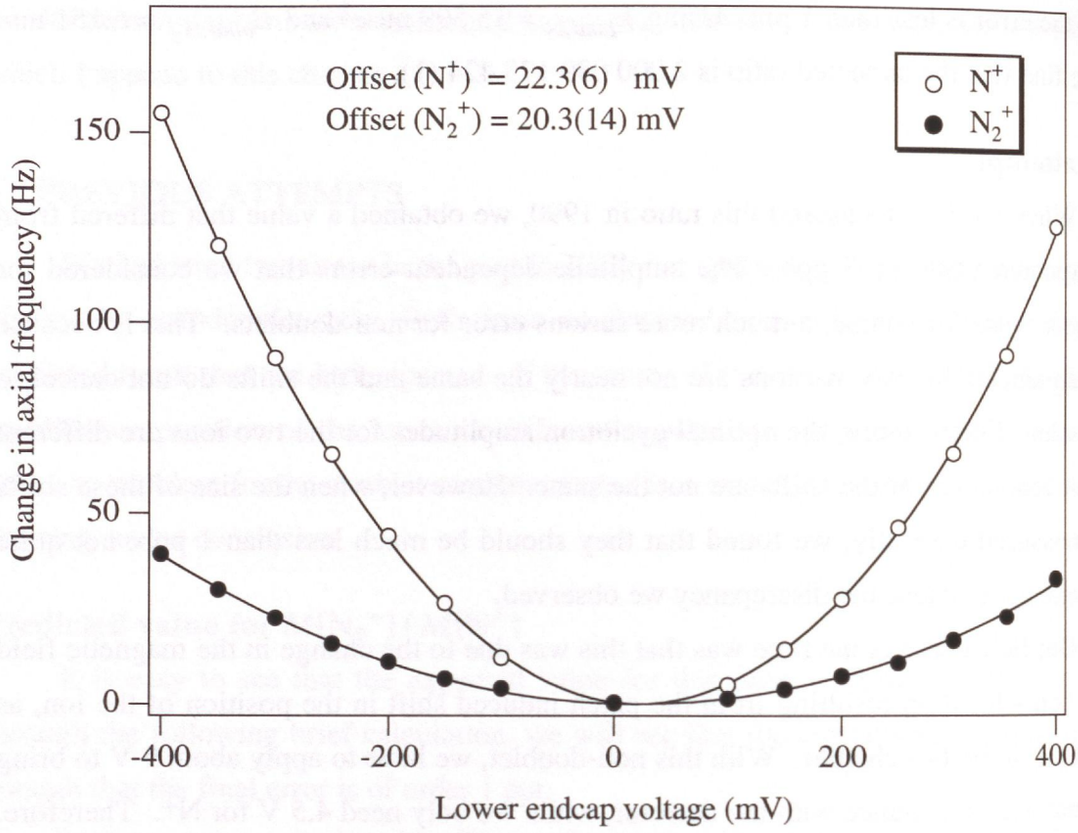

Fig. 4-1 Axial patch effect measurement with N^+ and N_2^+. The axial frequency shifts quadratically with the applied voltage on the lower endcap. The minimum of the parabola indicates the electrical center of the trap and should lie at 0 applied voltage if there were no patch effect offset.

The 22 mV patch offset is close to our earlier estimate of its size. So we were hoping to substantially reduce our error when we repeated the N_2^+ vs. N^+ measurement, this time with an externally applied 22 mV offset on the lower endcap to null the patch effect shift in axial position. But, as shown in the figure in our paper, the systematic error remained. The most likely explanation, and in retrospect something we should have thought of in the first place, is that there are radially asymmetric potentials that also shift the position of the ion. We cannot measure this in our azimuthally symmetric trap, but it is likely that they are of the same order as the axial patch and should cause similar error (assuming our linear gradient in the radial direction is as large).

2 SEPARATED OSCILLATORY FIELDS TECHNIQUE

The obvious solution to the above problem is to measure the cyclotron frequency of both ions with exactly the same voltage on the trap. Then we can be certain that the frequencies are measured at the same location. But now the two ions have axial frequencies that are about 50 kHz apart and cannot both be seen with our narrow band (5 Hz wide) detector. We can use our PNP technique on one ion by adjusting the trap voltage so that it is resonant with the detector. For the other ion, we have to measure the cyclotron frequency when its axial motion cannot directly be detected, i.e. it is in a non-resonant or "dark" trap. We have solved this by using a variant of the Ramsey separated oscillatory fields (SOF) method.

The basic idea is to store the cyclotron resonance information in the cyclotron *amplitude* with the SOF method while the ion is invisible to the detector, and then read out this amplitude with a π-pulse after the trap voltage is adjusted to bring the ion back into axial resonance with the detector (the amplitude should not change when the voltage changes). The SOF technique works by giving two identical cyclotron excitation pulses from a signal generator, separated by a time T, so that the final amplitude represents the interference between the driving frequency and the ion's natural frequency.

Measuring the trap cyclotron frequency

The actual SOF procedure to measure the trap cyclotron frequency is conceptually simpler than the PNP technique but takes somewhat longer because it is not phase sensitive. To see how it works on an N^+ ion (measured with the trap voltage at 9V, which brings an N_2^+ ion into resonance with the detector), we will refer to Fig. 4-2 which shows the amplitudes of the drives and the ion modes at different times. As for PNP, the cyclotron mode is coherently excited by the drive pulse so that, at the end of the pulse, it has an amplitude determined by the drive strength, and a phase that is shifted from the driving phase by a fixed transfer function phase ϕ_{tf}.

Mapping the x-y plane of the cyclotron motion into the complex domain, we find that its complex amplitude (**C**) at the end of the pulse is given by:

$$\mathbf{C} = A\exp\left[i\left(\phi_d(t_0) + \phi_{tf}\right)\right], \tag{4-3}$$

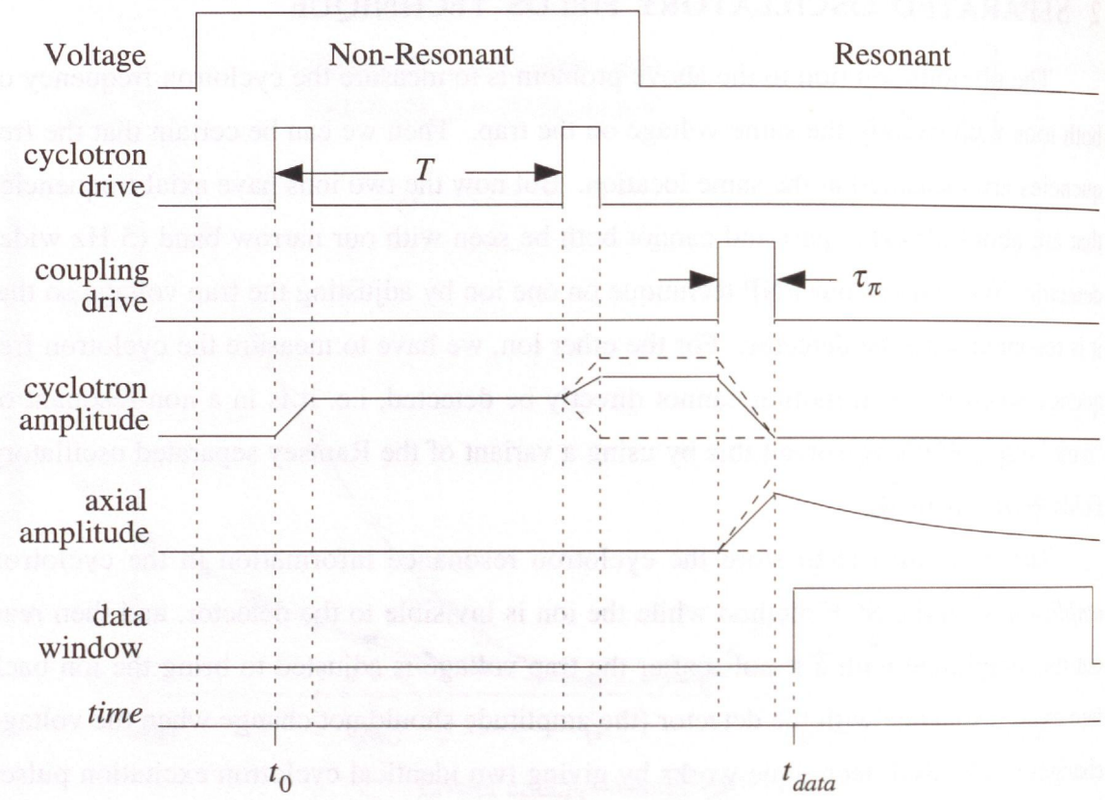

Fig. 4-2 Driving sequence for the SOF measurement (not to scale). The voltage settings are selected for driving (non-resonant) and coupling to the axial (resonant). The cyclotron amplitude depends on the separation time between the pulses T, but is bounded between 0 and $2A$. Except for T, the timing of all the other pulses is non-critical.

where $\phi_d(t_0)$ is the initial phase of the drive generator. The second pulse comes after a time T, when the phase of the cyclotron motion and drive source have advanced to:

$$\begin{aligned} &\text{Drive generator} \quad \phi_d = \omega_d T + \phi_d(t_0) \\ &\text{Cyclotron mode} \quad \phi_c = \omega_c' T + \phi_d(t_0) + \phi_{tf} \end{aligned} \tag{4-4}$$

If the cyclotron mode had not been excited earlier, a second pulse identical to the first one would give the cyclotron mode the same amplitude as in (4-3), except that the phase would be shifted by $\omega_d T$. Since the cyclotron mode already has a complex amplitude, the final amplitude is the vectorial sum of the two:

$$\begin{aligned} \mathbf{C} &= A\exp\left[i\left(\omega_c' T + \phi_d(t_0) + \phi_{tf}\right)\right] + A\exp\left[i\left(\omega_c' T + \phi_d(t_0) + \phi_{tf}\right)\right] \\ &= A\exp\left[i\left(\phi_d(t_0) + \phi_{tf}\right)\right]\left\{\exp(i\omega_c' T) + \exp(i\omega_d T)\right\} \\ &= \mathbf{A}'\left\{\exp(i\omega_c' T) + \exp(i\omega_d T)\right\} \end{aligned} \tag{4-5}$$

where **A'** is defined to subsume all the uninteresting phases. The term inside the curly brackets can be simplified using trigonometric identities as follows.

$$\begin{aligned}
&\left\{\exp(i\omega_c' T)+\exp(i\omega_d T)\right\} \\
&=\cos(\omega_c' T)+i\sin(\omega_c' T)+\cos(\omega_d T)+i\sin(\omega_d T) \\
&=2\cos\left(\frac{\omega_c'+\omega_d}{2}T\right)\cos\left(\frac{\omega_c'-\omega_d}{2}T\right)+2i\sin\left(\frac{\omega_c'+\omega_d}{2}T\right)\cos\left(\frac{\omega_c'-\omega_d}{2}T\right) \\
&=2\cos\left(\frac{\omega_c'-\omega_d}{2}T\right)\exp\left(i\frac{\omega_c'+\omega_d}{2}T\right)
\end{aligned} \tag{4-6}$$

From this we obtain the resultant complex amplitude after the two pulses.

$$\mathbf{C}=2A\cos\left(\frac{\omega_c'-\omega_d}{2}T\right)\exp\left[i\left(\frac{\omega_c'+\omega_d}{2}T+\phi_d(t_0)+\phi_{tf}\right)\right] \tag{4-7}$$

This equation shows that the resonance information is stored in the magnitude C of the complex amplitude of the cyclotron motion:

$$C=2A\left|\cos\left(\frac{\omega_c'-\omega_d}{2}T\right)\right| \tag{4-8}$$

As we vary the separation time T, the amplitude shows a fringe pattern at half the difference between the ion's natural frequency and the driving frequency. The disadvantage with using a phase insensitive detection scheme, i.e. only measuring the amplitude of the cyclotron motion, is that the resonance appears as a rectified cosine curve and the fringes appear at twice the rate at which the phase is wrapping. If we had a phase sensitive detector, then we would not need the second pulse at all, we just read the phase after a time T. This is indeed what our PNP technique does.

There are some nuances to the actual measurement. First of all, the frequency of the rectified beat pattern is the difference between ω_c' and ω_d, but it does not tell us what the sign of this difference is. We determine this unambiguously by deliberately detuning the drive 2 Hz below the expected cyclotron frequency, which we know to 0.1 Hz from the avoided crossing. Then we know that the fringes appear at about 2 Hz, what we want to measure is whether it is exactly 2.049...? A typical measurement is shown in Fig. 1 of our paper.

A measured point on the fringe pattern has the steepest constraint on the frequency when it lies close to the origin, i.e. the detected amplitude is near 0 (destructive

interference). If the amplitude lies close to the maximum (constructive interference), then it does not constrain the frequency very well at all. But this poses a problem for us. When the amplitude is close to 0, we have the lowest signal to noise ratio and the parameter estimation algorithm may lock to the largest noise peak nearby. Furthermore, even though the slope of amplitude vs. frequency is largest near 0, it is also easiest to miss a fringe because the two points with the same amplitude on neighbouring fringes are closest to each other. When the amplitude is maximum, our signal is at its highest, the next fringe is farthest away, but the determination of the frequency is poorest. We therefore like to optimize the separation time T so that the measured points lie near the 45° phase (or have $1/\sqrt{2}$ of the peak amplitude).

Of course, we cannot *a priori* predict where our points are going to lie (otherwise we would not be doing the measurement!), so we have to take two points close to each other. We do know that the unrectified fringe frequency is approximately 1 Hz, therefore if we take two points 150 ms (54° in phase) apart, it is very likely that one of them has near optimal amplitude.

We measure the cyclotron amplitude by applying a π-pulse to convert it into axial motion, but only after we change the trap voltage to 4.5 V, which makes N^+ resonant with the detector. The voltage changes adiabatically and results in a small change in the cyclotron amplitude (because the trap cyclotron frequency changes), but that is below our detection limit and, in any case, only rescales the overall amplitude of the fringe pattern. We optimize our signal to noise ratio for the 45° points by adjusting the drive pulse so that the axial amplitude after a π-pulse on these points is $a_{z,\mathrm{opt}}$ (defined in Chapter 3). This means that the peak cyclotron amplitude ($2A$) is $\sqrt{2}\rho_{c,\mathrm{opt}}$, yielding:

$$A_{\mathrm{opt}} = \rho_{c,\mathrm{opt}} / \sqrt{2} \,. \tag{4-9}$$

As we will see later, this happens to be exactly the right amplitude for canceling the effect of special relativity when measuring the N_2^+/N^+ ratio, or any ratio close to 2.

As in the PNP technique, we build up the frequency precision by increasing the integration time in steps. Instead of counting phase wraps, we now count fringes. But the fringes repeat after every 180°, so we can increase T only by a factor of 2 or so each time if we are not to lose count. Also, we have to take 2 points near each value of T. This

makes the whole measurement somewhat longer and it takes about 10 minutes to finish a sequence of SOF pulses with three 50 s integrations.

Obtaining free space cyclotron frequency

Converting the trap cyclotron frequency to a free space frequency is a little more indirect than in the PNP technique. This is because we cannot measure ω_z for N^+ during the trap cyclotron frequency measurement (at 9V); we only know its axial frequency in a resonant trap (4.5 V). We could scale the measured axial frequency with the square root of the voltage ratio between the resonant and non-resonant trap if we knew all the patch effect offsets and could measure the voltage with better than part in 10^7 precision!

Lacking this technology of the future, we use the measured axial frequency of N_2^+ as a sensitive voltmeter to infer the axial frequency of N^+. That is, we use the relation:

$$\omega_{z,N} = \sqrt{\frac{M[N_2^+]}{M[N^+]}}\,\omega_{z,N_2}\,. \tag{4-10}$$

In this specific case, of course, we know the exact mass ratio to use. In a general case, we can use the mass values from the standard table to determine the ratio since the required precision for ω_z is less than a part in 10^8. Once we measure the final ratio (to much higher precision), we can check back to see that using the more precise ratio makes no difference to the measured value.

The axial frequency of the N_2^+ ion is, of course, not measured at exactly the same time as the cyclotron frequency measurement on N^+. This is a potential source of concern if the voltage is drifting significantly with time (we show in our paper that this is not really a problem right now). For a given N^+ measurement, we always use the axial frequency from the previous measurement on N_2^+. We could try to eliminate any voltage drift by averaging the axial frequencies of the previous and next N_2^+ measurements, but we feel that this introduces unwanted correlations between successive measurements on N^+.

There is one other technical point worth mentioning here. It turns out that the axial frequency for N_2^+ is measured at a voltage that is slightly different from the one used during the N^+ measurement, so we have to correct the above expression for this. The reason for this is the following. The voltage on the trap is switched with a computer controlled digital relay that chooses between the two channels on the voltage box, one

adjusted for resonating N^+ and the other for N_2^+. Since we cannot adjust the manual potentiometers with sufficient precision so that each ion's axial frequency is exactly centered on the detector response, the computer supplies a single small offset (~50 μV) to the set voltages. The problem is that this offset will generally be different for N^+ and N_2^+. We can change the digital state of the channel select relay in a well timed manner, but changing the analog output of the computer with precise timing is not easily programmed. Therefore, during the entire measurement on N^+, we leave the computer offset at the value needed to center N^+ when applying the π-pulse. But this means that there is a small difference in the voltages used for N^+ and N_2^+ arising from the difference in the computer generated offset (~15 μV). However, the axial frequency difference due to this (~200 mHz) can be determined to better than 1 mHz and does not present a problem.

Typical non-doublet run

A run with non-doublets is only slightly different from one with doublets. The two channels in the voltage box are first tuned for the two kinds of ions. The ion on which we use the PNP technique is then measured exactly as before on one channel.

For the ion measured in a non-resonant trap, we first set the trap to the resonant voltage. Then we find and cool the magnetron and cyclotron modes. We use the avoided crossing estimate of the trap cyclotron frequency to determine the free space cyclotron frequency (using Eq. 1-11). We now scale the axial frequency with the square root of the mass ratio to find the ion's axial frequency in the non-resonant trap, and use this to find the trap cyclotron frequency in the non-resonant trap. The frequency of the SOF drive pulses is then set at 2 Hz below this estimate. For each SOF sequence, we cool the cyclotron motion with a π-pulse on the resonant channel of the voltage box, select the opposite channel and allow the voltage to stabilize, apply the two SOF pulses, select the resonant channel again, and finally apply the π-pulse to determine the cyclotron amplitude.

Due to the longer time for each SOF measurement, we usually get only 10 switches between the ions in one run. Therefore, it would be nice to be able to speed up the measurement process by making it phase sensitive. This is the development we turn to now.

Modified PNP for non-doublets

We cannot use the PNP technique when the ion is not resonant with the detector because we cannot detect the axial motion to determine the cyclotron phase when the π-pulse is applied. But now consider the following procedure. Say that we excite the cyclotron motion with a known phase as before, but then just before applying the π-pulse, we change the trap voltage to make it resonant. The voltage change has two consequences. First, the equilibrium position of the ion changes. Second, all the three frequencies - axial, magnetron and trap cyclotron- change because the electric field is different. Actually, the trap cyclotron frequency changes from both these effects, the electric field effect causes a large shift of a few parts in 10^3, while the position change coupled with the linear magnetic field gradient causes a negligible shift of a few ppb.

If we consider our N_2^+/N^+ example again, the change in the cyclotron frequency can be determined as follows. In an ideal trap,

$$\omega_c' = \omega_c - \omega_m. \tag{4-11}$$

The magnetron frequency for N_2^+ is about 2.76 kHz and, for a given trap voltage, is nominally independent of mass (recall that $\omega_m \approx \omega_z^2/2\omega_c$). Therefore the magnetron frequency for N^+ at 9 V is also 2.76 kHz, while it is only 1.38 kHz at 4.5 V. As we change the trap voltage from 9 to 4.5 V, the trap cyclotron frequency increases by 1.38 kHz. This change takes place over a few milliseconds, limited by the low pass filters in our DC lines, and is adiabatic. The additional shift in ω_c' due to the change in position is only about 30 mHz and can be neglected for this discussion.

As a function of time, the cyclotron frequency "chirps" from its old to its new value. If we excite the cyclotron mode at $t = 0$, start changing the trap voltage at $t = T$, and apply the π-pulse at $t = T + 1$ allowing 1 s for the voltage to stabilize, then the phase we detect is the phase evolved in time T plus the additional phase accumulated in the 1 second when the frequency was chirping. Now, the beauty of the PNP technique is that we do not care about the additional phase as long as it is the same for points with different T.

So what can cause it to be different? Well, the only reason this phase will change is if the trap cyclotron frequency changes or the chirp time changes. The chirp time depends on the low frequency transfer function in the cryofilters, so it should remain

constant. The frequency can change if the voltage drifts, but we constantly monitor it to center the ion's axial frequency on the coil frequency, so that is not a problem. The frequency can also change if the magnetic field changes. The total phase accumulated in 1 s at 9.35 MHz is 3.366×10^9 degrees, and our magnetic field changes are about 0.5 ppb, therefore the resulting phase error is a negligible 1.7° compared to the 10° estimation noise.

To see that it really works, I show in Fig. 4-3 some data taken with an Ar^{++} ion measured in an Ar^{+} trap. The cyclotron motion was excited in a non-resonant trap, allowed to evolve for 150 ms, then the trap was made resonant, and finally the π-pulse was applied after a 2.85 s stabilization time. As can be seen, the detected phase remains constant. The phase noise is slightly larger than the estimation noise because the

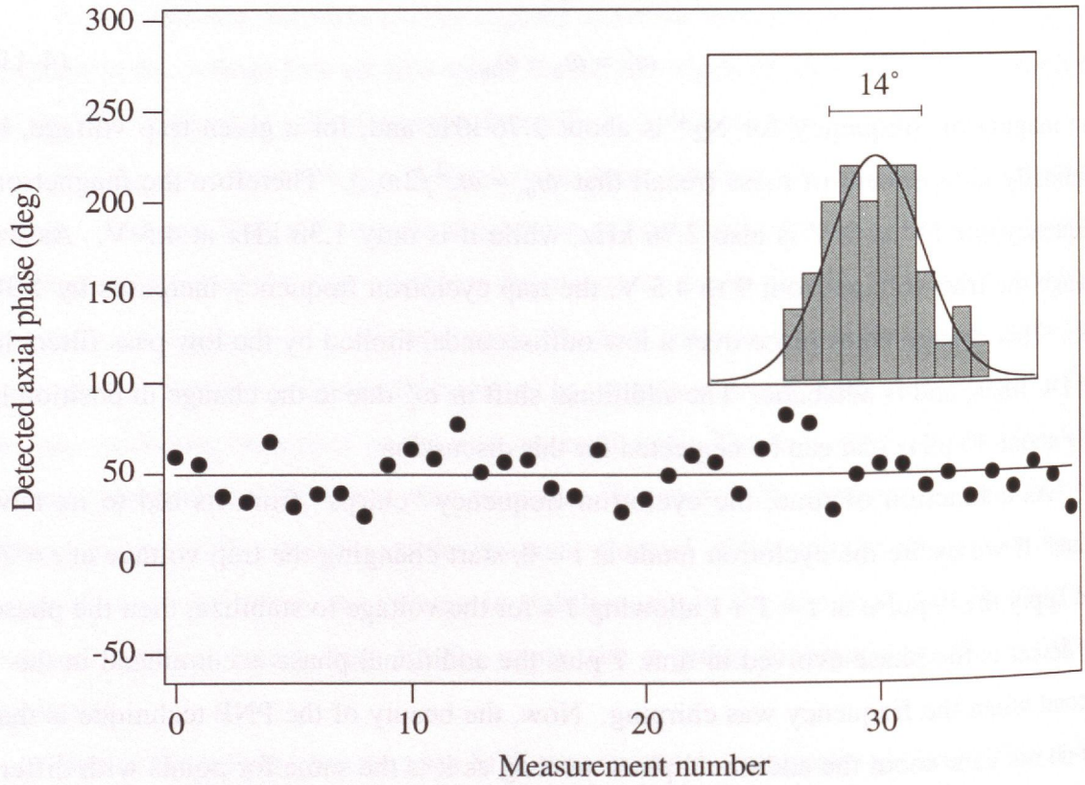

Fig. 4-3 Modified PNP for non-doublets. Each plotted point corresponds to the detected phase in the axial motion of an Ar^{++} ion after the following experiment. The cyclotron motion was first excited in a non-resonant trap, allowed to evolve for 250 ms, then the trap voltage was changed to make Ar^{++} resonant, and finally a π-pulse was applied after a 2.85 s wait to allow the voltage to stabilize. Some of the phase noise is due to actual magnetic field noise in the 3 seconds of total phase integration. If the correlation with the external magnetometer is removed, the residual phase noise is 11°.

measurements were performed during the day when the field fluctuations can be as large as 5 ppb. We are certain that this is due to external noise because the phase is well correlated with the reading from our external magnetometer.

There are many reasons we have not used this promising technique for the results in this thesis. The SOF technique is very different from PNP because we are now relying on the estimated amplitudes of the signals, not the phase. Therefore, it should have different errors if we are misinterpreting the axial signal, though that is not very likely. And the modified PNP technique only buys us 50% more switches per night; the price we have to pay for using SOF is not that heavy. The more important reason for using SOF though, as will become clear from Chapter 6, is that it may adapt very well to our new ideas of simultaneously measuring the cyclotron frequency of two very dissimilar ions in the trap.

3 SYSTEMATIC ERRORS

The sources of systematic error for non-doublets are the same as for doublets. But the economy of errors is quite different because the frequencies and amplitudes for the two ions are so dissimilar. The most important amplitude independent error comes, of course, from the patch induced shift, but the whole SOF method was developed to eliminate that. The only other such error of consequence is the axial frequency pulling from the detector.

Tuned circuit pulling

The fact that we measure the axial frequency only for the ion on which we use PNP (call it type P) and infer it for the ion on which we use SOF (call it type S) causes this error to appear slightly differently than for a doublet measurement. The axial frequency of ion S is of course 60 kHz off the detector and is not perturbed at all. If the small perturbation due to the detector on ion P causes a relative error in the axial frequency of $\delta\omega_{zP}/\omega_{zP}$, then the relative shift in its cyclotron frequency is:

$$\frac{\delta\omega_{cP}}{\omega_{cP}} = \frac{\omega_{zP}^2}{\omega_{cP}^2}\frac{\delta\omega_{zP}}{\omega_{zP}}. \qquad (4\text{-}12)$$

Denoting the mass ratio of the ions as R_M, the frequencies for ion S are,

$$\omega_{cS} = R_M\omega_{cP} \;;\quad \omega_{zS} = \sqrt{R_M}\,\omega_{zP}\,. \qquad (4\text{-}13)$$

Because we scale the measured axial frequency of ion P by $\sqrt{R_M}$ to determine the axial frequency for ion S in Eq. (4-10), the *relative* error from the circuit pulling on the axial frequency is the same for both ions. But the relative shift in the cyclotron frequency for ion S is given by:

$$\frac{\delta\omega_{cS}}{\omega_{cS}} = \frac{\omega_{zS}^2}{\omega_{cS}^2}\frac{\delta\omega_{zS}}{\omega_{zS}} = \frac{\omega_{zP}^2}{R_M\omega_{cP}^2}\frac{\delta\omega_{zP}}{\omega_{zP}}. \tag{4-14}$$

Using this and (4-12), we obtain the effect on the measured ratio as:

$$\begin{aligned} R_M &= \frac{\omega_{cS}\left(1+\delta\omega_{cS}/\omega_{cS}\right)}{\omega_{cP}\left(1+\delta\omega_{cP}/\omega_{cP}\right)} \\ &\approx \frac{\omega_{cS}}{\omega_{cP}}\left(1+\frac{\omega_{zP}^2}{R_M\omega_{cP}^2}\frac{\delta\omega_{zP}}{\omega_{zP}}-\frac{\omega_{zP}^2}{\omega_{cP}^2}\frac{\delta\omega_{zP}}{\omega_{zP}}\right). \\ &= \frac{\omega_{cS}}{\omega_{cP}}\left(1-\frac{R_M-1}{R_M}\frac{\omega_{zP}^2}{\omega_{cP}^2}\right) \end{aligned} \tag{4-15}$$

In our canonical N_2^+/N^+ example, $R_M \approx 2$ and the effect on the ratio is half the effect on the frequency of N_2^+. On a particularly bad day, we might be detuned from the detector frequency by 0.5 Hz, which causes a shift of 6 mHz and therefore a relative error of $4\text{x}10^{-8}$ in ω_{z1}. The error in the measured ratio due to this is only 0.045 ppb.

Amplitude dependent errors

The amplitude dependent errors come from the same matrix as for the doublets. But now it is not possible to cancel the effects of B_2, C_4 and relativity to first order by simply choosing the same amplitude for both ions since all the scaling frequencies are very different. But the effect of relativity and the effect of the field inhomogeneities differ in one fundamental way. For relativity, we need to know the exact absolute amplitude for the cyclotron mode (and therefore the ion's velocity). However, B_2 and C_4 are defined and measured in terms of the drive strength and the absolute calibration is not needed. Due to this difference, we always adjust the cyclotron amplitudes for the two ions so that the effect of relativity cancels, and then use the measured B_2 and C_4 coefficients to account for the amplitude dependent shifts, if need be.

To cancel the effect of the relativistic mass shift, we want to measure the two ions at the same tangential velocity, i.e.

$$\omega_{cP}\rho_{cP} = \omega_{cS}\rho_{cS} \;\Rightarrow\; \rho_{cP} = R_M\rho_{cS}. \tag{4-16}$$

We defined in Chapter 3 an optimal cyclotron radius $\rho_{c,\mathrm{opt}}$ such that the harmonic region of the trap is maximally utilized after a π-pulse. The values of $\rho_{c,\mathrm{opt}}$ for the two ions are related by,

$$\rho^2_{cP,\mathrm{opt}} = \frac{\omega'_{cS}}{\omega'_{cP}}\rho^2_{cS,\mathrm{opt}} = R_M\rho^2_{cS,\mathrm{opt}}. \tag{4-17}$$

We always use $\rho_{cP,\mathrm{opt}}$ to optimize our signal during the PNP measurement on ion P; thus the radius for ion S to cancel the effect of relativity is:

$$\rho_{cS,\mathrm{canc}} = \frac{1}{R_M}\rho_{cP,\mathrm{opt}} = \frac{1}{\sqrt{R_M}}\rho_{cS,\mathrm{opt}}. \tag{4-18}$$

As mentioned earlier (Eq. 4-9), for ratios close to 2, this is also the radius for optimizing the SOF measurement. For other ratios, we still use this radius and accept the slightly sub-optimal average signal during the SOF measurement.

With this cyclotron radius, the shift due to the B_2 and C_4 terms is around 0.1 ppb, as shown in Table 1 of our paper. We can correct for these shifts to about 20% of the total shift, which is our limit in determining the value of the B_2 and C_4 coefficients. But, for all the ratios measured in this study, the trap was tuned well enough that the shifts were negligible compared to the 0.15 ppb final statistical error in the ratio. For example, in the N_2^+ vs. N^+ measurement, the error due to these effects is estimated to be only 0.06 ppb.

4 PHYS. REV. LETT. PAPER ON NON-DOUBLETS

I conclude this chapter with a copy of a paper we have submitted for publication in Physical Review Letters detailing our new technique and its results.

Precision Penning Trap Mass Comparison of Non-Doublets

Vasant Natarajan, Kevin R. Boyce,[a] Frank DiFilippo, and David E. Pritchard

Research Laboratory of Electronics, Department of Physics,
Massachusetts Institute of Technology, Cambridge, MA 02139

We have compared the cyclotron frequency of two single ions in a Penning trap to obtain their mass ratio with a precision close to 0.1 ppb. This precision was extended to mass ratios far from unity (non-doublets) by measuring the frequency of both ions at the same trap voltage, eliminating errors from shifts in the equilibrium position of the ions with different voltages. We have tested our technique with "calibrated" non-doublet ratios such as $M[N_2^+]/M[N^+]$. By comparing isotopically pure methane ions to C^+, we obtain the masses of H, D, and the neutron with up to 40 times improved precision over current values.

PACS numbers: 07.75.+h, 35.10.Bg, 35.80.+s, 06.30.-k

Single charged particles stored in Penning traps have been used for some of the most precise fundamental measurements in science.[1] Comparison of the masses of trapped ions is the first technique to achieve precision below 1 ppb and promises to introduce a new era in mass spectrometry.[2] Recent work by Van Dyck *et al.*[3] and our group,[4,5] with accuracy close to 0.1 ppb, has improved the precision of some atomic masses by 10-10^3 times over the standard nuclear mass table.[6] This improved level of precision opens up several new experiments. Measurement of the endpoint of the tritium decay spectrum to 0.3eV can aid ongoing beta ray spectroscopy experiments to determine the rest mass of the electron neutrino.[7] An accurate knowledge of the binding energy of nuclei (in amu) when combined with a precise wavelength measurement of the associated γ ray would yield the value of $N_A h$, and, in conjunction with the M_e/M_p ratio and the Rydberg constant, an independent value for α^2.[8]

The phenomenal accuracy of Penning trap mass measurements comes from the ability to precisely measure the cyclotron frequency of single ions trapped in a highly uniform magnetic field. In order to overcome systematic shifts in the frequency due to various imperfections in the trapping fields, precision work has heretofore been done on a doublet, i.e., two ions with nominally the same mass to charge ratio.[2-4] Differences in these shifts for the two ions are then scaled down by the factor $\Delta m/m$, which is usually below 10^{-3}.

In this paper, we report on a new technique that allows precision measurements of mass ratios for non-doublets, i.e., ions with a ratio far from unity. This opens the possibility of absolute measurement of mass by direct comparison to a C^+ ion, and also permits much more stringent checks on systematics by measurements on ratios such as $M[N_2^+]/M[N^+]$, which may be calculated with part in 10^{12} precision from the known electron mass and the binding energies. Absolute masses have been previously obtained[3] by comparing a given ion to C^{n+}, with a suitable value of n to make a doublet; our technique works for arbitrary ratios and avoids potential systematics due to induced-dipole shifts from the trap electrodes which affect the two ions differently if they have different charge states.[9]

The ideal Penning trap consists of a strong, uniform magnetic field and a quadrupole electric field typically applied using three hyperboloidal electrodes. The motion of a single ion decomposes into three normal modes; an axial mode (at ω_z) along the

magnetic field axis, and two radial modes - an electric field modified cyclotron motion (at ω_c') and an ExB magnetron drift (at ω_m) - perpendicular to it. In our 8.5T field, these frequencies are respectively 160kHz, 4.5MHz and 2.8kHz for an ion of mass 28 u. The "free space" cyclotron frequency of the ion is recovered from[10]

$$\omega_c = \frac{qB}{mc} = \sqrt{\omega_c'^2 + \omega_z^2 + \omega_m^2} \tag{1}$$

by measuring the three normal mode frequencies to appropriate precision. Mass ratios are obtained by loading the trap with a single ion of one species, measuring its cyclotron frequency, and then repeating with a single ion of the other species. Temporal variation of the magnetic field and other smaller statistical uncertainties are averaged by alternately measuring the frequencies of the two ions a number of times.

Most of the details of our trap and detector are discussed elsewhere and will only be briefly reviewed here. We detect the presence of the ion only through its axial motion, by measuring the image current induced in the endcaps. The axial mode is resonantly coupled to a high Q (~25000) superconducting tank circuit by adjusting the trap voltage ($\omega_z \propto \sqrt{qV/m}$), and then detected with an rf SQUID.[11] We have developed a scheme of π-pulses at the appropriate coupling frequency to *coherently* swap the action (i.e., $\left|\oint p.dq\right|$) from an initially excited radial mode into the axial mode, which can then be cooled and detected.[12] We measure the cyclotron frequency from the phase accumulated in the cyclotron mode in a given length of time, using what we call our pulse and phase (PNP) technique. The trap cyclotron mode is excited to an amplitude a_c with a short duration pulse from a phase-locked source, allowed to evolve unperturbed for a given length of time, and finally coupled to the axial motion with a π-pulse to determine its phase.[2]

The leading sources of systematic error in these measurements come from the second-order spatial inhomogeneities in the magnetic and electric fields, usually designated B_2 and C_4 respectively,[2,10] and the mass shift due to special relativity. All these effects cause a shift in the cyclotron frequency varying as a_c^2 (see Table I), but do not cause a systematic error for a doublet measurement if the values of a_c for the two ions are equal. Linear gradients in the magnetic field can also cause errors if the two ions have different equilibrium positions in the trap. The mean position of the ion is determined by the point at which the applied electric field cancels the stray fields due to surface potentials, which are probably caused by charged dielectric patches adsorbed on the

Table I. Systematic errors. The expressions in the second column give the effect of the different corrections on ω_c' to lowest order in the cyclotron amplitude, where $d = 0.549\,\text{cm}$ is the characteristic size of our trap. The typical values (in ppb) shown in the third and fourth columns are with $a_c \approx 0.010\,\text{cm}$ for N^+ and with $a_c \approx 0.020\,\text{cm}$ for $N_2{}^+$, chosen to cancel the effect of relativity. The field inhomogeneities were shimmed to $B_2 = 0.4(2)\times10^{-6}\,\text{cm}^{-2}$ and $|C_4| \le 1.0\times10^{-4}$. The last column gives an upper limit on systematic errors (in ppb) for this non-doublet comparison after correcting for the effects of B_2 and C_4.

Correction	Form of $\Delta\omega_c'/\omega_c'$	Mean value of $\Delta\omega_c'/\omega_c'$ (ppb)		Upper limit on systematic error for N^+ vs. $N_2{}^+$
		N^+	$N_2{}^+$	
Magnetic	$-(B_2/2)a_c{}^2$	0.020	0.080	0.020
Electric	$\frac{3}{2}(C_4/d^2)(\omega_m/\omega_c')a_c{}^2$	0.007	0.119	0.030
Relativity	$-\frac{1}{2}(\omega_c'{}^2/c^2)a_c{}^2$	0.191	0.191	0.020

trap electrodes, irregularities in the work function, or thermal EMF's. For a doublet, the difference in the trap voltage to bring the two ions into resonance with our detector is only a few mV, and the resulting shift (few nm) in the position of the two ions causes negligible error.

As seen from Table I, the error budget for non-doublets is very different. We will consider as our representative non-doublet the ions N^+ and $N_2{}^+$, whose mass ratio is exactly 2 except for some small corrections. In order to eliminate the effect of relativitistic mass shifts on this measurement, we need to measure the cyclotron frequency for the two species at the same tangential velocity, i.e., at amplitudes that differ by a factor of 2. The requirement on the cyclotron amplitude for nulling the differential effects of B_2 and C_4 is not the same (see Table I), hence the two sources of amplitude dependent errors cannot be nulled simultaneously. We have overcome this problem by carefully measuring B_2 and C_4 and correcting for their effects to an accuracy of 20%, which does not cause any serious error at the 0.1 ppb level.

The problem with the mean position of the ion is much more serious. The trap voltage needed to bring N^+ into resonance with our detector is about 5V, while we need 10V for $N_2{}^+$. This can cause a significant difference in the location of the ion depending on the size of our surface potentials. We have taken great care to have a clean vacuum in

order to minimize adsorbed patches when we cool our trap from room temperature to 4.2K, and we also coat the surface of our electrodes with a graphite film to reduce the effect of surface potentials near the trap center.[13] We can measure the effective stray potential in the axial direction by applying known offsets between the endcaps and studying the quadratic shift in ω_z; we found that the minimum of this parabola was shifted from 0 offset by about 22 mV. With our measured linear field gradient of about $1\times10^{-6}\text{cm}^{-1}$, this should cause a 2 ppb shift for the $M[N_2^+]/M[N^+]$ ratio. Indeed, we obtained a systematic difference of this order from the predicted value when we measured the ratio with our PNP technique. The systematic error remained after we repeated the measurement with the axial offset nulled (see Fig.2), suggesting that there are radial components to the stray fields of the same order (which we cannot measure or null in our azimuthally symmetric trap).

This offset error is eliminated by measuring the frequencies of both ions with the same trap voltage applied. In our example, this means that we have to measure ω_c for both N^+ and N_2^+ with 10V on the trap, the voltage at which our PNP technique works for N_2^+. However, at 10V, the axial frequency of N^+ is $\sqrt{2}$ times higher than the fixed frequency of our narrow band detector, and we cannot measure its cyclotron frequency with this technique.

Our solution is to use the Ramsey separated oscillatory fields (SOF) technique[15] to store the cyclotron resonance information in the cyclotron *amplitude* in a non-resonant trap and then determine this amplitude after bringing the ion into resonance with the detector. Thus, to measure the frequency of N^+ at 10V, we first excite its cyclotron mode with a short pulse from a signal generator. After a length of time T, during which the cyclotron motion evolves freely, we apply a second identical pulse to the ion. The resultant amplitude then represents the interference between the ion's natural frequency and the drive frequency, and displays a characteristic Ramsey fringe pattern at the beat frequency, as shown in Fig.1. In order to measure this amplitude, we change the trap voltage to 5V, which brings N^+ into axial resonance with our detector, then apply the usual π pulse and detect the resultant axial motion. We repeat this process for a series of interference times allowing us to determine the order of each Ramsey fringe unambiguously. The change in the trap voltage takes place over a few milliseconds; the small (adiabatic)

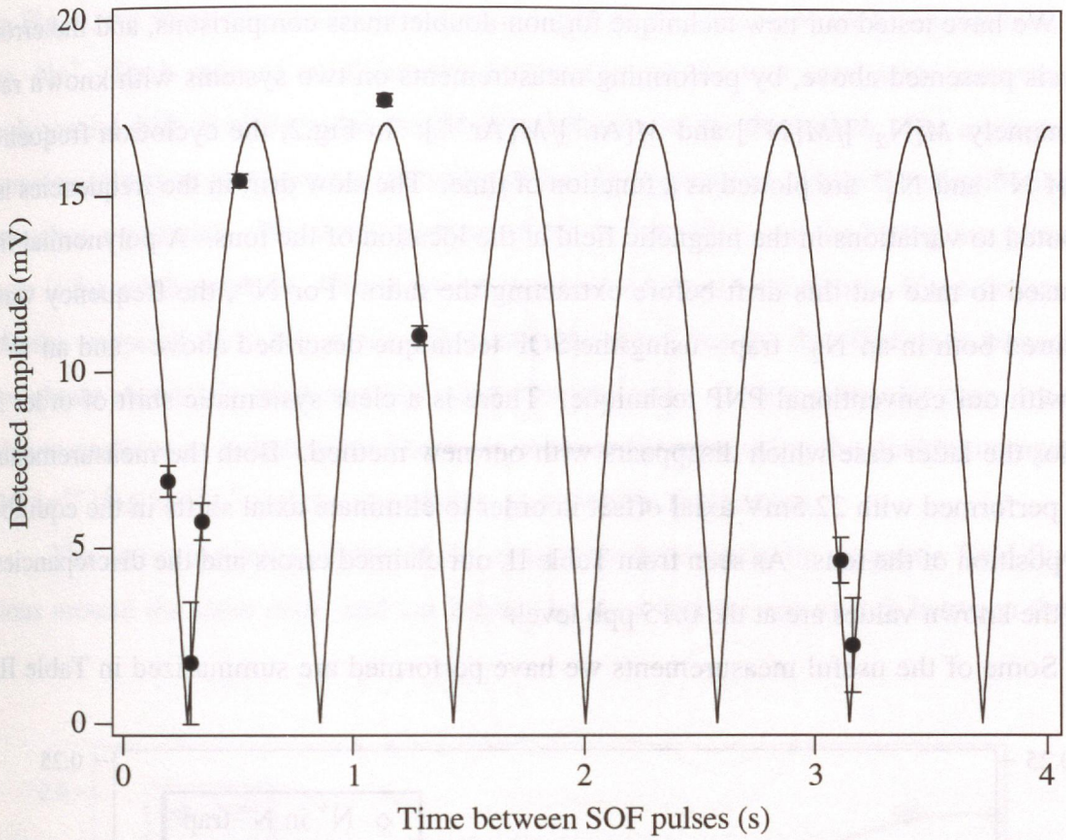

Fig. 1 SOF technique for determining ω_c'. For each point, the cyclotron mode was given two pulses centered at $\omega_c'/2\pi - 1.75$ Hz and separated by time T, and the resultant amplitude detected by changing the trap voltage to bring the ion into axial resonance and applying a π-pulse. We can determine the order of each fringe unambiguously if the separation times are incremented by a factor less than three. The precision measurement of ω_c' comes from points with $T = 50$ s.

change resulting in the cyclotron amplitude is below our detection limit and, in any case, only rescales the overall amplitude of the fringe pattern.

In order to obtain the free space cyclotron frequency for N^+ and $N_2{}^+$ as in Eq.1, we need to know their axial frequencies. We can directly measure ω_z for $N_2{}^+$ on our detector, but for N^+ we infer it by scaling the value of ω_z for $N_2{}^+$ with the square root of the mass ratio. The precision with which this scale factor needs to be known is much smaller than the ultimate precision, and we can use the mass values from the standard table.[6] We can measure ω_z with a precision of about 20mHz, and our axial frequency drift (mostly due to drift in our voltage source) over the few minutes between the N^+ and $N_2{}^+$ measurements is less than 10mHz; this causes an error of only 0.04 ppb in ω_c.

We have tested our new technique for non-doublet mass comparisons, and the error analysis presented above, by performing measurements on two systems with known ratios, namely $M[N_2^+]/M[N^+]$ and $M[Ar^+]/M[Ar^{++}]$. In Fig.2, the cyclotron frequencies of N^+ and N_2^+ are plotted as a function of time. The slow drift in the frequencies is attributed to variations in the magnetic field at the location of the ions. A polynomial fit was used to take out this drift before extracting the ratio. For N^+, the frequency was measured both in an N_2^+ trap - using the SOF technique described above - and an N^+ trap with our conventional PNP technique. There is a clear systematic shift of order 3 ppb for the latter case which disappears with our new method. Both the measurements were performed with 22.5mV axial offset in order to eliminate axial shifts in the equilibrium position of the ions. As seen from Table II, our claimed errors and the discrepancies from the known values are at the 0.15 ppb level.

Some of the useful measurements we have performed are summarized in Table II.

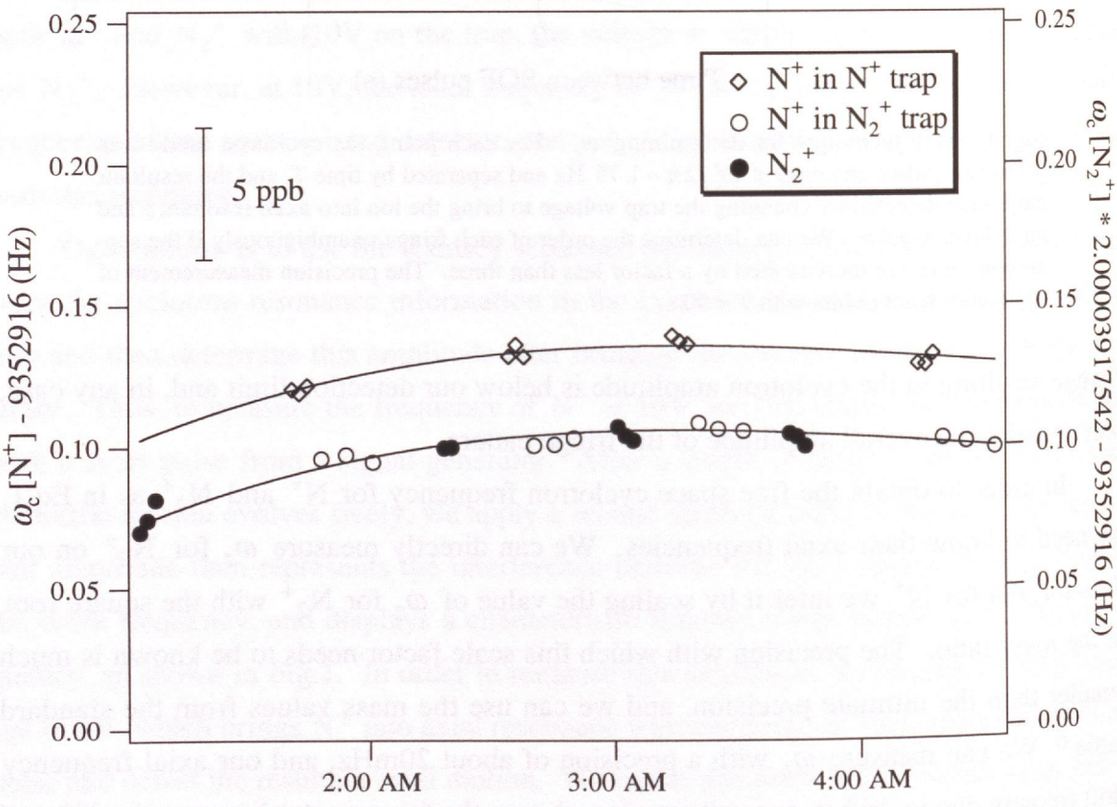

Fig. 2 Free space cyclotron frequencies for N^+ and N_2^+. The frequency for N^+ was measured both in an N^+ trap (with 5V) and in an N_2^+ trap (with 10V). The frequency for N_2^+ has been scaled by the known ratio of $M[N_2^+]/M[N^+]$, so that the plotted points for the two ions should line up if there are no systematic errors. The solid line is a 3rd order polynomial fit to the magnetic field drift.

In Fig. 3, we show the results of a typical night of measurement on a non-doublet, Ar^+ vs. Ne^+. Each ratio of neighbouring frequencies on the two ions, after removing the polynomial drift, is taken as an independent measure of the mass ratio. The average ratio remains robust as we increase the order of the fit polynomial, while the distribution approaches a gaussian. We rarely go beyond 6th or 7th order, and the histogram presented here is for a 5th order fit. There are no apparent non-gaussian errors. If we do not take out the temporal drift, the average is nearly the same, but the distribution is bimodal as we obtain alternately high and low values for the ratio. In this particular case, we were able to perform an independent check on our measurement using the doublet comparison $M[Ar^{++}]/M[Ne^+]$,[5] and the two results agree within their errors.

The errors quoted in Table II are caused predominantly by magnetic field fluctuations around the slow drift, and are limited by how fast we can switch between the two

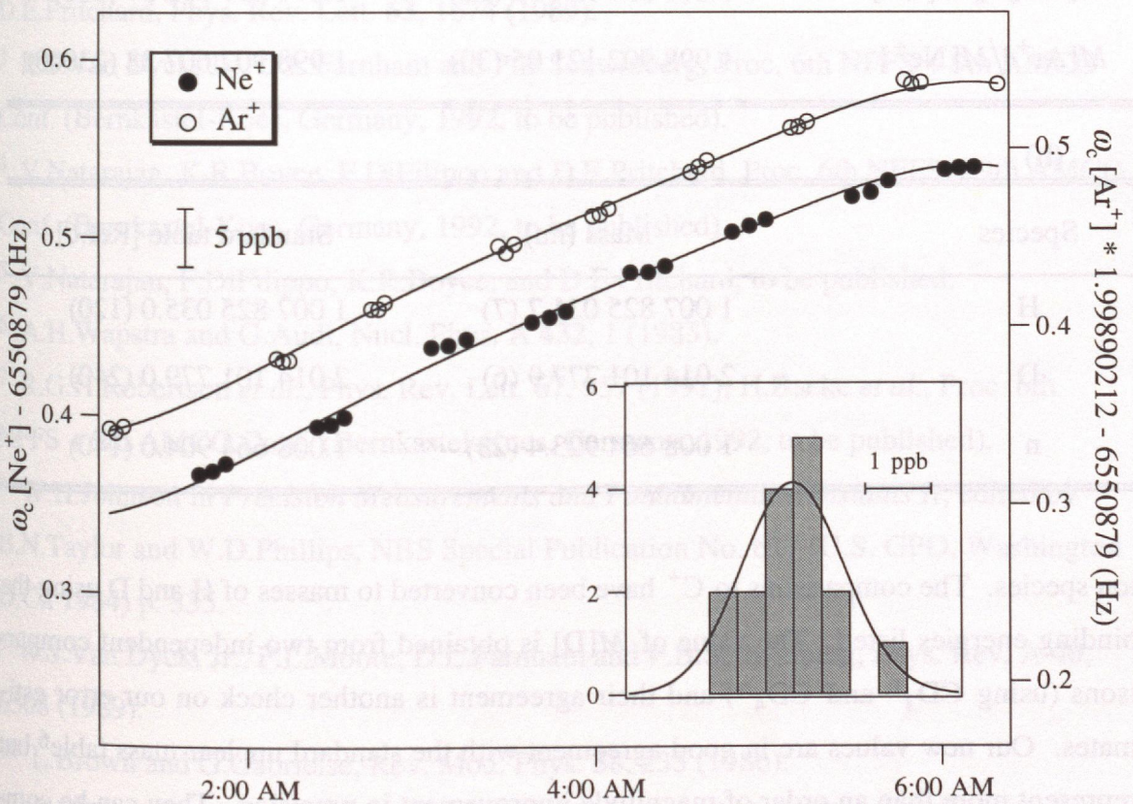

Fig. 3 Mass ratio measurement for a typical non-doublet Ar^+ vs. Ne^+. The cyclotron frequency for Ne^+ was measured using the SOF technique in an Ar^+ trap. The magnetic field drift was taken out with a 5th order polynomial fit. Each ratio of neighbouring frequencies was taken as an independent measure of the mass ratio, to obtain the histogram presented.

Table II. Non-doublet ratios and atomic masses. In (a), we list the non-doublet ratios measured and the values obtained using the current nuclear mass table (see Ref.6). Note that the first two ratios (designated with an *) are known to a few ppt accuracy, and depend only weakly on the masses in Ref.6. In (b), we have converted the comparisons to C^+ into masses of H, D, and the neutron (in nu) using the following corrections (also in nu):
$M[e] = 548\,579.903$; $M[C^+] + M[e] - M[C] = 12.10$; $M[CH_4^+] + M[e] - M[C+4H] = -4.42$;
$M[CD_3^+] + M[e] - M[C+3D] = -2.82$; $M[CD_4^+] + M[e] - M[C+4D] = -4.42$; and
$M[H] + M[n] - M[D] = 2\,388\,177.2(22)$.

(a)

Non-Doublet	Measured value	Standard table [Ref.6]
$M[N_2^+]/M[N^+]$	2.000 039 175 61 (29)	2.000 039 175 424 (1) *
$M[Ar^+]/M[Ar^{++}]$	2.000 027 454 12 (36)	2.000 027 454 084 (1) *
$M[CH_4^+]/M[C^+]$	1.335 957 033 78 (23)	1.335 957 034 89 (300)
$M[CD_3^+]/M[C^+]$	1.503 548 462 35 (20)	1.503 548 462 71 (400)
$M[CD_4^+]/M[C^+]$	1.671 397 950 39 (31)	1.671 397 950 57 (480)
$M[Ar^+]/M[Ne^+]$	1.998 902 121 05 (30)	1.998 902 607 38 (23000)

(b)

Species	Mass (nu)	Standard table [Ref.6]
H	1 007 825 031.7 (7)	1 007 825 035.0 (120)
D	2 014 101 777.9 (6)	2 014 101 779.0 (240)
n	1 008 664 923.4 (23)	1 008 664 904.0 (140)

ion species. The comparisons to C^+ have been converted to masses of H and D using the binding energies listed. The value of $M[D]$ is obtained from two independent comparisons (using CD_3^+ and CD_4^+) and their agreement is another check on our error estimates. Our new values are in good agreement with the standard nuclear mass table[6] but represent more than an order of magnitude improvement in precision. They can be combined with the average value of the deuteron binding energy[16] to yield the neutron mass; the improvement by only a factor of 6 is limited by the imprecision of the deuteron binding energy.

We have achieved precision below 0.1 ppb in some cases while comparing doublets[5] and the error analysis in Table I shows that this should be possible for non-doublets too, if we can get sufficient statistics in one run. Nevertheless, the size of the field fluctuations will probably limit us around 0.05 ppb, and we feel the route to greatly increased precision lies in measuring the frequency of the two ions simultaneously.[14]

This work was supported by NSF Grant No. 8921769-PHY and Joint Services Electronics Program Grant No. DAAL03-92-C-0001. One of us (F.D.) acknowledges additional support from an NSF Graduate Fellowship.

References

(a) Present address: NASA Goddard Space Flight Center, Greenbelt, MD

[1] R.S.Van Dyck, Jr., P.B.Schwinberg and H.G.Dehmelt, Phys. Rev. Lett. **59**, 26 (1987).

[2] E.A.Cornell, R.M.Weisskoff, K.R.Boyce, R.W.Flanagan,Jr., G.P.Lafyatis and D.E.Pritchard, Phys. Rev. Lett. **63**, 1674 (1989).

[3] R.S.Van Dyck, Jr., D.L.Farnham and P.B.Schwinberg, Proc. 6th NFFS + 9th AMCO Conf. (Bernkastel-Kues, Germany, 1992, to be published).

[4] V.Natarajan, K.R.Boyce, F.DiFilippo and D.E.Pritchard, Proc. 6th NFFS + 9th AMCO Conf. (Bernkastel-Kues, Germany, 1992, to be published).

[5] V.Natarajan, F.DiFilippo, K.R.Boyce, and D.E.Pritchard, to be published.

[6] A.H.Wapstra and G.Audi, Nucl. Phys. A **432**, 1 (1985).

[7] R.G.H.Robertson *et al.*, Phys. Rev. Lett. **67**, 957 (1991); H.Backe *et al.*, Proc. 6th NFFS + 9th AMCO Conf. (Bernkastel-Kues, Germany, 1992, to be published).

[8] W.H.Johnson in *Precision Measurements and Fundamental Constants II*, edited by B.N.Taylor and W.D.Phillips, NBS Special Publication No. 617 (U.S. GPO, Washington D.C., 1984) p. 335.

[9] R.S.Van Dyck, Jr., F.L.Moore, D.L.Farnham and P.B.Schwinberg, Phys. Rev. A **40**, 6308 (1989).

[10] L.Brown and G.Gabrielse, Rev. Mod. Phys. **58**, 233 (1986).

[11] R.M.Weisskoff, G.P.Lafyatis, K.R.Boyce, E.A.Cornell, R.W.Flanagan,Jr. and D.E.Pritchard, J. Appl. Phys. **63**, 4599 (1988).

[12] E.A.Cornell, R.M.Weisskoff, K.R.Boyce and D.E.Pritchard, Phys. Rev. A **41**, 312 (1990).

[13] J.B.Camp, T.W.Darling and R.E.Brown, J. Appl. Phys. **69**, 7126 (1991). The graphite film is sprayed on using Aerodag G, Acheson Colloids Company, Port Huron, MI.

[14] E.A.Cornell, K.R.Boyce, D.L.K.Fygenson and D.E.Pritchard, Phys. Rev. A **45**, 3049 (1990).

[15] N.Ramsey, *Molecular Beams* (Clarendon, Oxford, 1956).

[16] A.H.Wapstra, Nucl. Intrum. Meth. Phys. Res. A **292**, 671 (1990).

5 ATOMIC MASS TABLE

We have so far described two different techniques for measurement, one for doublets and one for non-doublets. As mentioned earlier, the doublet ratios were chosen so that they can be inverted to yield the absolute masses of the atoms involved. We also have direct measurements of the masses of H and D from the non-doublet comparisons to C^+. In this chapter, we will see that the two methods of obtaining these masses yield consistent results and allow us to make an atomic mass table that is probably the most precise one to date.

For the doublet results, there are several consistency checks that we can perform using overdetermined sets. This verifies both our ratio extraction technique and our analysis of systematic errors. The non-doublets intrinsically allow for stringent systematic checks and hence provide results about which we feel confident. We have therefore used the non-doublet results to further check on the doublet measurements.

1 DOUBLET AND NON-DOUBLET RESULTS

Listed in Table 5-1 are all the doublet and non-doublet mass ratios that we have measured in this study, and the binding energies used to convert them to neutral atom mass ratios. Several of the doublet ratios were measured more than once with the runs spaced up to a few weeks apart. As shown in Table 5-2, the results were always consistent within the error bars and the values listed in Table 5-1 are the weighted averages. During the time between the repeated measurements, the magnetic field drifted down a bit, the patch effects changed, the coil frequency moved by a few Hz and all the trap fre-

quencies were slightly different. Since the ratio remained the same, we conclude that there is no systematic time dependence in our measurements from these effects. The overall reduced χ^2 from all the time dependent tests is 0.42, indicating good consistency for repeated measurements.

Table 5-1 Doublet and non-doublet ratios. In (a), we list the doublet ratios measured in this study and in (b), the non-doublet ratios . Also listed are the total binding energies (in nu-c^2) for the two ions as defined in Chapter 3, used to convert each ionic ratio to a ratio of masses of constituent atoms.

(a)

Doublet	Measured value	Binding energy	
		Ion 1	Ion 2
$M[N^+]/M[CH_2^+]$	0.999 102 679 26 (16)	15.599	2.641
$M[O^+]/M[CH_4^+]$	0.997 730 269 42 (8)	14.611	- 4.423
$M[CD_3^+]/M[CD_2H_2^+]$	0.999 914 190 77 (10)	- 2.823	- 4.423
$M[Ar^{++}]/M[Ne^+]$	0.999 437 341 28 (11)	46.570	23.146
$M[Ne^+]/M[CD_4^+]$	0.996 810 562 56 (13)	23.146	- 4.423
$M[Ar^{++}]/M[CD_4^+]$	0.996 249 698 10 (10)	46.570	- 4.423
$M[CO^+]/M[N_2^+]$	0.999 598 887 51 (13)	3.081	6.151
$M[Ar^+]/M[C_3H_4^+]$	0.998 278 399 35 (9)	16.984	- 20.097

(b)

Non-Doublet	Measured value	Binding energy	
		Ion 1	Ion 2
$M[CH_4^+]/M[C^+]$	1.335 957 033 78 (23)	- 4.423	12.099
$M[CD_3^+]/M[C^+]$	1.503 548 462 35 (20)	- 2.823	12.099
$M[CD_4^+]/M[C^+]$	1.671 397 950 39 (31)	- 4.423	12.099
$M[Ar^+]/M[Ne^+]$	1.998 902 121 05 (30)	16.984	23.146

Table 5-2 Repeated doublet ratio measurements. The measured values were obtained from independent runs on the dates shown. The reduced χ^2 in each case is also listed. The values in Table 5-1(a) are weighted averages of the values listed here.

Doublet	Date	Measured value	χ^2
$M[CD_3^+]/M[CD_2H_2^+]$	11/11/92	0.999 914 190 82 (11)	0.93
	12/5/92	0.999 914 190 60 (20)	
$M[Ar^{++}]/M[Ne^+]$	10/1/92	0.999 437 341 30 (15)	0.06
	10/22/92	0.999 437 341 25 (15)	
$M[CO^+]/M[N_2^+]$	5/12/92	0.999 598 887 35 (30)	0.36
	5/16/92	0.999 598 887 55 (15)	
$M[Ar^+]/M[C_3H_4^+]$	11/21/92	0.998 278 399 30 (13)	0.32
	12/30/92	0.998 278 399 40 (12)	

We have also studied some of our measurement errors by looking at the following overdetermined sets among the ratios. Each set checks a different kind of error and the strongest check comes from a set that involves both doublet and non-doublet measurements.

Overdetermined set at mass 20

The first kind of overdetermined set comes from the three ratios at mass 20 - $M[Ar^{++}]/M[Ne^+]$, $M[CD_4^+]/M[Ar^{++}]$ and $M[Ne^+]/M[CD_4^+]$. The product of these ratios should be exactly 1 and the value we measure is 1.000 000 000 30 (20). This consistency is a good test of our ratio extraction technique. If we were over-analyzing the data to fit every little wiggle on the frequency drift with time, we would be grossly underestimating our final errors. Then the three errors would not be consistent within 1σ.

The above test does not however check our systematic errors in a strict sense. This is because we can define an equivalent "*trap mass*" for the measured cyclotron frequency of the ions in our apparatus, which could actually be systematically shifted from the true mass due to unknown effects. The above check then only tells us that we always measure the same *trap mass*. Of course, the fact that the ratio is consistent with the values from

the standard table implies that we are not off at the 1 ppb level. But in order to really check our systematic errors at 0.1 ppb, we need a different kind of overdetermined set.

Overdetermined set at different masses

This set consists of the three ratios $M[CO^+]/M[N_2{}^+]$, $M[N^+]/M[CH_2{}^+]$ and $M[O^+]/M[CH_4{}^+]$ at mass 28, 14 and 16 respectively. To see that this is indeed an overdetermined set, we go back to our discussion at the beginning of Chapter 3. There we saw that the first ratio strongly constrains the difference $M[C+O-2N]$. The other two ratios can also be combined to obtain the same difference (in fact this was the source of our singularity problem). Therefore, we can think of this as two ways of obtaining the $M[CO^+]/M[N_2{}^+]$ mass ratio. The value obtained by combining the two measurements at mass 14 and mass 16 is 0.999 598 887 44 (17), which agrees well with the directly measured value of 0.999 598 887 51 (13).

This is a good check on both our statistical errors (obtained while extracting the ratio) and some of our systematic errors. The systematic errors at mass 14, for example, are governed by such factors as the differential shift in position between the ions with 4.5 V on the trap, the flatness of the RF transfer function at 9.35 MHz, and the effect of field inhomogeneities at the optimal cyclotron amplitude for a mass 14 ion. The errors at mass 16 and mass 28 should not only be independent, but quite different in magnitude. As can be seen from the error analysis in Chapter 3, these errors scale as some high power of the ion's mass. The three doublets we have used for this check also have mass ratios with very different deviations of the ratio from unity, which should again make the size of their systematics different.

We therefore feel that our earlier error analysis is adequate at this level of precision.

Check on M[Ar]/M[Ne] from the non-doublet result

A third check on our errors compares a doublet result with a non-doublet ratio. We have measured the ratio $M[Ar^+]/M[Ne^+]$ using the non-doublet technique presented in the last chapter. We can convert this to a value for the doublet ratio $M[Ar^{++}]/M[Ne^+]$, which we have directly measured with our doublet procedure. The value we obtain from the non-doublet measurement is 0.999 437 341 21 (15), in quite good agreement with the doublet measurement of 0.999 437 341 28 (11).

This is probably the single most stringent test on our errors because the two techniques are so different. In the non-doublet measurement, the cyclotron frequency of Ne^+ is determined with 12.8 V on the trap, with a trap cyclotron frequency that is 2 kHz different from the doublet value, a cyclotron amplitude $\sqrt{2}$ smaller than its optimal value, and a magnetron frequency that is twice as big as for the doublet measurement. It is a testament to our understanding of the trap dynamics and to the invariance theorem that we obtain the same free space frequency as in the doublet case.

M[H] and M[D] from doublets and non-doublets

We saw in our solution to singularity problem in Chapter 3 that the three doublet ratios $M[CD_3^+]/M[CD_2H_2^+]$, $M[Ar^{++}]/M[CD_4^+]$ and $M[Ar^+]/M[C_3H_4^+]$ can be combined with the known ratio $M[Ar^+]/M[Ar^{++}]$ to obtain the masses of H, D and Ar. The relative precision with which these masses are obtained is different. The mass of H in both CD_2H_2 and C_3H_4 is only about 10% of the total mass, so its mass is not very precisely obtained from the ratios. On the other hand, the mass of D is 40% of the total mass and we only lose a factor of 2.5 in precision. For the mass of Ar, the relative precision is almost the same as the precision of the measured ratio.

The mass of H was also obtained in the last chapter from the non-doublet comparison $M[CH_4^+]/M[C^+]$ at mass 16. This gives a more precise value because H now forms 25% of the total mass of the ion. Similarly, the mass of D was obtained by measuring the ratio $M[CD_4^+]/M[C^+]$ at mass 20. We also had a second independent way of obtaining this mass, from the ratio $M[CD_3^+]/M[C^+]$ at mass 18.

The results from these different methods are summarized in Table 5-3. All the masses agree quite well within 1σ of each other. In fact, this was how we discovered the systematic error that was plaguing our doublet measurements. When we first did this comparison, we found a 7 nu lower mass of D from the doublet route, giving a discrepancy of 13 times the convolved errors. By then we knew that we had been inadvertently using different guard ring voltages for the two ions, but the resulting C_4 difference seemed to be too small to account for the discrepancy. We finally resolved it by repeating the Ar^+ to $C_3H_4^+$ doublet comparison with the same guard ring setting. We found a much larger dependence of the cyclotron frequency on V_{gr} than expected, as discussed in Chapter 3, with the likely explanation that it is caused by a higher order electrostatic

Table 5-3 Comparison of different ways of obtaining atomic masses of H and D. The doublet route involves a combination of the three ratios explained in the text. The non-doublet way comes from a direct comparison to C^+.

Method	M[H] (nu)	M[D] (nu)
Doublets	1 007 825 030.3 (13)	2 014 101 777.1 (10)
Non-doublet (CH_4^+/C^+)	1 007 825 031.7 (7)	—
Non-doublet (CD_4^+/C^+)	—	2 014 101 778.5 (9)
Non-doublet (CD_3^+/C^+)	—	2 014 101 777.5 (8)

term. We have looked at all our old data for this error and found that the CO^+ to N_2^+ comparison we reported at the AMCO-9 conference [VBD92, BOY92] was systematically shifted up by 0.2 ppb. Our new number is corrected for this effect and is an average of two independent measurements (see Table 5-2).

Summary of systematics checks

In summary, we have performed several different consistency checks on the measured ratios, apart from the lack of time dependence demonstrated in Table 5-2. The different checks are listed in Table 5-4 along with the reduced χ^2 obtained in each case. The overall χ^2_{sys} is 0.91, indicating that our systematic checks have reasonable deviations from the expected values.

Table 5-4 Summary of systematic checks. The χ^2 obtained for each of the consistency checks is listed.

Systematic check	χ^2
Overdetermined set at mass 20	2.31
Overdetermined set at different masses	0.11
M[Ar]/M[Ne] from doublets and non-doublets	0.14
M[H] from doublets and non-doublets	0.89
M[D] from doublets and non-doublets	1.11

2 ATOMIC MASSES

The icing on this delicate cake we have built up is to obtain the precise atomic masses of the atoms that can actually be used by researchers. This is achieved by performing a least squares fit to all the data presented in the last section.

Global least squares fit

With all our results now being consistent, we can do a global fit to the data from both the doublets and the non-doublets. The atomic masses we obtain are listed in Table 5-5. The reduced χ^2 of the overall fit is 0.73, indicating the excellent internal consistency of all our ratios and error estimates. Also shown for comparison are the masses from the 1983 adjustment [WAA85]. Most of our values are in good agreement with the currently accepted masses; our precision is however 20-1000 times better! - a major breakthrough by the standards of precision metrology.

The 1000-fold improvement in the mass of Ne is of course not typical. We included Ne (and Ar) in our present study precisely because of their previous imprecision, as suggested by Audi and Wapstra [AUD93, WAP93]. There is also a 2.5 σ deviation in our mass of Ne from the old value, which is surprising given the large imprecision in the old number. But according to Wapstra [WAP93], the deviation (and the large error) is because the mass of Ne was determined from the measured mass of ^{35}Cl and a combination of some 10 nuclear reaction energies. In fact, such an offset has been suspected for some

Table 5-5 Atomic masses. The list of masses (in nu) represents a least squares fit to all the ratios in Table 5-1. For comparison, the current values from the standard nuclear mass table are also presented [WAA85].

Atom	Mass (nu)	Standard table [WAA85]
^{1}H	1 007 825 031.4 (5)	1 007 825 035.0 (120)
^{2}H	2 014 101 777.9 (5)	2 014 101 779.0 (240)
^{14}N	14 003 074 007.2 (18)	14 003 074 002.0 (260)
^{16}O	15 994 914 619.8 (25)	15 994 914 630.0 (500)
^{20}Ne	19 992 440 175.0 (22)	19 992 435 600.0 (22000)
^{40}Ar	39 962 383 121.6 (35)	39 962 383 700.0 (14000)

time and the correction causes no serious concern when it is spread over all the nuclear energies.

Comparison with Van Dyck *et al.*

Van Dyck and his group have reported several atomic masses of light atoms by comparing different ions to suitable charge states of C (to make a doublet) in a Penning trap [VFS92, VFS93a]. They have a significant edge over us in the comparison of low mass (below 10 u) ions because they use a smaller trap and higher axial frequencies (since their FET amplifier can go to about 1 MHz), resulting in a much higher signal for the same amplitude. We are limited to an axial frequency of 160 kHz by the RF SQUID. Still our precision for the masses of H and D is a factor of 2 better.

As can be seen from the comparison of atomic masses in Table 5-6, most of their results agree quite well with ours. The only serious discrepancy is in the mass of D that they reported at the AMCO conference [VFS92]. Since we pointed out this difference, they have reported a new value [VFS93a] for the mass of D that differs from the old one by 3σ (with very little change in σ and only a small increase in statistics from 5 to 8 runs), but brings it into agreement with our value. Some of their other results are also not very stable.

Table 5-6 Comparison with atomic masses reported by Van Dyck *et al.* The list of masses (in nu) measured in this work and reported by Van Dyck *et al.* at AMCO-9 [VFS92, denoted by 1] and at the 1993 APS meeting [VFS93a, denoted by 2].

Atom	This work	Van Dyck *et al.*
^{1}H	1 007 825 031.4 (5)	1 007 825 032.6 (10) [1]
^{2}H	2 014 101 777.9 (5)	2 014 101 774.0 (9) [1] 2 014 101 776.9 (11) [2]
^{3}H	—	3 016 049 267.3 (15) [1,2]
^{3}He	—	3 016 029 310.0 (10) [1,2]
^{4}He	—	4 002 603 235.3 (32) [1] 4 002 603 249.8 (10) [2]
^{14}N	14 003 074 007.2 (18)	14 003 074 005.6 (18) [2]
^{16}O	15 994 914 619.8 (25)	15 994 914 622.9 (60) [1] 15 994 914 626.3 (30) [2]
^{20}Ne	19 992 440 175.0 (22)	—
^{40}Ar	39 962 383 121.6 (35)	—

Traditional mass differences

Finally, in keeping with tradition in the mass spectrometry community and a request from Audi [AUD93], we have converted the measured ratios into mass differences both for the doublets and the non-doublets. In order to do this we need to know the masses of the constituents, albeit to 3 orders of magnitude lower precision. Usually, the masses from the standard mass table have sufficient precision, but in view of the large imprecision and deviation in the mass of Ne, we have used the atomic masses from Table 5-5 to obtain the mass differences. The results are listed in Table 5-7.

Table 5-7 Mass differences from ratios. The doublet and non-doublet ratios listed in Table 5-1 have been converted into the following mass differences (in nu).

Ratio	Difference quantity	Value (nu)
$M[N^+]/M[CH_2^+]$	M[C + 2H - N]	012 576 054.2 (22)
$M[O^+]/M[CH_4^+]$	M[C + 4H - O]	036 385 506.0 (13)
$M[CD_3^+]/M[CD_2H_2^+]$	M[2H - D]	001 548 283.5 (18)
$M[Ar^{++}]/M[Ne^+]$	M[2Ne - Ar]	022 497 224.6 (44)
$M[Ne^+]/M[CD_4^+]$	M[C + 4D - Ne]	063 966 933.6 (26)
$M[Ar^{++}]/M[CD_4^+]$	M[2C + 8D - Ar]	150 431 104.1 (40)
$M[CO^+]/M[N_2^+]$	M[2N - C - O]	011 233 392.7 (36)
$M[N_2^+]/M[C_2H_4^+]$	M[2C + 4H - 2N]	001 548 283.5 (18)
$M[Ar^+]/M[C_3H_4^+]$	M[3C + 4H - Ar]	068 917 004.9 (36)
$M[CH_4^+]/M[C^+]$	M[12H - C]	093 900 380.0 (83)
$M[CD_3^+]/M[C^+]$	M[6D - C]	084 610 665.3 (48)
$M[CD_4^+]/M[C^+]$	M[6D - C]	084 610 670.9 (56)
$M[Ar^+]/M[Ne^+]$	M[2Ne - Ar]	022 497 227.6 (60)

6 TOWARDS HIGHER PRECISION

In this final chapter, I propose two new techniques that might help us reach our goal in precision of a few ppt. Our current primary limitation in accuracy is the temporal fluctuations in the magnetic field while switching between the two species. An obvious solution to this problem is to measure the cyclotron frequencies of the two ions simultaneously. One such technique involving the simultaneous trapping of a doublet was indeed considered by Eric Cornell about 4 years ago [CBF92] and looks quite promising. The alternative scheme I present here relies on the trapping of a non-doublet pair of ions. It is easier to implement and has many advantages for testing systematic errors in the measurement.

Whatever technique we use to overcome temporal field fluctuations, there is another source of measurement noise that will limit us at a precision of about 0.05 ppb per measurement. This is due to thermal fluctuations in the cyclotron radius from the finite sideband cooling limit. These fluctuations, coupled with the field flaws and the effect of special relativity, cause fluctuations in the cyclotron frequency each time we measure it. Though it does not represent a source of systematic error, we will have to develop some method of overcoming it if we are not to spend an inordinately long time averaging the noise. A technique of amplitude squeezing [DNB92] proposed here will reduce the amplitude noise in the cyclotron motion at the expense of an increase in phase noise. While this may mean a somewhat longer integration time to get the same precision, it is still advantageous because the frequency noise is reduced.

1 SIMULTANEOUS TWO-ION MEASUREMENT

The alternate ion mass measurement scheme is analogous to comparing two masses with a spring balance. We put each mass on the balance, take the reading, and compare the readings. This method relies on the properties of the spring and the gravitational field remaining the same between the two measurements. In an analogous manner, our method relies on the electric and magnetic fields not changing between measurements on the two ions. A simpler scheme would be to use a simple balance that directly measures the difference between the two masses, at the same time.

Extending this to two ions in a Penning trap would mean measuring the cyclotron frequency difference between the two ions simultaneously. But the analogy is not so straightforward because the electromagnetic interaction between two ions in the trap is orders of magnitude stronger than the gravitational interaction between two neutral masses on opposite sides of a balance.

Previous analysis

Eric Cornell [COR90, CBF92] did a detailed analysis of the dynamics of two ions in a Penning trap when the ions are members of a doublet. The Coulombic interaction between the ions can be linearized when the inter-ion spacing is a constant of the motion. Then the normal modes can be solved for and the perturbations calculated. For a typical mass doublet, the splitting in the cyclotron frequencies of the two ions is a few kHz while the perturbation is of order a few mHz (with a 1 mm separation between the ions), therefore the cyclotron mode is only weakly perturbed. Similarly, the axial frequency splitting is a few 10's of Hz and the two axial modes remain only weakly coupled, at least when the axial amplitude is small. But the magnetron mode is nominally independent of mass (Eq. 1-12), and for a doublet the splitting is only a few 100's of μHz. Therefore, even when the inter-ion distance is 1 mm, the magnetron mode remains strongly coupled. The result of this is that the "magnetron" normal modes for the two-ion system are no longer independent motions of the two ions, but some linear combination of the two.

In particular, we can think of a stretch and common mode of the magnetron motions in analogy with a system of tightly coupled pendula, with the stretch mode corresponding to the two ions chasing each other around their center of motion, and the common mode corresponding to tandem bicycle wheel motion with the ions taking turns coming towards

and moving away from the trap center. The different symmetries of the two modes can be used to cool them preferentially by coupling to the cooled axial mode. If the common mode is cooled completely, then the two ions just chase each other around the trap and therefore sample essentially the same field inhomogeneities. The only source of systematic error is that the position of the two ions is not exactly symmetric with respect to the trap center (because of the small mass difference) and therefore the average fields sampled are not the same.

The error budget for such a measurement from field flaws (B_2 and C_4) and relativity showed that systematic errors could be kept below 0.01 ppb in a narrow range of inter-ion spacing (around 1 mm or so). This was after the common mode magnetron motion was cooled to its sideband cooling limit.

The most significant advantage of this scheme is that one needs to precisely measure only the *difference* cyclotron frequency between the two ions. Since this is wrapping phase at a rate of only a few kHz, we can integrate the phase for half an hour without fear of losing track of the phase wraps from random fluctuations in the magnetic field. In the alternate ion scheme, this integration time is currently limited to about five minutes.

Two-ion scheme using a reference ion

The new scheme I propose here for doing a simultaneous two-ion measurement uses a pair of ions that form a non-doublet, i.e. the ions are very dissimilar in their trap frequencies. The idea is to put one ion in a small magnetron orbit near the trap center and the other one in a large magnetron orbit. Then the ratio of the cyclotron frequencies that we measure is perturbed due to ion-ion interaction and due to the fact that the two ions are not measured at the same location. However, if we repeat this measurement with the inner ion replaced with a different (but similar) ion and without disturbing the magnetron orbit of the outer ion, then the ratio of the cyclotron frequencies is again perturbed, but to greatly the same extent as before. Therefore, the ratio of the ratios gives a unperturbed value of the mass ratio of the two inner ions. In effect, we have used the outer ion as a *reference* field monitor to eliminate field variations between the two measurements.

There are two crucial requirements for this method to work successfully. First of all, the two ions must stay in their respective magnetron orbits, i.e. the magnetron modes must only be weakly coupled. Secondly, and more critically, there must be no change in

the orbit of the reference ion while the inner ion is being changed. Our technique for ejection of the first inner ion and loading with a second inner ion must be done with negligible perturbation of the outer ion. We will quantify both these conditions in the following considerations.

In order to find the radial normal mode frequencies in the trap when two ions are present, we turn to the radial equation of motion first considered in Chapter 1 (Eq. 1-8). The only additional term is a Coulombic interaction term between the ions. We can therefore write the equations of motions for the two ions as:

$$\ddot{\boldsymbol{\rho}}_1 - \omega_{c1}\dot{\boldsymbol{\rho}}_1 \times \hat{z} - \tfrac{1}{2}\omega_{z1}{}^2\boldsymbol{\rho}_1 - \frac{e^2(\boldsymbol{\rho}_1 - \boldsymbol{\rho}_2)}{m_1|\boldsymbol{\rho}_1 - \boldsymbol{\rho}_2|^3} = 0, \tag{6-1}$$

$$\ddot{\boldsymbol{\rho}}_2 - \omega_{c2}\dot{\boldsymbol{\rho}}_2 \times \hat{z} - \tfrac{1}{2}\omega_{z2}{}^2\boldsymbol{\rho}_2 + \frac{e^2(\boldsymbol{\rho}_1 - \boldsymbol{\rho}_2)}{m_2|\boldsymbol{\rho}_1 - \boldsymbol{\rho}_2|^3} = 0. \tag{6-2}$$

These equations are not solvable exactly because of the nonlinear coupling term. We linearize the system by making the assumption that the magnetron modes of the two ions are only weakly perturbed and that throughout the motion $\rho_1 \approx$ const. and $\rho_1 >> \rho_2$, where 1 signifies the outer reference ion. Then the cubic term in the denominator can be approximated as $|\boldsymbol{\rho}_1 - \boldsymbol{\rho}_2|^3 \approx \rho_1{}^3$, and the equations of motion simplify to:

$$\ddot{\boldsymbol{\rho}}_1 - \omega_{c1}\dot{\boldsymbol{\rho}}_1 \times \hat{z} - \tfrac{1}{2}\omega_{z1}{}^2\boldsymbol{\rho}_1 - \Omega_1{}^2(\boldsymbol{\rho}_1 - \boldsymbol{\rho}_2) = 0, \tag{6-3}$$

$$\ddot{\boldsymbol{\rho}}_2 - \omega_{c2}\dot{\boldsymbol{\rho}}_2 \times \hat{z} - \tfrac{1}{2}\omega_{z2}{}^2\boldsymbol{\rho}_2 + \Omega_2{}^2(\boldsymbol{\rho}_1 - \boldsymbol{\rho}_2) = 0, \tag{6-4}$$

where we have defined the coupling constants

$$\Omega_i = \left(e^2/m_i\rho_1{}^3\right)^{1/2},\ i = 1, 2. \tag{6-5}$$

The normal mode frequencies can be obtained by assuming that, to lowest order, the radial orbits remain unperturbed. We plug solutions of the form $\mathrm{Re}\left(\boldsymbol{\rho}_{i,0}e^{i\omega t}\right)$ and solve the resultant characteristic equation:

$$\left(\omega^2 - \omega_{c1}\omega + \omega_m'\omega_{c1}\right)\left(\omega^2 - \omega_{c2}\omega + \omega_m'\omega_{c2}\right) - \omega_{c1}\omega_{c2}\omega_{\mathrm{int}}^2 = 0, \tag{6-6}$$

where we have introduced two new quantities,

$$\omega_{\text{int}} = \frac{{\Omega_1}^2}{\omega_{c1}} = \frac{{\Omega_2}^2}{\omega_{c2}} \ ,$$
$$\omega'_m = \frac{{\omega_{z1}}^2}{2\omega_{c1}} + \omega_{\text{int}} = \frac{{\omega_{z2}}^2}{2\omega_{c2}} + \omega_{\text{int}} \ . \tag{6-7}$$

The modification due to the interaction is contained in the quantity ω_{int}, while ω'_m is close to the interaction modified magnetron frequency. In the absence of ion-ion interaction, ω_{int} goes to 0 and we obtain the decoupled characteristic equation in Chapter 1 (Eq. 1-9). We can gain insight into the perturbation by considering the magnitude of ω_{int}.

With the outer ion in a 1 mm magnetron orbit, the interaction frequency is about 27 mHz. We can rewrite Eq. 6-6 by defining the four frequencies:

$$\omega'_{c1,2} = \tfrac{1}{2}\left(\omega_{c1,2} + \sqrt{\omega_{c1,2}^2 - 4\omega'_m\omega_{c1,2}}\right) \ ,$$
$$\omega'_{m1,2} = \tfrac{1}{2}\left(\omega_{c1,2} - \sqrt{\omega_{c1,2}^2 - 4\omega'_m\omega_{c1,2}}\right) \ , \tag{6-8}$$

so that the characteristic equation becomes,

$$(\omega - \omega'_{c1})(\omega - \omega'_{m1})(\omega - \omega'_{c2})(\omega - \omega'_{m2}) - \omega_{c1}\omega_{c2}\omega_{\text{int}}^2 = 0. \tag{6-9}$$

The four frequencies are the *exact* cyclotron and magnetron eigenfrequencies for the two ions if we neglect the last term and consider the simpler equation,

$$(\omega - \omega'_{c1})(\omega - \omega'_{m1})(\omega - \omega'_{c2})(\omega - \omega'_{m2}) = 0. \tag{6-10}$$

It can be verified that this assumption causes negligible error when the cyclotron frequencies are of order a few MHz and the magnetron frequencies are a few kHz. Let us take for a numerical example that the inner ion has mass 20 (*e.g.* Ne^+) while the outer ion has a mass of 40 (*e.g.* Ar^+). Then the difference between the true solution to Eq. 6-9 and the approximate ω'_{m1} is only 1 mHz, or 5 parts in 10^7, while the difference in the cyclotron frequency is below 0.5 ppt.

The four eigenfrequencies can be expanded in powers of powers of $\omega'_m/\omega_{c1,2}$ to see that the primary modification to the unperturbed frequencies comes from ω_{int}. For a mass 20 and mass 40 ion, the cyclotron frequencies are split by 3.2 MHz and it is virtually impossible to get the two ion modes strongly coupled. For the magnetron modes, the splitting is 600 mHz, while the interaction frequency is only 27 mHz at 1 mm separation. The coupling is weak if $\omega_{m1} - \omega_{m2} >> \omega_{\text{int}}$, i.e. the interaction causes a shift that is much

smaller than the splitting in the frequencies, which is satisfied quite well in our case. Therefore, our earlier assumption that the magnetron orbits of the two ions remain unperturbed (to lowest order) and the ions stay in their respective locations is quite valid. We can use perturbation theory to write the first order corrected magnetron orbits as

$$\begin{aligned}\boldsymbol{\rho}_1' &\approx \mathrm{Re}\left(\boldsymbol{\rho}_{1,0}e^{i\omega_{m1}'t} + \frac{\omega_{\mathrm{int}}}{\omega_{m1}-\omega_{m2}}\boldsymbol{\rho}_{2,0}e^{i\omega_{m2}'t}\right), \\ \boldsymbol{\rho}_2' &\approx \mathrm{Re}\left(\boldsymbol{\rho}_{2,0}e^{i\omega_{m1}'t} + \frac{\omega_{\mathrm{int}}}{\omega_{m2}-\omega_{m1}}\boldsymbol{\rho}_{1,0}e^{i\omega_{m2}'t}\right).\end{aligned} \tag{6-10}$$

This means that there is a 4% mixing of one ion's orbit into the other which causes a slow (600 mHz) variation in each orbit.

So far, we have tacitly assumed that the cyclotron and axial amplitudes of the two ions are negligible compared to the magnetron orbit separation. As long as this remains valid, the analysis that the magnetron modes are only weakly coupled is correct. The cyclotron radii used during the cyclotron frequency measurement are about 0.15 to 0.25 mm, which is not exactly negligible compared to 1 mm, but does not change the dynamics significantly. The axial amplitudes can be as large as 1 mm. But as we will see below, only one ion has significant axial amplitude at any given time. Furthermore, the axial amplitude is perpendicular to the radial plane of magnetron separation and therefore only decreases the interaction between the ions. Thus the magnetron perturbation decreases and the modes remain weakly coupled throughout.

SOF technique for mass ratio

The precision measurement of the mass ratio requires detecting the axial motions of both ions. As explained in Chapter 4, this poses a problem if the two ions have widely different frequencies as in the case of a non-doublet. The SOF technique for measuring the cyclotron frequency adapts quite well to the two-ion situation as well. The procedure when the inner ion is resonant with the detector and the outer one is non-resonant would be as follows: excite the cyclotron modes of both ions with short coherent pulses, allow them to evolve for a length of time T, then simultaneously apply a π-pulse to the inner ion and a second SOF pulse to the outer ion. The axial signal from the inner ion after the π-pulse can be immediately detected to determine its phase. For the outer ion, we wait until

the axial motion of the inner ion has cooled, change the trap voltage to make the outer ion resonant with the detector, then apply a π-pulse to determine its cyclotron amplitude.

The only problem with this straightforward extension is inferring the axial frequency for the outer ion using Eq. 4-10,

$$\omega_{z2} = \sqrt{M_1/M_2}\,\omega_{z1}. \tag{6-11}$$

This equation is valid in the absence of ion-ion perturbation and when both ions are measured at the same location, as in our alternate ion scheme. But when the outer ion is in a large magnetron orbit, its axial frequency can be shifted by a few parts in 10^6. However, as before, this causes a shift in the cyclotron frequency of a few ppb but the shift should be the same when we change the inner ion. Therefore the ratio of ratios remains unperturbed at the ppt range.

Perturbation in reference ion orbit

We finally turn to the all important question of how much perturbation in the orbit of the reference ion we can tolerate if we wish to reach a precision below 0.01 ppb. First of all, let us assume that the fields are perfect and the only perturbation comes from ion-ion interaction. If the two inner ions are measured with the reference ion in exactly the same orbit, the ratio of the ratios remains unperturbed at the 1 ppt level. But if the reference ion magnetron orbit changes by 0.1%, then the interaction changes enough to change the measured ratio at the 0.01 ppb level.

The second source of systematic error is that the field flaws sampled by the outer ion are different if its radius changes. Using the perturbation matrix (Eq. 3-21), we see that the shift in the cyclotron frequency of the reference ion (mass 40) when it is in a 1 mm magnetron orbit is about 5 ppb for our values of B_2 and C_4. If the radius of this orbit changes by $\delta\rho$, the change in ρ^2 is $2\rho\delta\rho$, so again the orbit should remain the same during both measurements to 0.1% to keep errors below 0.01 ppb.

This seems like a draconian requirement if the reference ion is in any way disturbed during the process of loading the second ion. It is difficult to theoretically estimate the changes in the orbit from our current ion loading process and we can only study this effect experimentally. So far, we have been able to load an Ar^+ reference ion into the trap, pulse it out into a large magnetron orbit, and then successfully load a Ne^+ ion near the center of our trap. We can also preferentially eject the Ne^+ ion and replace it with an-

other Ne^+ ion without noticeably perturbing the Ar^+ ion. But we have not yet performed a precision measurement of the cyclotron frequency ratios to determine if there is a change in the Ar^+ radius. If it turns out to be much worse than 0.1%, we will have to modify the loading technique or use a larger inter-ion separation to reduce the effect of ion-ion interaction (and shim the field inhomogeneities better since they will have a worse effect at larger radii).

Still this technique has several advantages over the doublet two-ion method. The most important one is that systematic errors arising from changes in the reference ion orbit can be studied easily. This can be done by trying to measure the exact ratio 1.000.... In other words, we measure the ratio of Ne^+ to Ar^+ with Ar^+ in the reference orbit, eject the Ne^+, reload with a second Ne^+, and again measure the ratio of Ne^+ to Ar^+. If the two ratios are not identical, the reference ion was unacceptably perturbed. The second advantage of using non-doublets is akin to the advantages of using calibrated ratios in Chapter 4. Using a pair of ions such as Ar^+ and Ar^{++} in the trap, the shifts in the ratio can be studied as a function of the radius of the reference magnetron orbit since the unperturbed ratio is already known.

The doublet two-ion scheme cannot be tested for systematic errors in this manner, *e.g.* by measuring the exact ratio of unity. This is because two identical ions is not a good limit to the analysis of the two-ion dynamics. Two identical ions have all their modes strongly coupled by ion-ion interaction because the unperturbed splitting is 0, i.e. the unperturbed modes are degenerate and any interaction lifts the degeneracy. The only way to study systematic errors is to use a loop of overdetermined ratios with doublets at different masses (as in our search for systematic errors in the doublet results). However, as mentioned before, the doublet technique has the significant advantage that the precision quantity to be measured is the simultaneous difference cyclotron frequency, which is only a few kHz. The non-doublet scheme requires us to measure two frequencies that differ by a few MHz and take their ratio. With our field fluctuations of 0.3 ppb, we will be limited to a 5 minute integration time before we start losing track of the phase. The resulting precision might only be 0.02 ppb or so, not unacceptably low but still a disadvantage.

2 CLASSICAL AMPLITUDE SQUEEZING

The size of the relativistic shift for light mass ions (below mass 20) is higher than 3 ppb. The thermal fluctuation in the cyclotron amplitude from the finite radius after the last π-pulse cooling then results in a fluctuation in the cyclotron frequency, which is about 10-20% of the mean shift. In order to reduce these fluctuations below our desired precision of 0.01 ppb, we have to figure out a scheme of reducing the amplitude noise in the cyclotron mode. The high frequency cooling discussed in Chapter 2 is one way of lowering the effective temperature of the cyclotron mode, but in this section we will describe an alternate scheme where we *squeeze* the amplitude noise into the cyclotron phase. The actual process of squeezing with a parametric drive is easily implemented in the axial mode, where we can modulate the trapping potential by applying a drive at $2\omega_z$. The squeezed distribution can then be transferred into the cyclotron mode with a π-pulse.

Quadrature squeezing using a parametric drive to decrease the noise in one phase quadrature at the expense of the other is now well established in the optical regime. But as shown in our paper, there is a limit to the amount of *amplitude* noise reduction that is possible using quadrature squeezing. Our problem therefore was to develop a scheme of amplitude squeezing the noise in our classical oscillator. The key idea to achieve this was to use the nonlinearity in the oscillator to effectively stop the parametric amplification at an amplitude determined by the size of the nonlinearity. As the amplitude of the oscillator increases due to the parametric drive, it passes a threshold where the amplitude is large enough to shift the frequency significantly and the oscillator begins to dephase with respect to the drive. The actual details of using this technique are given in the following section.

The solution to the problem of a parametrically driven nonlinear oscillator was initially determined by Frank DiFilippo using a numerical integration method.

Phys. Rev. Lett. paper on squeezing

The details of our proposed amplitude squeezing technique and the results of computer simulations were originally published in Physical Review Letters. I attach a reprint of this paper in this section.

PHYSICAL REVIEW
LETTERS

VOLUME 68 | 11 MAY 1992 | NUMBER 19

Classical Amplitude Squeezing for Precision Measurements

Frank DiFilippo, Vasant Natarajan, Kevin R. Boyce, and David E. Pritchard
Research Laboratory of Electronics, Department of Physics, Massachusetts Institute of Technology, Cambridge, Massachusetts 02139
(Received 21 January 1992)

In analogy to squeezing of light, noise in a classical oscillator can be squeezed to reduce amplitude uncertainty. While this can be achieved to some extent in a harmonic oscillator parametrically driven at $2\omega_0$, true amplitude squeezing is possible in anharmonic oscillators, either by driving at $2\omega_0$ or allowing amplitude-dependent dephasing. These techniques can reduce the uncertainty in measurements of the frequency of an oscillator; for example, the thermal uncertainty in the relativistic frequency shift in single ion mass spectroscopy can be reduced by more than a factor of 5.

PACS numbers: 06.20.−f, 07.75.+h, 42.50.Dv, 46.10.+z

In recent years, understanding of squeezed light [1,2] has evolved to the point that detection below the shot-noise limit has been demonstrated [3,4], and several applications of these nonclassical states are being considered [5]. Although the emphasis has been in the quantum regime, where the source of noise is the uncertainty principle, there is a classical correspondence [6] which suggests that noise of a thermal or technical origin can be squeezed to minimize its unwanted effects on a particular measurement. Such a reduction of thermal noise in a quadrature component has been observed in a high-Q classical oscillator by parametric excitation and has applications to atomic force microscopy and gravity wave detection [7]. A similar reduction in amplitude uncertainty would be useful for determining the frequency of an anharmonic oscillator in the presence of noise. Since the frequency is amplitude dependent, fluctuations in amplitude will result in fluctuations in the measured frequency. This paper describes three schemes for amplitude squeezing in a classical anharmonic oscillator: by driving parametrically at $2\omega_0$ in the anharmonic and harmonic regimes, and by dephasing in an undriven oscillator. As an illustration, this concept is applied to high-precision mass spectroscopy of a single trapped ion.

We begin by considering the motion of a classical anharmonic oscillator parametrically driven at twice the resonant frequency. A simple treatment is presented, with emphasis on the phase diagram, of an undamped resonant oscillator to lowest order in the parametric drive strength and the anharmonicity. (Higher-order expansions, detuning, and damping [8,9] can be neglected for the mass spectroscopy example.) Afterwards, the special cases of no anharmonicity and no parametric drive are considered.

The potential for a one-dimensional oscillator with a small ($\alpha z^2 \ll 1$) quartic anharmonic correction whose frequency is modulated at $2\omega_0$ by a weak ($\varepsilon \ll 1$) parametric drive is

$$U(z,t) = \tfrac{1}{2} m\omega_0^2 z^2 (1 + \varepsilon \sin 2\omega_0 t + \tfrac{1}{2}\alpha z^2) . \tag{1}$$

To lowest order in α and ε, higher harmonics can be neglected, and one expects oscillation only at ω_0:

$$\begin{aligned} z(t) &= r(t)\cos(\omega_0 t - \theta(t)) \\ &= C(t)\cos\omega_0 t + S(t)\sin\omega_0 t . \end{aligned} \tag{2}$$

In this approximation, $C(t)$ and $S(t)$ are slowly varying (i.e., $dC/dt, dS/dt \ll r\omega_0$). Thus d^2C/dt^2 and d^2S/dt^2 can be neglected in the equation of motion, yielding the autonomous system of equations

$$\frac{dC}{dt} = \kappa(C + \gamma r^2 S), \quad \frac{dS}{dt} = -\kappa(S + \gamma r^2 C) , \tag{3}$$

where

$$\kappa = \varepsilon\omega_0/4, \quad \gamma = 3\alpha/2\varepsilon .$$

Rewriting in terms of r and θ leads to the first integral of the motion:

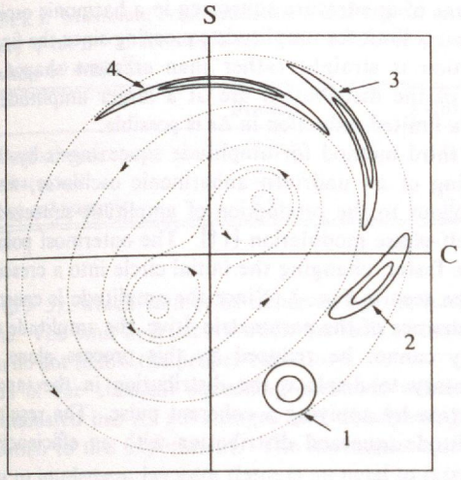

FIG. 1. Amplitude squeezing for an anharmonic oscillator driven at $2\omega_0$ for $\gamma<0$. Initial Gaussian contours (1) are transformed along the phase trajectories in the C-S plane (dotted lines) through intermediate states (2) and (3) until amplitude uncertainty is reduced (4). (The $\gamma>0$ diagram is obtained by reflecting about either axis.)

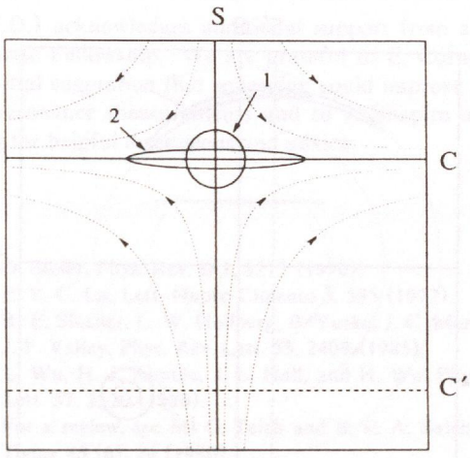

FIG. 2. Quadrature squeezing for a harmonic oscillator driven at $2\omega_0$. An initial Gaussian distribution (1) at the origin is transformed along the hyperbolic phase trajectories into an elliptical distribution (2). A coherent pulse displaces the distribution so that its major axis is in the tangential direction, resulting in a reduced amplitude uncertainty with respect to the final coordinates (C',S).

$$a^4=r_1^2r_2^2=r^4+2r^2\sin2\theta/\gamma+1/\gamma^2\,, \tag{4}$$

which specifies the trajectories in phase space (Fig. 1). They are Cassinian ovals, defined as the loci of points which maintain a constant product of the distances r_1 and r_2 from the two fixed points (centers) located at (r^*,θ^*):

$$r^*=|\gamma|^{-1/2},\quad \theta^*=\mathrm{sgn}(\gamma)\tfrac{1}{4}\pi\pm\tfrac{1}{2}\pi\,. \tag{5}$$

This enables the system of equations to be decoupled, and the time evolution along the trajectories is obtained by solving the resultant elliptic integral equation for $r(t)$ or $\theta(t)$. There are two topologically distinct types of phase trajectories. The "outer" trajectories (case $a>r^*$) encircle both centers, and the time evolution is determined from

$$\kappa t=-(1/2\gamma a^2)[F(\Theta_>(\theta)|1/\gamma^2a^4)]_{\theta=\theta(0)}^{\theta=\theta(t)}\,, \tag{6}$$

where

$$\sin\Theta_>(\theta)=\frac{\sin2\theta}{(1-\cos^2 2\theta/\gamma^2a^4)^{1/2}}$$

and $F(\phi|m)$ is the Legendre elliptic integral of the first kind [10]. The "inner" trajectories (case $0<a<r^*$) encircle just one of the centers. From (4), there are two solutions for r, and the trajectories evolve according to

$$\kappa t=\tfrac{1}{2}[\pm F(\Theta_<(\theta)|\gamma^2a^4)]_{\theta=\theta(0)}^{\theta=\theta(t)}\,, \tag{7}$$

where

$$\sin\Theta_<(\theta)=\cos2\theta/|\gamma a^2|\,.$$

This phase diagram can be qualitatively understood as a competition between the parametric excitation and the anharmonicity. The parametric drive amplifies the in-phase component and attenuates the out-of-phase component, resulting in a flow towards large $|C|$ and small $|S|$. The anharmonicity causes dephasing, appearing as a rotation about the origin. At the centers, the two effects cancel.

The well-known cases of the parametrically driven harmonic oscillator and the undriven anharmonic oscillator can be recovered by letting $\alpha\to0$ and $\varepsilon\to0$, respectively. For the driven harmonic case, the only fixed point is a saddle point at the origin. The phase trajectories are hyperbolic (Fig. 2), flowing towards large $|C|$ and small $|S|$. They are specified by the constant of the motion $\lambda'=r^2\sin2\theta$, and their time evolution is given by $C(t)=C(0)e^{\kappa t}$ and $S(t)=S(0)e^{-\kappa t}$. For the undriven anharmonic case, the fixed points merge into a center at the origin. The amplitude r is the constant of the motion, and the phase trajectories are concentric circles (Fig. 3) evolving according to $\theta(t)=\kappa\gamma r^2t/\omega_0$.

The above equations can be used to study how the thermal noise statistics are affected by parametric amplification and anharmonicity. The noise is simply modeled so that the quadrature components C and S for an ensemble of identically cooled oscillators are Gaussian with equal standard deviations: $\Delta C=\Delta S=\sigma$. If this noise is displaced to a large mean amplitude ($\langle r\rangle\gg\sigma$), the polar components r and θ are approximately Gaussian near the center of the distribution. In this limit, the amplitude uncertainty and the phase uncertainty are about equal: $\Delta r\cong\langle r\rangle\Delta\theta\cong\sigma$.

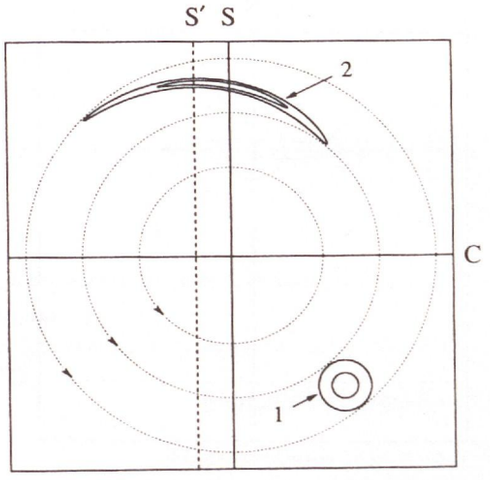

FIG. 3. Amplitude squeezing for an undriven anharmonic oscillator. An initial Gaussian distribution (1) dephases with constant amplitude, becoming a crescent distribution (2). After aC displacement in the tangential direction, the distribution is amplitude squeezed with respect to the new coordinates (C,S').

The thermal noise can be "amplitude squeezed" by a transformation which produces a crescent-shaped distribution while maintaining the same phase-space density (by Liouville's theorem), thereby reducing the amplitude uncertainty at the expense of the phase uncertainty. If this process is fast enough, further thermal effects may be ignored. An ideal amplitude-squeezing process preserves the product $\langle r\rangle\Delta r\Delta\theta$, just as a minimum uncertainty quantum state. This fact can be used to characterize the quality of squeezing by defining a "squeezing efficiency" η as

$$\eta=\sigma^2/\langle r\rangle\Delta r\Delta\theta\,, \tag{8}$$

which is unity for a "minimum uncertainty" classical distribution.

In the driven anharmonic oscillator, the initial circular distribution is distorted into a crescent along the outer trajectories, as shown in Fig. 1. Amplitude squeezing occurs where the flow is toward smaller amplitude, in this case near the S axis. The points with larger amplitude move faster in phase space and reach this region first, thereby reducing the amplitude uncertainty. Squeezing efficiencies close to 1 can be attained by this method. Reduced amplitude uncertainty can also result from propagation along the inner trajectories, but to a much lesser extent.

Quadrature squeezing can be achieved by driving the oscillator at $2\omega_0$ in the harmonic regime. The initial circular distribution becomes elliptical, preserving the relationship $\Delta C\Delta S=\sigma^2$. In order to achieve reduction in Δr, a coherent force pulse must be applied to displace the distribution such that the major axis is along the tangential direction [5] (Fig. 2). Although there is no limit to the amount of quadrature squeezing in a harmonic oscillator, there is a limit for amplitude squeezing since the final distribution is straight rather than crescent shaped. The tails of the distribution are at a larger amplitude; thus only a limited reduction in Δr is possible.

A third method for amplitude squeezing is by the dephasing of an undriven anharmonic oscillator, which is analogous to the production of amplitude-squeezed light by self-phase modulation [11]. The outermost points dephase faster, changing the initial circle into a crescent, as can be seen in Fig. 3. Since the amplitude is constant in the absence of the parametric drive, the amplitude uncertainty cannot be reduced by this process alone. It is necessary to displace the distribution in the tangential direction by applying a coherent pulse. The result is an amplitude-squeezed distribution with an efficiency close to 1.

The techniques discussed so far can have important applications in single-ion mass spectroscopy. To date, relative mass measurements have been made up to an accuracy of 4×10^{-10} in a Penning trap [12,13]. When the precision is improved to the 10^{-11} range, relativistic effects will cause significant error if the mode amplitudes are known only to their thermal cooling limits. To lowest order, the velocity of a trapped ion is $v=\omega_c'\rho_c$, where $\omega_c'\cong eB/mc$ and ρ_c are the trap cyclotron frequency and radius. Thus the relativistic mass shift δm is amplitude dependent, and the thermal uncertainty in ρ_c will cause a mass uncertainty of

$$\Delta\left(\frac{\delta m}{m}\right)=\frac{\omega_c'^2}{2c^2}\Delta(\rho_c^2)\cong\frac{\omega_c'^2}{c^2}\langle\rho_c\rangle\Delta\rho_c\,. \tag{9}$$

A single trapped ion [14] is well suited for the above squeezing schemes. The ion's amplitude and phase can be controlled by applying coherent pulses to the endcaps, and the trap anharmonicity can be adjusted by tuning the compensation electrodes. The ion can be decoupled from the resonant detector by changing the trapping potential, becoming effectively undamped. By squeezing the thermal noise, the precision can be improved by the factor β:

$$\beta=\frac{\Delta(\rho_c^2)(\text{unsqueezed})}{\Delta(\rho_c^2)(\text{squeezed})}\,. \tag{10}$$

Computer simulations of the evolution of an initial Gaussian noise distribution of 10000 points were done using typical experimental parameters to calculate the squeezing efficiencies and error reductions that would be possible. The final amplitude was adjusted to be 20 times the initial rms amplitude after cooling, ensuring that the ion would stay within the region where the anharmonicity can be controlled. All the additional parameters were adjusted to maximize the error reduction β for a specific squeezing time. Table I summarizes β and η for the three methods. Both anharmonic schemes can achieve true amplitude squeezing ($\eta\cong1$) with large error reduc-

TABLE I. Maximum error reduction β and typical squeezing efficiency η (at $\beta=5$) for single-ion mass spectroscopy simulations where $\langle r\rangle=20\sqrt{2}\sigma$.

	β(max)	η (for $\beta=5$)
Driven anharmonic	5.8	0.97
Driven harmonic	2.5	...
Undriven anharmonic	8.7	0.98

tions ($\beta>5$), which cannot be achieved by the harmonic scheme. The limit in β occurs when the tails of the distribution do not follow the proper curvature.

Each of the classical squeezing methods which have been discussed has its advantages and disadvantages for application to this experiment. The harmonic squeeze is easiest to implement because there is no need to introduce anharmonicity, but it has a low β and η. Nonetheless, because of its simplicity, the harmonic squeeze would be useful as a first step before exploring the anharmonic methods. The main advantage of the driven anharmonic squeeze is that a final pulse is not needed. The undriven anharmonic squeeze offers the most error reduction, but like the harmonic squeeze, it requires a final pulse whose phase must be precisely controlled with respect to the evolved distribution. In this experiment, however, having β greater than about 5 is not desirable because the increased phase uncertainty substantially increases the measurement time. Also, since the same measurement is performed many times, a squeezing process with fewer steps would be more practical. Thus the driven anharmonic method appears to be the most appropriate for this application.

This work was supported by National Science Foundation Grant No. 8921769-PHY and Joint Services Electronics Program Grant No. DAAL03-92-C-0001. One of us (F.D.) acknowledges additional support from a NSF Graduate Fellowship. We are grateful to E. Cornell for the initial suggestion that squeezing could improve cyclotron resonance measurements and to J. Shapiro and F. Wong for helpful discussions and advice.

[1] D. Stoler, Phys. Rev. D **1**, 3217 (1970).
[2] E. Y. C. Lu, Lett. Nuovo Cimento **3**, 585 (1972).
[3] R. E. Slusher, L. W. Hollberg, B. Yurke, J. C. Mertz, and J. F. Valley, Phys. Rev. Lett. **55**, 2409 (1985).
[4] L. Wu, H. J. Kimble, J. L. Hall, and H. Wu, Phys. Rev. Lett. **57**, 2520 (1986).
[5] For a review, see M. C. Teich and B. E. A. Saleh, Phys. Today **43** (6), 26 (1990).
[6] F. Hong-Yi and J. VanderLinde, Phys. Rev. A **40**, 4785 (1989).
[7] D. Rugar and P. Grütter, Phys. Rev. Lett. **67**, 699 (1991). In this damped case, the $2\omega_0$ drive was operated below the threshold for parametric amplification, allowing a maximum noise reduction of a factor of 2.
[8] N. N. Bogoliubov and Y. A Mitropolsky, *Asymptotic Methods in the Theory of Non-Linear Oscillations* (Gordon and Breach, New York, 1961).
[9] C. Hayashi, *Nonlinear Oscillations in Physical Systems* (McGraw-Hill, New York, 1964).
[10] M. Abramovitz and I. A. Stegun, *Handbook of Mathematical Functions* (Dover, New York, 1970).
[11] M. Kitagawa and Y. Yamamoto, Phys. Rev. A **34**, 3974 (1986).
[12] E. A. Cornell, R. M. Weisskoff, K. R. Boyce, R. W. Flanagan, Jr., G. P. Lafyatis, and D. E. Pritchard, Phys. Rev. Lett. **63**, 1674 (1989).
[13] E. A. Cornell, Ph.D. thesis, Massachusetts Institute of Technology, 1990 (unpublished).
[14] L. Brown and G. Gabrielse, Rev. Mod. Phys. **58**, 233 (1986).

Proposed experiment to demonstrate squeezing

The simplest way to demonstrate the reduction in cyclotron amplitude fluctuations by the squeezing technique is to convert the amplitude noise to axial frequency fluctuations using the effective bottle shift (Chapter 3, Eq. 3-21):

$$\delta\omega_z = \omega_z\left(\frac{\omega_c' B_2}{4\omega_m} - \frac{3C_4}{2d^2}\right)\rho_c^{\,2} = \omega_z\left(\frac{\omega_c' B_{2,\mathrm{eff}}}{4\omega_m}\right)\rho_c^{\,2}\,. \tag{6-12}$$

If the thermal RMS radius of the cooled cyclotron mode is $\rho_{c,th}$, and the drive pulse results in a radius $\rho_{c,0}$, then the resulting fluctuation in $\rho_c^{\,2}$ is given by $\sqrt{2}\rho_{c,0}\rho_{c,th}$. This causes an RMS thermal scatter in the measured axial frequency given by:

$$\Delta\omega_{z,rms}(\mathrm{thermal}) = \omega_z\left(\frac{\omega_c' B_{2,\mathrm{eff}}}{4\omega_m}\right)\sqrt{2}\rho_{c,0}\rho_{c,th}. \tag{6-13}$$

The RMS scatter in the axial frequency should decrease below the thermal value as we squeeze the amplitude noise. For the simple case of quadrature squeezing, the RMS noise level oscillates around the thermal value as we vary the phase between the squeeze pulse and the drive pulse, with an optimal reduction by a factor of about 2.

The thermal RMS radius after cooling the cyclotron mode with a π-pulse is given from the sideband cooling limit (Eq. 1-15) as:

$$\rho_{c,th} = \left(\frac{2T_z}{m\omega_z\omega_c'}\right)^{1/2}, \tag{6-14}$$

where T_z is the temperature of the cooled axial mode. This value is nearly independent of mass since we use the same axial frequency for all ions and ω_c' scales inversely with mass. Using a typical value of 10 K for the axial temperature, we obtain $\rho_{c,th}$ as 0.001 cm. If we use a mass 20 ion for the squeezing experiment (say Ar^{++}, which gives twice the signal and has half the damping time of a singly charged ion), we would use a pulsed amplitude $\rho_{c,0}$ of 0.17 cm, which is 17 times larger than the thermal RMS value. We can measure the axial frequency with a precision of about 15 mHz, so in order to measure the thermal RMS fluctuation in ω_z from Eq. 6-13, we have to ensure that the fluctuation is at least 30 mHz. This can be achieved if the value of $B_{2,\mathrm{eff}}$ is about 1×10^{-5}, which results in thermal fluctuations in the axial frequency of 38 mHz, an easily detectable value. Such a high value of $B_{2,\mathrm{eff}}$ can be attained either by turning up B_2 using the shim coils of the magnet, or by changing the guard ring voltage and turning up C_4. Increasing C_4 is easier

to implement but has the disadvantage of spoiling the axial response, while changing B_2 involves a more complicated procedure of energizing the shim coils but does not affect the harmonicity of the axial response.

The actual measurement would involve a sequence of cooling the cyclotron mode with a π-pulse, applying a squeeze pulse to the axial mode and transferring the squeezed noise to the cyclotron mode, exciting the cyclotron mode with a drive pulse, and finally measuring the axial frequency. Each sequence will take about 35 s, and it has to be repeated about 200 times (to obtain a good measure of $\Delta\omega_{z,rms}$) for a given phase relation between the squeezed noise and the drive pulse. The advantage with measuring the noise in the axial frequency is that these measurements can be done during the day since magnetic field fluctuations are not important in this scheme.

3 FUTURE DIRECTIONS

In this forward looking last section, I will point the directions towards achieving some of the goals mentioned in the first chapter. We will see our attempts at making the important mass 3 measurement for the neutrino mass and how they might be solved soon. Reaching higher precision might ultimately come down to a choice between a mechanical solution of stabilizing the magnetic field, or one of the techniques of two-ion resonance measurements.

Attempts at ^3H - ^3He

Our earliest attempts at the helium-tritium mass comparison were plagued by vacuum problems. We only attempted to load HD^+ ions and could not get the trap tuned well enough to be able to see the ion's pulsed response. We had to abandon the attempts when the number of bad ions being produced started increasing dramatically, indicating that the vacuum was going bad.

Our second attempt took place last summer. This time we were able to tune the trap quite well and see an HD^+ ion both with the two-drive scheme and in a pulsed transient mode. In order to improve the signal to noise ratio, we had to move the ion off the center of the coil frequency where the noise floor drops noticeably. We were also able to make a preliminary measurement of the cyclotron frequency using the avoided crossing method. We did not have any problems with the vacuum probably because of our more

efficient ion-making scheme and the charcoal cryo-sorber (see Chapters 1 and 2). The only drawback this time was that we could not automate the bad ion killing process well enough to get a good single ion each time. This was presumably due to the fact that all the impurity ions were now much heavier and had axial frequencies around 10-50 kHz when the voltage was set to make HD^+ resonate at 160 kHz. Our transformers are designed not to pass a lot of energy in this range and we had to pump a lot of noise power in order to excite the impurity ions. But this also caused the good ion to get excited (despite the -30 dB notch filter at 160 kHz) because it is much lighter. When we dipped the cloud, we almost always lost the good ion too.

The solution we attempted was to turn up the trap voltage so that the axial frequency of HD^+ was close to 500 kHz and then apply the noise (without the notch filter). Now the impurity ions have axial frequencies in the 30-160 kHz range and hopefully see much more noise power. This worked quite well even though we did not perfect the technique.

Our concern this time for not pursuing the measurement was the fear of introducing tritium onto the trap surfaces. We estimated that if we used up the total dose of tritium we had purchased (75 mCi), there would be enough of it adsorbed on the inside surfaces of the trap electrodes that an atom would be undergoing beta decay every 10 seconds or so. This means that there would be an 18 kV electron coming out of the trap walls every few seconds, with the potential to ionize either some background gas atom or something off the opposite trap wall and thereby introduce a bad ion. This would make a long measurement quite impossible and probably contaminate the trap for ever.

So what are the solutions? If either of the two-ion schemes work, we have the potential to do this measurement easily and quickly. With two ions, we need to make ions only a few times, which translates to a low radioactive dose. Secondly, we can probably get to much higher precision. The other solution is to get the external ion-loader working. Then the bad ion problem is much reduced and so is the total gas load. We will still have to make many measurements to average the magnetic field variations, but at least we understand the systematics for the alternate single ion scheme. And the required precision to help the ß ray spectroscopists is only about 0.1 ppb.

Higher precision

The fundamental choice on the road to higher precision is whether we want to reduce the magnetic field noise with clever mechanical design or finesse the whole problem with two-ion techniques. Using a superconducting loop around the trap can dramatically improve the shielding of external magnetic noise but, since the loop conserves flux, it is necessary to keep it dimensionally stable. We found a significant improvement in the magnet stability after we added a pressure regulator over the magnet liquid He bath. Adding pressure control over the experiment cryo-bore might be similarly useful as the temperature along the insert remains much more stable. This might also be necessary in keeping the superconducting shielding loop stable.

But our current inclination is that precision in the ppt range will be limited by factors other than just magnetic field noise. For instance, the applied voltage on the trap will have to be stable to a part in 10^8 or better. This may be right at the edge of current technology and definitely beyond the capability of the present voltage box. These kinds of problems are not true for two-ion mass spectroscopy where temporal fluctuations in the electric field is also the same for both ions. However, spatial variations in the trapping fields become more important because the two ions have to be spatially separated. Until we understand the exact dependencies of the fields with increasing radius, we cannot truly evaluate the systematic errors arising from them or hope to correct for the shifts. Our analysis shows that if the effects are dominated by the B_2 and C_4 terms, they can be shimmed sufficiently well and maybe even used to cancel each other's shifts and the shift due to special relativity. If the shifts come from higher order electrostatic terms though, we might need to modify the trap to have extra shim electrodes to compensate for them. Despite these obstacles, two-ion techniques seem to be the most promising approach to ppt precision.

BIBLIOGRAPHY

AUD93 G. Audi, private communications (1993).

BBB92 H. Backe *et al.*, "A new upper limit of the electron antineutrino rest mass from tritium β-decay", *Proc. 6th NFFS + 9th AMCO Conf.* (Bernkastel-Kues, Germany, 1992, to be published).

BHK92 G. Bollen *et al.*, "High-accuracy mass measurements on unstable Rb, Sr, Cs, Ba, Fr and Ra isotopes", *Proc. 6th NFFS + 9th AMCO Conf.* (Bernkastel-Kues, Germany, 1992, to be published).

BOY92 K.R. Boyce, "Improved Single Ion Cyclotron Resonance Mass Spectroscopy", (Ph.D. thesis, Massachusetts Institute of Technology, 1992).

BRG86 L.S. Brown and G. Gabrielse, "Geonium theory: Physics of an electron or ion in a Penning trap", *Rev. Mod. Phys.* **58**, 233 (1986).

CBF92 E.A. Cornell, K.R. Boyce, D.L.K. Fygenson, and D.E. Pritchard, "Two ions in a Penning trap: Implications for precision mass spectroscopy",*Phys. Rev. A* **45**, 3049 (1992).

CDB91 J.B. Camp, T.W. Darling, and R.E. Brown, "Macroscopic variations of surface potentials of conductors", *J. Appl. Phys.* **69**, 7126 - 7129 (1991).

COR90 E.A. Cornell, "Mass Spectroscopy Using Single Ion Cyclotron Resonance", (Ph.D. thesis, Massachusetts Institute of Technology, 1990).

CWB89 E.A. Cornell, R.M. Weisskoff, K.R. Boyce, R.W. Flanagan Jr., G.P. Lafyatis, and D.E. Pritchard, "Single-ion cyclotron resonance measurement of $M(CO^+)/M(N_2{}^+)$"*Phys. Rev. Lett.* **63**, 1674 (1989).

CWB90 E.A. Cornell, R.M. Weisskoff, K.R. Boyce, and D.E. Pritchard, "Mode coupling in a Penning trap: π pulses and a classical avoided crossing", *Phys. Rev. A* **41**, 312 (1990).

DNB92 F. DiFilippo, V. Natarajan, K.R. Boyce, and D.E. Pritchard, "Classical amplitude squeezing for precision measurements", *Phys. Rev. Lett.* **68**, 2859 (1992).

FLA87 R.W. Flanagan, "Trapping and Detection of Ions" (Ph.D. thesis, Massachusetts Institute of Technology, 1987).

GAT88 G. Gabrielse and J. Tan, "Self-shielding superconducting solenoid systems" *J. Appl. Phys.* **63**, 5143 (1988).

GFO90 G. Gabrielse *et al.*, "Thousandfold improvement in the measured antiproton mass", *Phys. Rev. Lett.* **65**, 1317 (1990).

GMN93 M.V. Gorshkov, A.G. Marshall, and E.N. Nikolaev, "Analysis and elimination of systematic errors originating from coulomb mutual interaction and image charge in Fourier transform ion cyclotron resonance precise mass difference measurements", submitted to *J. Am. Soc. Mass. Spec.* (1993).

GRR80 I.S. Gradshteyn and I.M. Ryzhik, *Table of Integrals, Series, and Products*, 451 (Academic Press, New York, 1980).

GWW90 C. Gerz, D. Wilsdorf, and G. Werth, "Measurement of the ^{4}He-D_2 mass difference", *Z. Phys. D* **17**, 119 (1990).

JHB67 W.H. Johnson, M.C. Hudson, R.A. Britten, and D.C. Kayser, "Recent results of measurements by the Minnesota 16-inch mass spectrometer", *Proc. Third International Conf. on Atomic Masses*, ed. R.C. Barber, 793 (University of Manitoba Press, 1967).

JOH84 W.H.Johnson, "The measurement of atomic masses by mass spectroscopic methods and a role for atomic masses in the determination of fundamental constants", *Precision Measurements and Fundamental Constants II*, eds. B.N.Taylor and W.D.Phillips, NBS Special Publication No. 617 (U.S. GPO, Washington D.C.) 335 (1984).

KAM81 S.M. Kay and S.L. Marple, Jr., "Spectrum analysis - A modern perspective", *Proc. IEEE* **69**, 1380 (1981).

KUT82 R. Kumaresan and D.W. Tufts, "Estimating the parameters of exponentially damped sinusoids and pole-zero modeling in noise", *IEEE Trans. Acous., Speech, and Sig. Proc.* **ASSP-30**, 833 (1982).

LMH88 M.A. Levine, R.E. Marrs, J.R. Henderson, D.A. Knapp, and M.B. Schneider, "The electron beam ion trap: A new instrument for atomic physics measurements", *Physica Scripta T22*, 157 (1988).

NBD92 V. Natarajan, K.R. Boyce, F. DiFilippo, and D.E. Pritchard, "Improved precision mass comparison in a Penning trap - techniques and results", *Proc. 6th NFFS + 9th AMCO Conf.* (Bernkastel-Kues, Germany, 1992, to be published).

NIR51 A.O.Nier and T.R. Roberts, "The determination of atomic mass doublets by means of a mass spectrometer", *Phys. Rev.* **81**, 507 (1951).

PEN36 F.M. Penning, "Die Glimmentladung bei niedrigem druck zwischen koaxialen zylindern in einem axialen Magnetfeld", *Physica* **3**, 873 (1936).

PFT88 W.H. Press, B.P. Flannery, S.A. Teukolsky, and W.T. Vetterling, *Numerical recipes in C - The art of scientific computing* (Cambridge University Press, 1988).

RBS91 R.G.H. Robertson *et al.*, "Limit on $\overline{\nu}_e$ mass from observation of the β decay of molecular tritium", *Phys. Rev. Lett.* **67**, 957 (1991).

RIB74 D.C. Rife and R.R. Boorstyn, "Single-tone parameter estimation from discrete-time observations", *IEEE Trans. Info. Theory* **IT-20**, 591 (1974).

VFS92 R.S. Van Dyck Jr., D.L. Farnham, and P.B. Schwinberg, "High precision Penning trap mass spectroscopy of the light ions", *Proc. 6th NFFS + 9th AMCO Conf.* (Bernkastel-Kues, Germany, 1992, to be published).

VFS93a R.S. Van Dyck Jr., D.L. Farnham, and P.B. Schwinberg, "Atomic mass measurements of H, He, and C, yielding neutron separation energies" and "Atomic mass measurements of ^{14}N and ^{16}O and the CO^+/N_2^+ comparison", Abstracts submitted for the Washington D.C. Meeting of the American Physical Society, Arpil 12-15, 1993. The first abstract was revised after we pointed out the discrepancy in the mass of D, and we thank Van Dyck for sending us an advance copy of the revised abstract.

VFS93b R.S. Van Dyck Jr., D.L. Farnham, and P.B. Schwinberg, "Tritium – Helium-3 mass difference using the Penning trap mass spectroscopy", *Phys. Rev. Lett.* **70**, 2888 (1993).

VMF86 R.S. Van Dyck, F.L. Moore, D.L. Farnham and P.B. Schwinberg, "Improved measurement of proton-electron mass ratio", *Bull. Amer. Phys. Soc.* **31**, 244 (1986).

VSD87 R.S. Van Dyck Jr., P.B. Schwinberg, and H.G. Dehmelt, "New high-precision comparison of the electron and positron *g* factors", *Phys. Rev. Lett.* **59**, 26 (1987).

WAA85 A.H. Wapstra and G. Audi, "The 1983 Atomic mass evaluation (I). Atomic mass table", *Nuc. Phys. A* **432**, 1 (1985).

WAP93 A.H. Wapstra, private communications (1993).

WEI88 R.M. Weisskoff, "Detecting Single, Trapped Ions" (Ph.D. thesis, Massachusetts Institute of Technology, 1988).

WID75 D.J. Wineland and H.G. Dehmelt, "Line shifts and widths of axial, cyclotron and g-2 resonances in tailored, stored electron (ion) cloud", *Int. J. Mass Spec. Ion Proc.* **16**, 338 (1975). See also the errata and addendum, *Int. J. Mass Spec. Ion Proc.* **19**, 251 (1976).

ACKNOWLEDGEMENTS

Its finally over and I have come to the easiest and, in many ways, the hardest part of writing the thesis - thanking and remembering to thank everyone who contributed to this work.

Dave Pritchard interviewed me while sitting in a hospital bed and offered me this opportunity to work in ion trapping, probably because he could not see very well that day! He provided both financial and much needed moral support when we seemed to be hitting up against the same wall over and over again. He let me pursue my ideas on the experiment, although his expert intuition about whether they would work often proved right. I am also indebted to Profs. Sorab Ghandhi and Ishwara Bhat who taught me a lot of my experimental skills and gave me a great introduction to graduate school at RPI before I came to MIT.

This experiment would not have been possible without the tireless efforts of the "ghosts of ICR past" - Greg Lafyatis, Bob Flanagan, Robert Weisskoff and Eric Cornell - who left behind volumes of notes, calculations, and useful theses, but most importantly, the knowledge that "if you build it (the trap), they (the single ions) will come!". It is infinitely easier to look for ions when you know that they have been seen before (though there was a time when I was beginning to suspect that it was all one big conspiracy). I overlapped with Eric Cornell only for a few months, but in that time he taught me to think intuitively about the dynamics in a Penning trap, both with one and two ions. He still remains one of the first persons I turn to (via the wonders of email) when I need to clear up some confusing detail about the physics inside a trap.

Kevin Boyce was the electronics guru for our experiment and most of the lab. He combined a physics background with radio and electronics experience to make the perfect experimentalist - don't give me those integrals, let me get my hands on the real stuff. He was also the link to the first two generations of the ICR experiment, and was always able to remember the "historical reasons" for having some useless thing in the apparatus (except the 1000/1111 switch, which he did not tell us about and cost us 2 weeks). Frank DiFilippo is the most meticulous and organized researcher in our group, and an ideal stabilizer to the impulses that Kevin and I were given to. He has taken great care of the apparatus, the magnet and our Mac. He is also responsible for much of our LabView control software (along with Kevin) and many of the jokes on our door. Mike Bradley, the newest member of our group, decided for me that it was high time I stopped taking data and started writing my thesis. But if his experimental skills are as good as his French, he should have a fun time in ICR world. I wish them both at least as much luck with the experiment as I had.

We were fortunate to have really good undergraduates - Matt Marjanovic, Dave Kern and currently Abe Stroock - working with us. They all matured quickly beyond the small projects that we started them off with and made important contributions to our apparatus.

It is a pleasure to acknowledge the useful knowledge gained from conversations with researchers around the world - among them Jordan Camp, Dave Wineland, Joe Tan, Van

Dyck, Georges Audi, Aaldert Wapstra, Tobias Engels, Georg Bollen, Günther Werth.... My friend and classmate (Dr.) Rajiv Vijayan lent his signal processing expertise to help me understand the tricks of spectral estimation, and got to sail with Dave in return.

On days when the experiment was not going well or I had some time to kill, Wolfgang Ketterle was always ready to discuss my crazy thoughts on QM and relativity. It was hard to talk to Kris Helmerson for five minutes before somebody wanted to know where to find a screwdriver or a gasket. I actually stopped asking him for help unless I was really desperate since he would invariably drop whatever he was doing and go to the nearest hardware store if necessary. Mike Joffe had a (good?) joke for every occasion and never demagnetized us though he kept threatening to. Chris Ekstrom took care of all the general purpose lab Macs and was nice to us as long as we let him steal our liquid nitrogen (all right, he also showed me how to get symbol **bold**). And Robert Lutwak kept me in contact with the outside world through email.

The other (ex-)people in the lab made graduate school the fun time that it is - Prof. Alex Nitram, Min Xiao, Ken Davis, Marc-Oliver Mewes, Jörg Schmiedmayer, David Keith, Quentin Turchette, Troy Hammond, Mike Chapman, Mike Haggerty, Scott Paine, Jon Sandberg, Jeff Holley, Hong Jiao, Warren Moskowitz, Brian Stewart, Rick Stoner, Ke-Xun Sun.... I am sure I owe them all for many favours.

Having Carol Costa around made administrative life easy for all of us. And she was the only one who knew when Dave was going to get in. Working on an experiment inevitably involves contact with companies; John Peck in RLE purchasing thankfully kept us shielded from much of the red tape. Bruce Russell in the RLE shop kept a stern face but had a complete set of drill bits that he let me borrow. And the custodians in our building (unlike some grad students) were most understanding when I had to shut down the freight elevator for taking data.

And finally I thank my family, for their understanding and support through all these years. I can only say that the large distance between us made me appreciate them that much better.

Thank you, Danke, merci, dhanyavad and nanri!